On Diversity in Wireless Communications

by

Wei Li
B.Eng, Beijing University of Posts and Telecommunications, 1995
M.Eng, Beijing University of Posts and Telecommunications, 1998

A Dissertation Submitted in Partial Fulfillment of the Requirements
for the Degree of

DOCTOR OF PHILOSOPHY

in the Department of Electrical and Computer Engineering

Supervisor: Dr. T. A. Gulliver

ABSTRACT

Diversity is a well known technique used to reduce the performance degradation in wireless communication systems caused by fading. Recently, much research has been directed to transmit diversity and receiver diversity. In this dissertation, we first study the capacity and error probability of space time block codes over correlated fading channels, and then generalize the results to the performance and capacity of maximal ratio combining (MRC) over correlated Nakagami fading channels. The performance analysis of a RAKE receiver employing MRC is given as a practical case study.

Table of Contents

List of Tables

List of Figures

List of Abbreviations

AWGN	Additive White Gaussian Noise
BEP	Bit Error Probability
BER	Bit Error Rate
BPSK	Binary Phase Shift Keying
CDMA	Code Division Multiple Access
CF	Characteristic Function
FDMA	Frequency Division Multiple Access
MAI	Multiple Access Interference
MGF	Moment Generating Function
MIMO	Multiple Input Multiple Output
MRC	Maximal Ratio Combining
OFDM	Orthogonal Frequency Division Multiplexing
PAM	Pulse Amplitude Modulation
PDF	Probability Density Function
PSK	Phase Shift Keying
QAM	Qudrature Amplitude Modulation
QPSK	Quadrature Phase Shift Keying
SNR	Signal to Noise Ratio
STC	Space-Time Code
STBC	Space-Time Block Code
STTC	Space-Time Trellis Code
TDMA	Time Division Multiple Access

Acknowledgement

A journey is easier when you travel together. I am taking this opportunity to thank all those who have assisted me in one way or another with my Ph.D. study. First of all, I would like to express my gratitude toward my supervisor Dr. T. Aaron Gulliver for his invaluable guidance and encouragement throughout my doctoral studies. His kindness, and attention to detail for his students made it a pleasure to work in his research group. I also would like to thank my committee members for their valuable suggestions for my research. Special thanks are due to Dr. Hong-Chuan Yang, who gave me the initial input for the results in Chapter 5 and spent lots of time to support my research on this topic. I am also very grateful to my dear friends and colleagues in the Electrical and Computer Engineering Department, namely Hao Zhang, Zeljko Blazek, Erik Laxdal, Caner Budakoglu, Richard Chen, Yihai Zhang, Yongsheng Shi, Poramate Tarasak, Ubolthip Sethakaset, Katayoun Farrahi, William Chow, Neil Carson, Mohammad Omar Farooq, Yousry Abdel-Hamid, Sabbir Ahmad, Ping Chen, Yajun Kou, and Nanyan Wang for their support. Their friendship has made my life here a wonderful memory.

Dedication

To Jing

Chapter 1

Introduction

1.1 Diversity for Wireless Communications

Today high speed and high quality data transmission are requirements of the wireless communication industry. However, wireless channels are characterized by large attenuation and vagaries termed as fading [1]. It is well known that diversity in signaling is very effective in countering the effects of fading. Diversity techniques are based on the notion that if the receiver can be provided with several copies of the signals with the same underlying data transmitted over independently fading channels, then the probability that all the signal components will fade simultaneously is reduced considerably.

Diversity is one of the key technologies for many current and emerging wireless communication systems. Indeed, diversity techniques, in which two or more copies of the same information-bearing signals are combined at the receiver to increase the overall signal-to-noise ratio (SNR), still offers one of the greatest potential for radio link performance improvement for many of the current and future wireless technologies. For example, to meet the stringent requirements for quality service requirements and spectrally efficient multilevel constellations, antenna (space) diversity is needed to offset the SNR penalty due to fading and the dense signal constellation. In addition, one of the most promising features of wideband code division multiple access (WCDMA) systems is their ability to resolve multipath signals, resulting in multipath diversity which can be exploited by RAKE reception.

There are many ways that we can provide the receiver with diversity [2][3][4]. Space diversity consists of receiving the transmitted signal through several separate antennas, whose spacing is wide enough with respect to the carrier wavelength so as to obtain sufficient decorrelation. This technique can be easily implemented at the base stations, and does not require extra radio spectrum occupancy. Frequency diversity is obtained by sending the same signal over different frequency carriers, whose separation should be larger than the coherence bandwidth of the channel. Clearly, frequency diversity is not a bandwidth efficient solution. We can achieve time diversity if the same information bearing signals are transmitted in different time slots separated by an interval longer than the coherence time of the channel.

1.1.1 Introduction to Space Time Block Codes

1.1.1.1 Background of Space Time Block Coding

The growing demand for high-rate data service through wireless channels experienced in recent years motivates the design of multiple antenna wireless systems to transmit increased data rates without substantial bandwidth expansion. In particular, antenna diversity can be used to improve the performance of wireless systems such as CDMA.

Recently, space-time coding (STC) has gained much attention as an effective transmit diversity technique. Space-Time Codes were firstly introduced by Tarokh *et al.* [5] to provide transmit diversity in wireless fading channels by using multiple transmit antennas. The STC scheme combines the idea of channel coding and diversity to improve the data rates and reliability of communication. The application of multiple transmit antennas is a relatively new and attractive area as it enables the designer to move the diversity burden from the mobile units to the base station. The overall system structure of STC is shown in Fig. 1. In a wireless communication system with STC, signals are first encoded by the space-time encoder, and then transmit with a multi-antenna system. The receiver combines the signals from the receive antennas and reproduces the transmitted signal.

Space-time coding can be thought of as a combination of channel coding and antenna arrays, it is essentially a joint design of coding, modulation, transmit and receive diversity, and can be considered as a generalization of other transmit diversity schemes, such as the bandwidth efficient transmit diversity scheme [6] and the delay diversity scheme [7]. However, the main problem in deploying transmit diversity is that the channel information is not available at the transmitter. To solve this problem, space-time codes create a relationship between spatially separated signals and temporarily separated signals. STC can achieve the same diversity advantage as the well-known maximal ratio combining (MRC) technique [8]. In addition to the diversity advantage, a certain amount of coding gain can also be achieved by a well-constructed STC. Thus, STC can guarantee good performance over a broad range of channel conditions.

There are two main types of space-time codes, namely space-time block codes (STBC) and space-time trellis codes (STTC). Space-time block codes operate on a block of input symbols, producing a matrix output whose rows represent time and columns represent different transmit antennas. In contrast to the single antenna block codes for the AWGN channel, space-time block codes do not generally provide coding gain, unless concatenated with an outer code. Their main feature is the provision of diversity gain with a very simple decoder. On the other hand, space-time trellis codes operate on one input symbol at a time, producing a sequence of vector symbols whose length represents the number of antennas. Like traditional trellis coded modulation (TCM) for a single-antenna channel, space-time trellis codes provide coding gain. Since they can also provide diversity gain, their key advantage over space-time block codes is the provision of coding gain. Their disadvantage is that they are very hard to design and in general the decoders are complex. This design problem is similar to that for TCM, convolutional codes, turbo codes, etc.

1.1.1.2 Mode of Operation for Space Time Block Coding

In this section, we present the principles of STBC following the approach in [8][9][10]. We consider a wireless system with N transmit antennas and M receive antennas. The channel

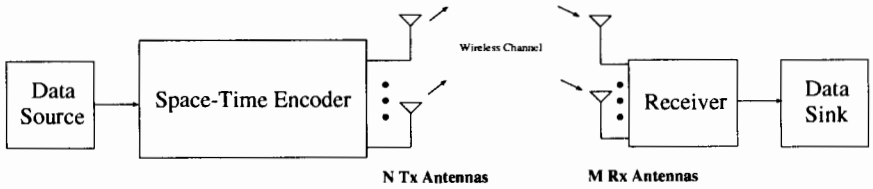

Figure 1.1. *System structure of Space Time Coding*

is assumed to be quasi-static with flat fading, which means that the channel is constant within one frame period, but varies independently between frames. Since we study the coding and decoding within one frame, we ignore the time index in the equations. Perfect channel state information is assumed available at the receiver, but the channel is unknown at the transmitter. Let T represent the number of time slots used to transmit S symbols. Hence, the transmission matrix of a STBC is

$$\mathbf{G} = \begin{pmatrix} g_{11} & g_{21} & \cdots & g_{N1} \\ g_{12} & g_{22} & \cdots & g_{N2} \\ \cdots & \cdots & \cdots & \cdots \\ \cdots & \cdots & \cdots & \cdots \\ g_{1T} & g_{2T} & \cdots & g_{NT} \end{pmatrix}, \tag{1.1}$$

where g_{ij} represents an element of the signal constellation and their conjugates, and are transmitted simultaneously from the ith transmit antenna in the jth time slot for $i = 1, 2, \ldots, N$ and $j = 1, 2, \ldots, T$. Since there are S symbols transmitted over T time slots, the code rate of the STBC is given by

$$R = \frac{S}{T}. \tag{1.2}$$

At a particular time nT, the received signal corresponding to the nth input block spanning T time slots is

$$\mathbf{Y}_{nT} = \mathbf{H}\mathbf{G}^T + \mathbf{W}_{nT}. \tag{1.3}$$

Time Slot	Transmit Antenna	
T	T_{x0}	T_{x1}
t_0	s_0	s_1
t_1	$-s_1^*$	s_0^*

Table 1.1. *Encoding and Transmission Process for the* $\mathbf{G}_2$ *STBC*

where $\mathbf{Y}_{nT}$ is an $M \times T$ matrix, $\mathbf{H}$ is an $M \times N$ fading channel coefficient matrix with i.i.d. (independent, identically distributed) entries modeled as circular complex Gaussian random variables, $\mathbf{G}^T$ is the transpose of $\mathbf{G}$ with size $N \times T$, and $\mathbf{W}_{nT}$ is an $M \times T$ receiver noise matrix with i.i.d. entries modeled as circular complex Gaussian random variables with zero mean and variance $N_0/2$ in each dimension. At the receiver, a combining technique [8][9][10] similar to MRC can be applied to obtain full diversity gain.

- **Two Transmit Antennas STBC**

  As mentioned above, the simplest form of STBC, which is a two transmit antenna based code associated with $N = 2$, was first proposed by Alamouti [8]. The corresponding transmission matrix is

$$\mathbf{G}_2 = \begin{pmatrix} s_0 & s_1 \\ -s_1^* & s_0^* \end{pmatrix}, \tag{1.4}$$

  For transmission matrix $\mathbf{G}_2$ there are $N = 2$ transmit antennas, $S = 2$ input symbols, namely s_0, s_1, and the code spans $T = 2$ time slots. s_0^* and s_1^* are the conjugates of symbols s_0 and s_1, respectively. Since $S = 2$ and $T = 2$, the code rate given by (1.4) is unity. The associated encoding and transmission are shown in Table 1.1.

  At any particular time instant T, two signals are simultaneously transmitted from transmit antennas T_{x0} and T_{x1}. For example, in time slot t_0, signal s_0 and s_1 are transmitted simultaneously from transmit antennas T_{x0} and T_{x1}, respectively. In the next time slot t_1, signal $-s_1^*$ and s_0^* are transmitted simultaneously from transmit antennas T_{x0} and T_{x1}, respectively.

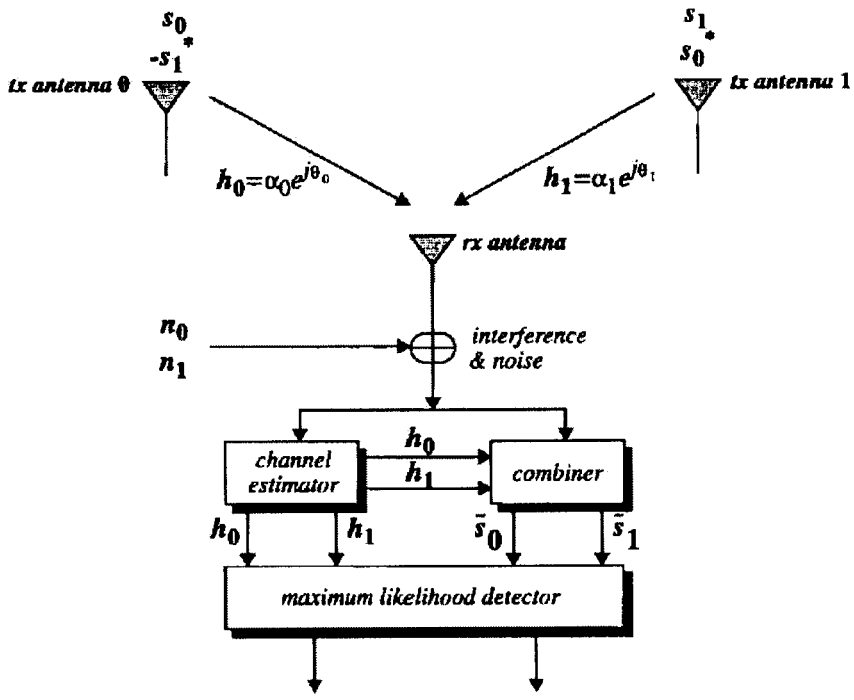

Figure 1.2. *Baseband representation of STBC* $\mathbf{G}_2$ *with one receive antenna.*

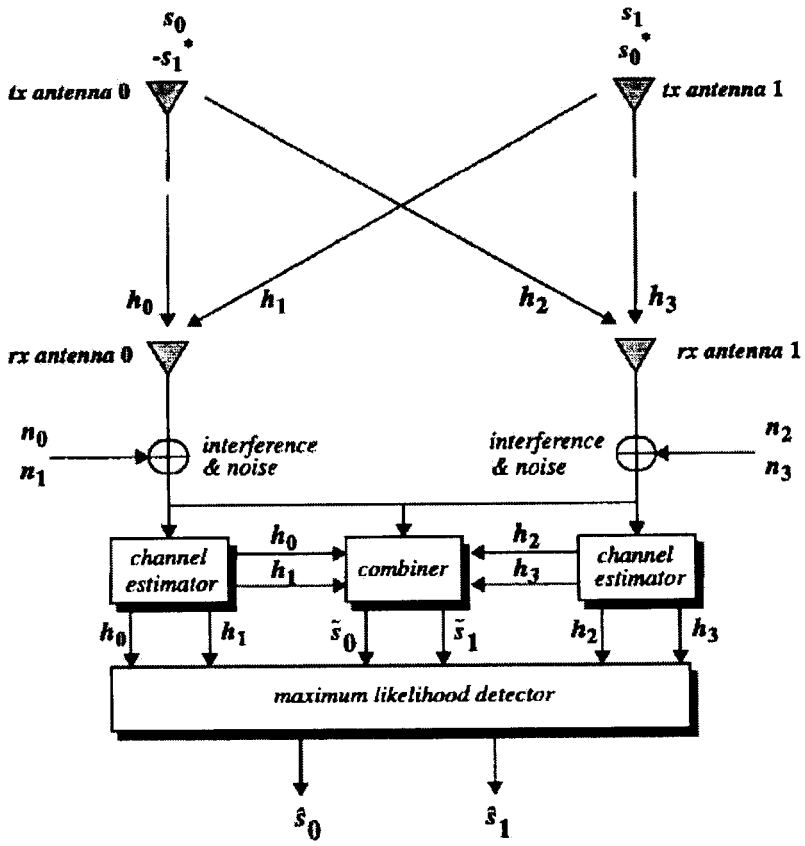

Figure 1.3. *Baseband representation of STBC* G_2 *with two receive antennas.*

Fig. 1.2 and Fig. 1.3 show the baseband representation of STBC $\mathbf{G}_2$ with one receive antenna and two receive antennas, respectively. As mentioned earlier, a flat fading channel is assumed so the complex fading envelop h_0 and h_1 are assumed to be constant across the corresponding two consecutive time slots. Independent additive white Gaussian noise (AWGN) is input at the receiver in each time slot. The received signals over flat fading channels can be expressed as

$$r_0 = h_0 s_0 + h_1 s_1 + n_0, \tag{1.5}$$

and

$$r_1 = -h_0 s_1^* + h_1 s_0^* + n_1, \tag{1.6}$$

where r_0 is the first received signal and r_1 is the second. Note that the received signal r_0 consists of the transmitted signals s_0 and s_1, while r_1 consists of their conjugates. In order to decode the transmitted signals, we have to extract the signals s_0 and s_1 from the received signals r_0 and r_1. With perfect channel state information available at the receiver, the received signals are combined as follows to decode s_0 and s_1

$$\tilde{s_0} = h_0^* r_0 + h_1 r_1^* = (|h_0|^2 + |h_1|^2) s_0 + h_0^* n_0 + h_1 n_1^* \tag{1.7}$$

and

$$\tilde{s_1} = h_1^* r_0 - h_0 r_1^* = (|h_0|^2 + |h_1|^2) s_1 + h_1^* n_0 - h_0 n_1^* \tag{1.8}$$

It is easy to see from (1.7) and (1.8) that s_0 and s_1 have been separated from r_0 and r_1 by simple multiplications and additions due to the orthogonality of the STBC [8][9]. Both signals $\tilde{s_0}$ and $\tilde{s_1}$ are then passed to the maximum likelihood detector as shown in Fig. 1.2 and Fig 1.3 to determine the most likely transmitted symbols s_0 and s_1. Note that the STBC combiner has a form very similar to MRC for receive diversity. Similarly, for STBC $\mathbf{G}_2$ with 2 receive antennas shown in Fig. 1.3, the received signals can be combined to generate s_0 and s_1 as follows

$$\tilde{s_0} = (|h_{00}|^2 + |h_{01}|^2 + |h_{10}|^2 + |h_{11}|^2)s_0 + h_{00}^* n_{00} + h_{01} n_{01}^* + h_{10}^* n_{10} + h_{11} n_{11}^*, \quad (1.9)$$

and

$$\tilde{s_1} = (|h_{00}|^2 + |h_{01}|^2 + |h_{10}|^2 + |h_{11}|^2)s_1 + h_{01}^* n_{00} - h_{00} n_{01}^* + h_{11}^* n_{10} - h_{10} n_{11}^*. \quad (1.10)$$

In the generalized form with M receive antennas, we have

$$\tilde{s_0} = \sum_{i=1}^{M} \left[(|h_{i0}|^2 + |h_{i1}|^2)s_0 + h_{i0}^* n_{i0} + h_{i1} n_{i1}^* \right] \quad (1.11)$$

and

$$\tilde{s_1} = \sum_{i=1}^{M} \left[(|h_{i0}|^2 + |h_{i1}|^2)s_1 + h_{i1}^* n_{i0} - h_{i0} n_{i1}^* \right] \quad (1.12)$$

It can be easily observed that STBC $\mathbf{G}_2$ with M receive antennas has the same diversity order as MRC with $2M$-order receive diversity.

- **STBC with more than Two Transmit Antennas**

  It is shown in [9] based on the theory of orthogonal designs that full rate STBCs exist for any number of transmit antennas using an arbitrary real constellation such as PAM modulation. For an arbitrary complex constellation such as PSK/QAM, half rate STBCs exist for any number of transmit antennas, while full rate STBCs only exist for 2 transmit antennas. In another words, $\mathbf{G}_2$ is the only full rate complex STBC. As specific cases for three and four transmit antennas, rate 1/2 and 3/4 STBCs are given in [9], and are denoted as $\mathbf{G}_3$, $\mathbf{G}_4$, and $\mathbf{H}_3$, $\mathbf{H}_4$, respectively, and are given by

$$\mathbf{G}_3 = \begin{pmatrix} +s_1 & +s_2 & +s_3 \\ -s_2 & +s_1 & -s_4 \\ -s_3 & +s_4 & +s_1 \\ -s_4 & -s_3 & +s_2 \\ +s_1^* & +s_2^* & +s_3^* \\ -s_2^* & +s_1^* & -s_4^* \\ -s_3^* & +s_4^* & +s_1^* \\ -s_4^* & -s_3^* & +s_2^* \end{pmatrix}, \tag{1.13}$$

and

$$\mathbf{G}_4 = \begin{pmatrix} +s_1 & +s_2 & +s_3 & +s_4 \\ -s_2 & +s_1 & -s_4 & +s_3 \\ -s_3 & +s_4 & +s_1 & -s_2 \\ -s_4 & -s_3 & +s_2 & +s_1 \\ +s_1^* & +s_2^* & +s_3^* & +s_4^* \\ -s_2^* & +s_1^* & -s_4^* & +s_3^* \\ -s_3^* & +s_4^* & +s_1^* & -s_2^* \\ -s_4^* & -s_3^* & +s_2^* & +s_1^* \end{pmatrix}, \tag{1.14}$$

and

$$\mathbf{H}_3 = \begin{pmatrix} +s_1 & +s_2 & +\frac{s_3}{\sqrt{2}} \\ -s_2^* & +s_1^* & +\frac{s_3}{\sqrt{2}} \\ +\frac{s_3}{\sqrt{2}}^* & +\frac{s_3}{\sqrt{2}}^* & -\frac{s_1+s_1^*-s_2+s_2^*}{2} \\ +\frac{s_3}{\sqrt{2}}^* & -\frac{s_3}{\sqrt{2}}^* & +\frac{s_1-s_1^*+s_2+s_2^*}{2} \end{pmatrix}, \tag{1.15}$$

and

$$\mathbf{H}_4 = \begin{pmatrix} +s_1 & +s_2 & +\frac{s_3}{\sqrt{2}} & +\frac{s_3}{\sqrt{2}} \\ -s_2^* & +s_1^* & +\frac{s_3}{\sqrt{2}} & -\frac{s_3}{\sqrt{2}} \\ +\frac{s_3}{\sqrt{2}}^* & +\frac{s_3}{\sqrt{2}}^* & -\frac{s_1+s_1^*-s_2+s_2^*}{2} & -\frac{s_1-s_1^*-s_2-s_2^*}{2} \\ +\frac{s_3}{\sqrt{2}}^* & -\frac{s_3}{\sqrt{2}}^* & +\frac{s_1-s_1^*+s_2+s_2^*}{2} & -\frac{s_1+s_1^*+s_2-s_2^*}{2} \end{pmatrix}. \quad (1.16)$$

Two simpler rate 3/4 STBCs are presented in [11][12][13], namely

$$\mathbf{G} = \begin{pmatrix} s_0 & s_1 & s_3 \\ -s_1^* & s_0^* & 0 \\ s_3^* & 0 & -s_1^* \\ 0 & s_3^* & -s_2^* \end{pmatrix}, \quad (1.17)$$

for three transmit antennas and

$$\mathbf{G} = \begin{pmatrix} s_0 & s_1 & s_3 & 0 \\ -s_2^* & s_1^* & 0 & s_3 \\ s_3^* & 0 & -s_1^* & s_2 \\ 0 & s_3^* & -s_2^* & s_1 \end{pmatrix}, \quad (1.18)$$

for four transmit antennas. In Table 1.2, we summarize the parameters associated with all STBC codes given in [6][7][9][10][11][12][13]. The decoding algorithms and the corresponding performance of these STBCs were given in [10].

1.1.2 Introduction to Maximal Ratio Combining

1.1.2.1 Background of Maximal Ratio Combining

As mentioned previously, diversity has long been recognized as a powerful communication receiver technique for mitigating the detrimental effects of channel fading. Diversity schemes can be classified according to the type of combining employed at the receiver, such as, maximal-ratio combining (MRC), equal gain combining (EGC), selection diversity combining (SDC) and generalized selection combining (GSC). In MRC, signals from

STBC	Code Rate	Transmit Antennas	Input Symbols	Code Length
G_2	1	2	2	2
G_3	1/2	3	4	8
G_4	1/2	4	4	8
H_3	3/4	3	3	4
H_4	3/4	4	3	4
G_5	7/11	5	7	11
G_6	3/5	6	18	30

Table 1.2. *Different STBC.*

each of the diversity branches are combined coherently and are individually weighted to optimize the SNR of the combiner. MRC is known to be optimum in the sense that it yields the best statistical reduction of fading in any linear diversity combiner. In an EGC combiner, the outputs of different diversity branches are first co-phased and weighted equally before being summed to give the resultant output. An EGC combiner does not require the estimation of the channel gains, and hence it results in reduced receiver complexity relative to MRC. However, the performance of EGC is inferior to that of MRC since the branch weights are all set to unity. SDC selects the branch that provides the highest instantaneous SNR, and so is the simplest and perhaps the most frequently used form of diversity combining. However, this is achieved at the expense of receiver performance. The complexity of MRC and EGC receivers depends on the number of diversity paths available, which can be quite high, especially for the multipath diversity of wideband CDMA and ultra wideband (UWB) signals. In addition, MRC is sensitive to channel estimation errors, and these errors tend to be more important when the SNR is low. On the other hand, SDC uses only one path out of the available paths. Consequently, it does not fully exploit diversity paths.

There are many practical applications for maximal ratio combining such as the RAKE receiver. A RAKE receiver uses several baseband correlators to individually process mul-

tipath signal components. The outputs from the correlators are combined to achieve improved reliability and performance. A detailed discussion of RAKE receiver can be found in Chapter 5.

1.1.2.2 Mode of Operation of Maximal Ratio Combining

Maximal ratio combining (MRC) takes better advantage of all the diversity branches in the wireless communication system. Fig. 1.4 shows its configuration for a two-branch diversity system. Both branches are weighted by their respective instantaneous amplitude-to-noise ratios. The branches are then synchronized and added together to get the best output SNR. The summed signals are then used as the received signal and sent to the demodulator. Maximal ratio combining will always perform better than either selection diversity or equal gain combining because it is an optimum combiner [1]. The information on all channels is used with this technique to get a more reliable received signal. The disadvantage of MRC is that it is complicated and requires accurate estimates of the instantaneous signal level and average noise power to achieve optimum performance. The advantage is that improvements can be achieved with this configuration even when both branches are completely correlated. The inputs to the maximal ratio combiner are both faded signals (with envelopes α_0 and α_1) with independent additive noise sources n_0 and n_1. n_0 and n_1 are zero mean white Gaussian random variables with variance σ^2. The input amplitude-to-noise ratios are given by

$$SNR_{input,amplitude} = \frac{\alpha_{0,1}}{\sigma}, \tag{1.19}$$

and the input signal to noise power ratio is

$$SNR_{input,power} = \frac{\alpha_{0,1}^2}{\sigma^2}. \tag{1.20}$$

Calculating the SNR after maximal ratio combining (MRC) requires the evaluation of the instantaneous signal power and noise power. The amplitude of the signal of interest after MRC at a given time, α_{out}, can be evaluated by multiplying the received signal envelopes α_0 and α_1 by their instantaneous amplitude to noise power ratios which when summed

gives

$$\alpha_{out} = \alpha_0^2 + \alpha_1^2. \tag{1.21}$$

The instantaneous signal power after maximal ratio combining, α_{out}^2, is defined as

$$\alpha_{out}^2 = (\alpha_0^2 + \alpha_1^2)^2. \tag{1.22}$$

The noise component after MRC is also multiplied by the gains in both branches and after co-phasing and branch addition is given by

$$n_{out} = n_0\alpha_0 + n_1\alpha_1. \tag{1.23}$$

The resulting noise power at the output of the maximal ratio combiner is

$$\sigma_{out} = \left[\alpha_0^2 + \alpha_1^2\right]\sigma^2. \tag{1.24}$$

The output signal to noise ratio after maximal ratio combining is given by the ratio of signal to noise power from (1.22) and (1.24)

$$SNR_{power,out} = \frac{\alpha_0^2 + \alpha_1^2}{\sigma^2} = SNR_{power,s_0} + SNR_{power,s_1}. \tag{1.25}$$

We can see from (1.25) that the SNR after MRC combining is the sum of the input SNRs. Results for more than two diversity paths are straightforward.

1.2 Motivation for This Research

The goal of wireless communications is to provide mobile, low cost, reliable systems with the capability of providing voice and high speed data with minimum latency and long battery life. However, there are still many obstacles and bottlenecks to achieve this in practice. Noise and fading are two of the major factors which make wireless channels hostile. Among all the technologies available, diversity is one of the most important methods to combat noise and fading. It can greatly improve system performance and capacity by providing the receiver with multiple signals generated by the same underlying data.

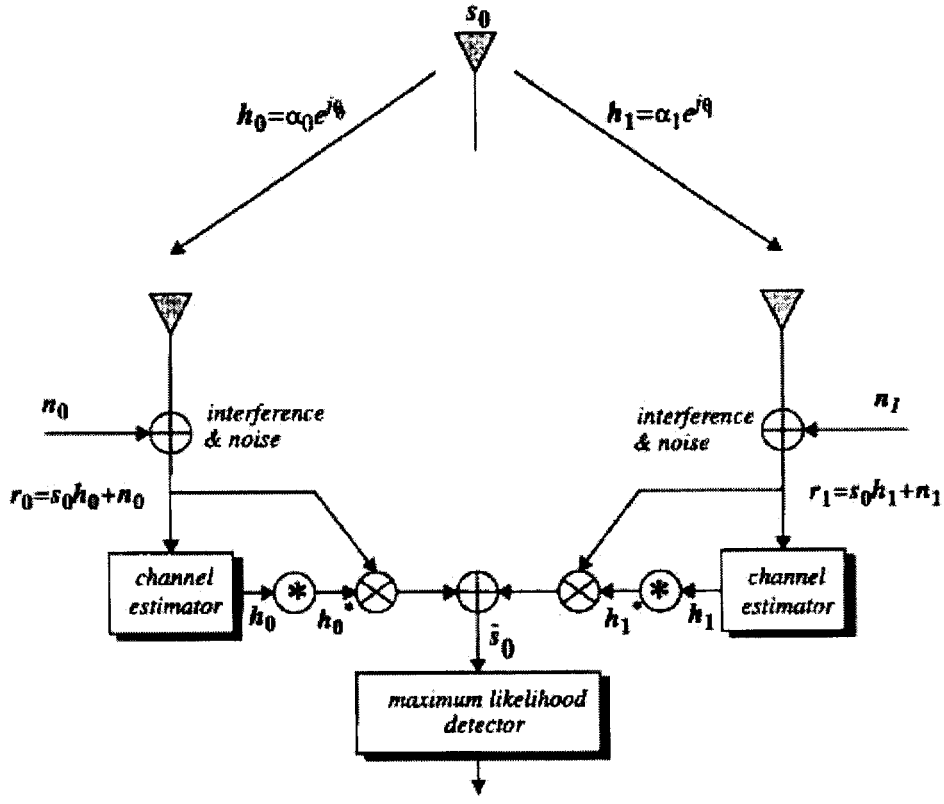

Figure 1.4. *Mode of operation of Maximal Ratio Combining.*

The motivation for this thesis is to evaluate the performance of wireless communication systems with transmit and/or receive diversity over correlated fading channels. Due to size constraints, the space between antenna elements is limited. When identical elements are closely spaced, the signal envelopes received by both elements can exhibit a large degree of correlation, or similarity. A large correlation implies that when one antenna receives a low power signal, the second element likely also receives a similarly degraded signal. A diversity system may have antennas that are close together so signals are correlated. The results presented in this thesis explore the error rates and capacity of wireless communication systems with STBC or MRC on correlated fading channels.

1.2.1 Literature Review

1.2.1.1 Current Research on STC

- **Improvements on STC**

  Since the introduction of space-time coding, there has been rapid progress in the field, targeted at finding better codes with improved diversity and with greater coding gains. In this area, Baro [14] et al. reported improved STTC that were found through exhaustive computer search; Ionescu et al. [6] reported improved 8 and 16 state STTC for 4-PSK in the case of two transmitters in Rayleigh fading via a modifed determinant criterion. Similarly, Yuan et al. [15] derived a more accurate code design criteria that yielded new STTC with better performance than the codes in [8].

- **Channel Correlation**

  The effects of receive and transmit channel correlation in multiple-input-multiple-output (MIMO) systems on the error performance of STC was firstly raised by Boleskei et al. [16]. He showed that the resulting maximum diversity order was given by the ranks of the receive and transmit correlation matrices. Further work has been undertaken to study the performance of STBC and STTC and to develop robust codes for correlated fading channels [17].

- **Channel State Information**

  Another research topic is to create STC systems for channels that are known neither to the transmitter nor to the receiver. The first step in this direction was undertaken by Hochwald etc., who proposed a systematic method for designing unitary space-time constellations for MIMO systems [18]. Unitary space-time signals are orthonormal in time across the antennas, and have been shown to be well-suited to Rayleigh fading channels where neither the transmitter nor the receiver has information about the fading channel [19].

- **Multilevel Designs**

  There has also been some interest in multilevel designs of STC, since they appear to be an efficient means of constructing and decoding codes when the number of antennas is large. Some recent work in this area includes investigating systematic designs of space-time codes employing multiple trellis coded modulation [20].

- **Applications in Practical Systems**

  Much research has been done regarding the application of STC to current mobile communication systems, such as OFDM, CDMA, MC-CDMA, etc. The incorporation of space-time coding into OFDM is a very hot research area. Recent work has shown that the performance of OFDM systems using STBC provides significant gains [21]. The SPINCOM group of at the University of Minnesota has proposed a novel generalized space-time OFDM transceiver. They considered a system with two transmit antennas and one receive antenna. In their system, STBC $\mathbf{G}_2$ was incoporated into a generalized OFDM transmitter to achieve transmitter diversity in frequency-selective propagation. In addition to performance improvement, the decoding complexity at the receiver is very low.

1.2.1.2 Current Research on MRC

Much research has been done on the performance of wireless systems employing MRC. In [22], the error probability for binary coherent multichannel reception over flat Ricean

fading channels was derived, but not in closed-form. Recently, a recursive solution for the error probability performance was developed [23] for multichannel PSK reception in frequency-selective Ricean fading channels. The error rate analysis in [23] was extended in [24] to coherent linear modulation systems over flat Rician fading channels, and specific results for rectangular q-ary QAM constellations were presented. In [25], a unified approach for calculating error rates of linearly-modulated signals over generalized fading channels was presented based on the moment generating function (MGF) of the SNR for multichannel reception. A similar analysis was given in [26] for binary maximum ratio combining (MRC) multichannel reception performance over a Nakagami fading channel. In [27], the authors extended the Khatri distribution of the largest eigenvalue of central complex Wishart matrices to the non-central case. This new result was applied to the performance analysis of multi-input multi-output (MIMO) MRC systems over Rician fading channels, and the error probability and outage capacity of MIMO systems with MRC was derived. In [28], the authors derived exact symbol error probability (SEP) expressions for coherent detection of PSK and QAM with hybrid selection MRC in multipath fading wireless channels.

1.2.2 Contributions of the Thesis

First presented in [8] for two transmit antennas, and generalized in [9][10] for an arbitrary number of transmit antennas, orthogonal space-time block coding (STBC) is a remarkable technique which can provide full diversity gain with very low computational complexity. However a loss in capacity, characterized by the code rate and the number of receive antennas, is shown in [29][30] for an arbitrary channel. The Shannon capacity

$$C = W \log_2(1 + SNR) \tag{1.26}$$

where SNR is the signal-to-noise ratio and W is the channel bandwidth, predicts the channel capacity C for an AWGN channel with continuous-valued inputs and outputs. However,

a channel employing STBC with PAM/PSK/QAM modulation has discrete-valued inputs and continuous-valued outputs, which imposes an additional constraint on the capacity calculation. Following the analysis in [10][30], a characterization based on an equivalent scalar Additive White Gaussian Noise (AWGN) channel multiplied by a coefficient, which is a function of the Frobenius norm of the channel matrix with multiple antennas, was given in [29] assuming a full code rate.

In Chapter 2 of this thesis, we continue the work by extending the capacity analysis for STBC to correlated fading channels. Closed form Shannon capacity expressions are derived for correlated Rayleigh and Nakagami fading channels. The capacity loss caused by the correlation is determined.

In Chapter 3 of this thesis, we explore the error probability for STBC to correlated fading channels. A unified approach has been introduced for various fading channels and modulation schemes. Closed form error probability expressions are derived for Rayleigh and Nakagami fading channels.

In Chapter 4 of this thesis, employing the same approach as in Chapters 2 and 3, we study the error probability and capacity for MRC on correlated Nakagami fading channels. We present simple error probability expressions for MRC multichannel reception of q-ary coherent systems over flat Nakagami fading channels. Closed-form symbol error probabilities for q-ary PAM, PSK and rectangular QAM systems are given in a very simple form. Closed form Shannon capacity expressions are also derived for correlated Nakagami fading channels.

Multipath is a troublesome effect in wireless channels. In addition to the direct path signal, many reflected path signals also arrive at the receiver with different delays and attenuations, resulting in fading and intersymbol interference. Employing a RAKE receiver is an efficient means of overcoming these multipath effects [1][31]. Actually, one of the advantages of code division multiple access (CDMA) systems is the capability of utilizing multipath signals that arrive with different time delays to improve performance. Other systems, such as frequency division multiple access (FDMA) or time division multiple

access (TDMA), cannot discriminate between multipath arrivals, and thus must rely on equalization to mitigate the negative effects of multipath. A RAKE receiver in a CDMA system can exploit multipath diversity to obtain better performance.

Significant effort has been devoted to improving the performance of RAKE receivers. The combining algorithm commonly used in CDMA RAKE receivers is conventional maximal ratio combining (MRC) which is known to maximize the signal-to-noise ratio (SNR) for diversity channels with equal noise power and perfect channel estimation [32]. However, combining all the diversity paths in MRC is not appropriate because weak paths contribute little to the combined SNR and add extra noise. In addition, implementing more fingers in the receiver will make it more complex and consume additional energy. Recently, other combining algorithms have been considered. generalized selection combining (GSC), which selects and combines the L_c best paths (i.e. with the highest SNR) among the L available multipaths, has been introduced and extensively studied [33][34][35][36][37]. In [38], a new minimum selection GSC (MS-GSC) scheme is introduced which selects the minimum number of paths such that the combined output SNR is larger than a threshold. In [39], a conditional diversity combining technique, namely absolute threshold GSC (AT-GSC), was introduced and analyzed. However, when all the paths are poor, this algorithm will not select any paths in which case the receiver will cease to function.

In Chapter 5 of this thesis, we study a practical RAKE combining scheme. We assume that the path obtained through synchronization will always be active, as is the case in practical systems. We assume that the receiver will try to use a small number of acceptable paths whose SNR is greater than a fixed threshold, from the set of resolvable ones. When there is no acceptable path, the synchronization path will still be used and the receiver will always function. When the receiver finds enough acceptable paths, it ceases path search. Therefore, the proposed scheme introduces smaller system delay since it is not always necessary to search for all resolvable paths. We study the performance of the proposed scheme over Rayleigh, Rician and Nakagami fading channels based on moment generating functions (MGF). In particular, we derive closed-form expressions for the average combined output

SNR and symbol error probability (SEP) over block fading channels. Outage probability and average number of estimated channels are also derived. To explore the performance of a practical RAKE receiver, the results are extended to the case when we have unequal average SNRs. In addition, the synchronized path is required to exceed an SNR threshold γ_{syn}.

1.3 Thesis Outline

The rest of this thesis is organized as follows. In Chapter 2, we analyze the capacity of space-time block codes for PAM/PSK/QAM modulation from an SNR perspective based upon the equivalent channel induced by the STBC over correlated fading channels. Using the PDF of the SNR, capacity is given for various combinations of modulation and fading channels. Chapter 2 is organized as follows. Section 2.1 gives the system model. Section 2.2 gives the capacity analysis of STBC over fading channels. Section 2.3 presents the analysis of a DS-CDMA system with STBC. Section 2.4 gives out some numerical resultes.

In Chapter 3, we analyze capacity and the error probability of STBC for PAM/PSK/QAM modulation from an SNR perspective based upon the equivalent channel induced by the STBC over correlated fading channels. Using the PDF of the SNR, symbol error probabilities are given for various combinations of modulation and fading channels. Chapter 3 is organized as follows. Section 3.1 first considers STBC $\mathbf{G}_2$ with one receive antenna, then extends the results to an arbitrary number of antennas. Closed-form error probability expressions are obtained for PAM, PSK, and QAM modulation in correlated Rayleigh fading. In Section 3.2 the BER of STBC over correlated Nakagami fading is derived. In Section 3.3 a unified approach to the error probability analysis of STBC with general branch correlation is presented for Ricean and Nakagami fading channels. Section 3.4 presents the BER analysis of a DS-CDMA system with STBC over correlated fading channels. Section 3.5 presents some performance results.

In Chapter 4, we analyze the error probability of MRC for PAM/PSK/QAM modulation

with the same approach introduced in Chapters 2 and 3. Chapter 4 is organized as follows. Section 4.1 presents the channel model and derives the characteristic function (CF) and probability density function (PDF) for Nakagami fading channels with MRC reception. The capacity analysis over correlated Nakagami fading channels with MRC reception is given in Section 4.2. In Section 4.3, error probabilities are derived for different modulation schemes over correlated Nakagami fading channels employing MRC. Section 4.4 presents some numerical results to illustrate and verify the analysis given in the previous sections.

In Chapter 5, we analyze the performance of a practical RAKE receiver with MRC combining over fading channels. Chapter 5 is organized as follows. Section 5.1 presents the system model and mode of operation. Section 5.2 presents a general analysis of the MGF of the combined output signal SNR, and gives specific results for Rayleigh, Rician and Nakagami fading channels. Section 5.3 evaluates the average combined SNR and SEP performance based on the MGFs obtained in Section 5.2. Results for system outage probability and number of channels estimated are also given. Section 5.4 generalizes the previous results to a more practical model in which the synchronized channel is chosen by an SNR threshold γ_{syn}, and the average SNRs of the diversity paths follow a non-i.i.d. (independent and identically distributed) rule. Section 5.5 presents some numerical results to support the analysis given.

In Chapter 6, we summarize our work and give some brief ideas for our future research work.

Chapter 2

Capacity Analysis of STBC over Correlated Fading Channels

2.1 Space Time Block Codes and the Channel Model

2.1.1 The Effective Scaled AWGN Channel

The channel model is the same as in [8][9][10][29] and [30]. Consider a wireless communication system with N transmit antennas and M receive antennas. The channel is assumed to be quasi-static with flat fading, which means that the channel is constant within one frame period, but varies independently between frames. Furthermore, perfect channel state information is assumed available at the receiver, but the channel is unknown at the transmitter.

The equivalent AWGN scaled channel for STBC is

$$\mathbf{y}_{nT} = \frac{1}{R}\|\mathbf{H}\|_F^2 \mathbf{X}_{nT} + \mathbf{W}_{nT}, \tag{2.1}$$

where $\mathbf{y}_{nT}$ is the $S \times 1$ complex matrix after STBC decoding from the received matrix $\mathbf{Y}_{nT}$, $\mathbf{X}_{nT}$ is the $S \times 1$ complex input matrix with each entry having energy E_s/N_0, E_s is the maximum total transmitted energy from the N transmit antennas per symbol time, $\mathbf{W}_{nT}$ is complex Gaussian noise with zero mean and variance $\frac{1}{R}\|\mathbf{H}\|_F^2 N_0/2$ in each real dimension, $\|\mathbf{H}\|_F^2 = \sum_{i=1}^{N}\sum_{j=1}^{M}\|h_{ij}\|^2$ is the squared Frobenius norm of $\mathbf{H}$, h_{ij} is the chan-

nel gain from the ith transmit antenna to the jth receive antenna. Therefore, the effective instantaneous SNR, denoted as γ_s, at the receiver is

$$\gamma_s = \frac{E_s}{NRN_0}\|\mathbf{H}\|_F^2 = \bar{\gamma_c}\|\mathbf{H}\|_F^2 = \sum_{i=1}^{N}\sum_{j=1}^{M}\bar{\gamma_c}\|h_{ij}\|^2 = \sum_{i=1}^{N}\sum_{j=1}^{M}\gamma_{ij}, \tag{2.2}$$

where

$$\bar{\gamma_c} = \frac{E_s}{NRN_0}, \tag{2.3}$$

is the average SNR of each fading path per symbol, and γ_{ij} is the instantaneous SNR of each fading channel. It can easily be shown that the instantaneous SNR per bit has the same PDF as γ_{ij} except that

$$\bar{\gamma_c} = \frac{E_s}{NRN_0 \log_2 q} \tag{2.4}$$

for a q-ary signal constellation.

2.1.2 CF and PDF of the SNR on Correlated Fading Channels

To facilitate the following analysis, we first define an $MN \times 1$ column complex matrix $\mathbf{z} = [h_{11}, h_{12}, \ldots, h_{1N}, h_{21}, \ldots, h_{MN}]$. Then (2.2) can be written as

$$\gamma_s = \mathbf{z}^{\dagger}(\bar{\gamma_c})\mathbf{z}, \tag{2.5}$$

where the superscript † denotes matrix transpose and conjugate.

2.1.2.1 Rayleigh Fading

With Rayleigh fading, h_{ij} can be modeled as a complex Gaussian variable with zero mean and variance σ_{ij}^2 in each dimension. The complex covariances of the h_{ij} are given by the elements R_{kl} of the $MN \times MN$ covariance matrix

$$\mathbf{R} = \mathrm{E}\left[[\mathbf{z} - \mathrm{E}[\mathbf{z}]]^*[\mathbf{z} - \mathrm{E}[\mathbf{z}]]'\right], \tag{2.6}$$

where E[.] is the expected value operator, $*$ is the conjugate operator, and $'$ is the transpose operator. From (2.6), it can readily be shown that the covariance matrix $\mathbf{R}$ is Hermitian, positive semi-definite. Note that $\mathrm{E}[\mathbf{z}] = 0$ for Rayleigh fading.

As shown in [3], the distribution of γ_s is then a Hermitian quadratic form distribution in complex Gaussian variates. Following the procedure in [3], the characteristic function (CF) of γ_s, which is defined as a Laplace transform on the PDF, is then

$$G_{\gamma_s}(s) = \frac{1}{|\mathbf{I} + s\bar{\gamma}_c \mathbf{R}^*|}. \tag{2.7}$$

Assume the rank of the covariance matrix $\mathbf{R}$ is r, where $r \leq MN$, and $\mathbf{R}$ has μ distinct nonzero eigenvalues, with the ith nonzero distinct eigenvalue of $\mathbf{R}$ denoted as λ_i, and repeated κ_i times, where $\sum_{i=1}^{\mu} \kappa_i = r$. Then (2.7) can be written as

$$G_{\gamma_s}(s) = \frac{1}{\prod_{i=1}^{\mu}(1 + s\bar{\gamma}_c\lambda_i)^{\kappa_i}}. \tag{2.8}$$

Using a partial fraction expansion [40], (2.8) is then

$$G_{\gamma_s}(s) = \sum_{i=1}^{\mu}\sum_{j=1}^{\kappa_i} \frac{D_{ij}}{(1 + s\bar{\gamma}_c\lambda_i)^j}. \tag{2.9}$$

where the coefficient D_{ij} is given by

$$D_{ij} = \frac{1}{(\kappa_i - j)!\,(\bar{\gamma}_c\lambda_i)^{\kappa_i - j}} \frac{\partial^{\kappa_i - j}}{\partial s^{m\kappa_i - j}} \left[(1 + s\bar{\gamma}_c\lambda_i)^{\kappa_i} G_{\gamma_s}(s)\right]|_{s=\frac{1}{\bar{\gamma}_c\lambda_i}} \tag{2.10}$$

An inverse Laplace transform will provide the PDF of γ_s. Utilizing the linearity of the Laplace transform, the PDF of the γ_s can be written as

$$p(\gamma_s) = \sum_{i=1}^{\mu}\sum_{j=1}^{\kappa_i} D_{ij} \frac{\gamma_s^{j-1} e^{-\frac{\gamma_s}{\bar{\gamma}_c\lambda_i}}}{\Gamma(j)\,(\bar{\gamma}_c\lambda_i)^j}. \tag{2.11}$$

where $\Gamma(.)$ is the Gamma function.

As a special case, for constant correlation with correlation coefficient ρ, i.e. $R_{kl} = \rho$ for $k \neq l$, and balanced fading channels, i.e. $\sigma_j^2 = \sigma^2$, the covariance matrix will have two

distinct eigenvalues $\lambda_1 = 2\sigma^2(1 + (M-1)\rho)$ and $\lambda_k = 2\sigma^2(1-\rho)$ for $k = 2, 3, \ldots, M$. The PDF of the instantaneous SNR γ_s from (2.11) is therefore

$$\begin{aligned} p(\gamma_s) &= \frac{(1+(MN-1)\rho)^{MN-2}}{(MN\rho)^{MN-1}\bar{\gamma}_c} \\ &\times \exp\left(-\frac{\gamma_s}{\bar{\gamma}_c(1+(MN-1)\rho)}\right) \\ &- \sum_{i=0}^{m(MN-2)} \frac{(1+(MN-1)\rho)^{MN-2-i}}{(MN\rho)^{MN-1-i}(1-\rho)^i\Gamma(i+1)\bar{\gamma}_c{}^{i+1}}\gamma_s^i \\ &\times \exp\left(-\frac{\gamma_s}{\bar{\gamma}_c(1-\rho)}\right). \end{aligned} \tag{2.12}$$

More specifically, for STBC $\mathbf{G}_2$ with one receive antenna, the PDF of the instantaneous SNR γ_s is

$$p(\gamma_s) = \frac{\exp(-\frac{\gamma_s}{\Gamma_1}) - \exp(-\frac{\gamma_s}{\Gamma_2})}{2\rho\bar{\gamma}_c} \tag{2.13}$$

Note that balanced fading channels are assumed in (2.12) and (2.13).

For STBC $\mathbf{G}_2$ with one receive antenna over unbalanced Rayleigh fading channels having coefficients h_{11} and h_{21} with variances σ_{11}^2 and σ_{21}^2, respectively, the PDF of the instantaneous SNR γ_s can be obtained using the procedure in [41]

$$p(\gamma_s) = \frac{\exp(-\frac{\gamma_s}{(1+\rho)\bar{\gamma}_c}) - \exp(-\frac{\gamma_s}{(1-\rho)\bar{\gamma}_c})}{\Gamma_1 - \Gamma_2}, \tag{2.14}$$

where

$$\Gamma_1 = \frac{1}{2}[\bar{\gamma}_{c1} + \bar{\gamma}_{c2} - \sqrt{(\bar{\gamma}_{c1} + \bar{\gamma}_{c2})^2 - 4\bar{\gamma}_{c1}\bar{\gamma}_{c2}(1-\rho^2)}], \tag{2.15}$$

$$\Gamma_2 = \frac{1}{2}[\bar{\gamma}_{c1} + \bar{\gamma}_{c2} + \sqrt{(\bar{\gamma}_{c1} + \bar{\gamma}_{c2})^2 - 4\bar{\gamma}_{c1}\bar{\gamma}_{c2}(1-\rho^2)}], \tag{2.16}$$

ρ is the correlation coefficient,

$$\bar{\gamma}_{c1} = \frac{2E_s}{NRN_0}\sigma_{11}^2, \tag{2.17}$$

and

$$\bar{\gamma}_{c2} = \frac{2E_s}{NRN_0}\sigma_{21}^2, \tag{2.18}$$

are the instantaneous SNRs for the two channels, respectively. By letting $\bar{\gamma}_{c1} = \bar{\gamma}_{c2}$, i.e. a balanced fading channel, the result is the same as (2.13), as expected.

2.1.2.2 Rician Fading

For Rician fading, h_{ij} can be modeled as a complex Gaussian variable with means m_I and m_Q for the real and imaginary parts, respectively, and variance σ_{ij}^2 in each dimension. The complex covariances of the h_{ij} are given by the elements R_{kl} of the $MN \times MN$ covariance matrix defined in (2.6).

Again, as in [3], the distribution of γ_s is a Hermitian quadratic form distribution in complex Gaussian variates. Following the procedure in [3], the characteristic function of γ_s, which is defined as a Laplace transform of the PDF, is then

$$G_{\gamma_s}(s) = \frac{\exp\left(-s(\mathrm{E}[\mathbf{z}])^\dagger \left(\frac{1}{\bar{\gamma}_c}\mathbf{I} + s\mathbf{R}^*\right)^{-1} \mathrm{E}[\mathbf{z}]\right)}{|\mathbf{I} + s\bar{\gamma}_c\mathbf{R}^*|}. \tag{2.19}$$

Note that (2.19) equals (2.7) if $\mathrm{E}[\mathbf{z}] = 0$, i.e. a Rayleigh fading channel. The Laguerre-series expansion [42] of (2.19) can be used to perform the inverse Laplace transform to obtain the PDF of the instantaneous SNR γ_s.

2.1.2.3 Nakagami Fading

For Nakagami fading, the amplitude of the channel coefficient $\|h_{ij}\|$ for the ijth diversity path has a Nakagami distribution with variance σ_{ij}^2 in each dimension. The random variable $y = \|h_{ij}\|^2$ then has PDF

$$p(y) = \frac{m^m}{(2\sigma_{ij}^2)^m \Gamma(m)} y^{m-1} e^{-\frac{y}{2\sigma_{ij}^2}}, \tag{2.20}$$

which follows a chi-square distribution. Compared with the corresponding result for Rayleigh fading in [43], the PDF of y for Nakagami fading has the same form as the PDF for independent Rayleigh fading with m diversity, i.e. a single Nakagami fading channel is equivalent to an m diversity system for a Rayleigh fading channel. Therefore, a set of MN-variate Nakagami random variables is equivalent to a set of $2m$ independent Gaussian vectors where each vector has dimension MN and covariance matrix $\mathbf{R}$ [44]. The instantaneous SNR γ_s can then be written as

$$\gamma_s = \bar{\gamma}_c \sum_{i=1}^{N} \sum_{j=1}^{M} \|h_{ij}\|^2 = \bar{\gamma}_c \sum_{i=1}^{N} \sum_{j=1}^{M} \sum_{k=1}^{2m} a_{ijk}^2, \tag{2.21}$$

where a_{ijk}^2 is a Gaussian random variable with zero mean and unit variance. Again, we transform the distribution of γ_s to a Hermitian quadratic form distribution in complex Gaussian variates [45]. The joint PDF of the instantaneous SNR of each multipath signal γ_{ij} is then

$$p(\gamma_{11}, \ldots, \gamma_{MN}) = \frac{\exp\left(-\frac{1}{2}\sum_{i=1}^{2m} \mathbf{a}_i^T \mathbf{R}^{-1} \mathbf{a}_i\right)}{(2\pi)^{mMN} |\mathbf{R}|^m}, \tag{2.22}$$

where $\mathbf{a_i}$ is an independent random Gaussian vector with dimension MN. The characteristics function (CF) of γ_s is then

$$\begin{aligned} G_{\gamma_s}(s) &= \int_0^\infty p(\gamma_s) \exp(-s\gamma_s) d\gamma_s \\ &= \frac{1}{|\mathbf{I} + s\frac{\bar{\gamma}_c}{m}\mathbf{R}|^m} \end{aligned} \tag{2.23}$$

Note that a full rank covariance matrix is assumed in (2.23).

Assume the convariance matrix $\mathbf{R}$ has μ distinct nonzero eigenvalues, with the ith nonzero distinct eigenvalue denoted as λ_i, and repeated κ_i times. Then (2.23) can be written as

$$G_{\gamma_s}(s) = \frac{1}{\prod_{i=1}^{\mu} |1 + s\frac{\bar{\gamma}_c}{m}\lambda_i|^{m\kappa_i}}. \tag{2.24}$$

Using a partial fractions expansion [40], (2.24) becomes

$$G_{\gamma_s}(s) = \sum_{i=1}^{\mu}\sum_{j=1}^{m\kappa_i} \frac{D_{ij}}{\left(1 + s\frac{\bar{\gamma}_c}{m}\lambda_i\right)^j}. \tag{2.25}$$

where the coefficient D_{ij} is given as

$$D_{ij} = \frac{1}{(m\kappa_i - j)!\left(\frac{\bar{\gamma}_c}{m}\lambda_i\right)^{m\kappa_i - j}} \frac{\partial^{m\kappa_i - j}}{\partial s^{m\kappa_i - j}} \left[\left(1 + s\frac{\bar{\gamma}_c}{m}\lambda_i\right)^{m\kappa_i} G_{\gamma_s}(s)\right] |_{s=\frac{m}{\bar{\gamma}_c\lambda_i}} \tag{2.26}$$

An inverse Laplace transform will provide the PDF of γ_s. Utilizing the linearity of the Laplace transform, the PDF of γ_s is

$$p(\gamma_s) = \sum_{i=1}^{\mu}\sum_{j=1}^{m\kappa_i} D_{ij} \frac{\gamma_s^{j-1} e^{-\frac{m\gamma_s}{\bar{\gamma}_c\lambda_i}}}{\Gamma(j)\left(\frac{\bar{\gamma}_c}{m}\lambda_i\right)^j}. \tag{2.27}$$

Note that (2.27) coincides with (2.11) if $m = 1$, i.e. a Rayleigh fading channel.

As a special case, for constant correlation with correlation coefficient ρ, i.e. $R_{kl} = \rho$ for $k \neq l$, and balanced fading channels, i.e. $\sigma_j^2 = \sigma^2$, the covariance matrix will have two distinct eigenvalues $\lambda_1 = 2\sigma^2(1 + (M-1)\rho)$ and $\lambda_k = 2\sigma^2(1-\rho)$ for $k = 2, 3, \ldots, M$. The PDF of the instantaneous SNR γ_s from (2.27) is therefore

$$\begin{aligned} p(\gamma_s) &= \sum_{j=1}^{m} \frac{(-1)^{m-j}(mMN - j - 1)!(1 + (MN-1)\rho)^{m(MN-1)-j}(1-\rho)^{m-j}\gamma_s^{j-1}}{(m-j)!(m(MN-1)-1)!(MN\rho)^{mMN-j}(j-1)!(\frac{\bar{\gamma}_c}{m})^j} \\ &\times \exp\left(-\frac{m\gamma_s}{\bar{\gamma}_c(1 + (MN-1)\rho)}\right) \\ &+ \sum_{j=1}^{m(MN-1)} \frac{(-1)^{m}(mMN - j - 1)!(1 + (MN-1)\rho)^{m(MN-1)-j}(1-\rho)^{m-j}\gamma_s^{j-1}}{(m-1)!(m(MN-1)-j)!(MN\rho)^{mMN-j}(j-1)!(\frac{\bar{\gamma}_c}{m})^j} \\ &\times \exp\left(-\frac{m\gamma_s}{\bar{\gamma}_c(1-\rho)}\right). \end{aligned} \tag{2.28}$$

Note that (2.28) coincides with (2.12) if $m = 1$. More specifically, for STBC $\mathbf{G}_2$ with one receive antenna, the PDF of the instantaneous SNR γ_s from (2.28) is

$$p(\gamma_s) = \sum_{j=1}^{m} \frac{(2m-j-1)!(1+\rho)^{m-j}(1-\rho)^{m-j}\gamma_s^{j-1}}{(m-j)!(m-1)!(2\rho)^{2m-j}(j-1)!(\frac{\bar{\gamma}_c}{m})^j} \times \left[(-1)^{m-j}\exp\left(-\frac{m\gamma_s}{\bar{\gamma}_c(1+\rho)}\right) + (-1)^m \exp\left(-\frac{m\gamma_s}{\bar{\gamma}_c(1-\rho)}\right)\right]. \quad (2.29)$$

Note that (2.29) coincides with (2.12) if $m = 1$.

2.2 Capacity Analysis of STBC over Fading Channels

The capacity of a multiple antenna wireless system over a fading channel with continuous-valued inputs and continuous-valued outputs is given in [46] as

$$C = \mathrm{E}\left[\log_2 \det\left(\mathbf{I} + \frac{E_s}{NN_0}\mathbf{H}\mathbf{H}^\dagger\right)\right], \quad (2.30)$$

where E[.] is the expected value operator, $\mathbf{I}$ is an identity matrix with dimension M, det denotes the determinant of matrix $\mathbf{X}$, and the superscript † denotes matrix transpose and conjugate. The capacity of the equivalent STBC channel in (2.1) with continuous-valued inputs and continuous-valued outputs for complex signals is given in [43] as

$$\bar{C} = \mathrm{E}\left[R\log_2\left(1 + \frac{E_s}{RNN_0}\|\mathbf{H}\|_F^2\right)\right] = \mathrm{E}[R\log_2(1+\gamma_s)], \quad (2.31)$$

Given the PDF of γ_s, the capacity of the equivalent STBC channel can be obtained from

$$\bar{C} = R\int_0^\infty \log_2(1+\gamma_s)p(\gamma_s)d\gamma_s, \quad (2.32)$$

Monte Carlo simulation can be employed to evaluate (2.32). However, in the remainder of this section, closed form Shannon capacity expressions are derived for Rayleigh and Nakagami fading channels.

2.2.1 Shannon Capacity over Fading Channels

2.2.1.1 Rayleigh Fading

Substituting (2.11) into (2.32), the Shannon capacity for STBC over a Rayleigh fading channel is

$$\bar{C} = R\sum_{i=1}^{\mu}\sum_{j=1}^{\kappa_i}\int_0^{\infty} D_{ij}\frac{\log_2(1+\gamma_s)\gamma_s^{j-1}e^{-\frac{\gamma_s}{\bar{\gamma}_c\lambda_i}}}{\Gamma(j)(\bar{\gamma}_c\lambda_i)^j}d\gamma_s. \tag{2.33}$$

To evaluate the integral in (2.33), we employ the following integral function

$$\begin{aligned} f(\bar{\gamma}_c, n) &= \int_0^{\infty}\ln(1+\gamma_s)\gamma_s^n e^{-\frac{\gamma_s}{\bar{\gamma}_c}}d\bar{\gamma}_c \\ &= (-1)^{n-1}\bar{\gamma}_c e^{\frac{1}{\bar{\gamma}_c}}\mathrm{Ei}\left(-\frac{1}{\bar{\gamma}_c}\right) \\ &+ \sum_{k=1}^{n}\frac{n!}{(n-k)!}\left[\sum_{j=0}^{k}\sum_{i=0}^{j-k-1}\frac{(-1)^{n-k}}{(k-j)(k-j-i-1)!}\bar{\gamma}_c^{\,i+j+2}\right] \\ &+ \sum_{k=1}^{n}\frac{n!}{(n-k)!}\left[(-1)^{n-k-1}\bar{\gamma}_c^{\,k+1}e^{\frac{1}{\bar{\gamma}_c}}Ei\left(-\frac{1}{\bar{\gamma}_c}\right)\right]. \end{aligned} \tag{2.34}$$

The proof of (2.34) is given in Appendix A. Ei(.) denotes the exponent integral function. The closed form Shannon capacity for a STBC over a correlated Rayleigh fading channel is then

$$\bar{C} = R\sum_{i=1}^{\mu}\sum_{j=1}^{\kappa_i}\frac{D_{ij}\log_2(e)}{\Gamma(j)\left(\bar{\gamma}_c\lambda_i\right)^j}f\left(\bar{\gamma}_c\lambda_i, j-1\right). \tag{2.35}$$

Assuming constant correlation, the capacity can be obtained by substituting (2.12) into (2.32) giving

$$\begin{aligned} \bar{C} &= R\frac{D_{ij}\log_2(e)(1+(MN-1)\rho)^{MN-2}}{\bar{\gamma}_c\left(MN\rho\right)^{MN-1}}f\left(\bar{\gamma}_c(1+(MN-1)\rho), 1\right). \\ &- \sum_{i=1}^{MN-2}R\frac{D_{ij}\log_2(e)(1+(MN-1)\rho)^{MN-2-i}}{\bar{\gamma}_c^{i+1}(1-\rho)^i\Gamma(i+1)\left(MN\rho\right)^{MN-1-i}}f\left(\bar{\gamma}_c(1-\rho), i\right). \end{aligned} \tag{2.36}$$

Similarly, the Shannon capacity for STBC $\mathbf{G}_2$ with one receive antenna over a correlated Rayleigh fading channel can be obtained by substituting (2.13) into (2.32)

$$\bar{C} = R\log_2(e)\frac{f((1+\rho)\bar{\gamma}_c, 0) - f((1-\rho)\bar{\gamma}_c, 0)}{2\rho\bar{\gamma}_c}. \tag{2.37}$$

The corresponding Shannon capacity over an unbalanced correlated Rayleigh fading channel can be obtained by substituting (2.14) into (2.32)

$$\bar{C} = R\log_2(e)\frac{f(\Gamma_1, 0) - f(\Gamma_2, 0)}{\Gamma_1 - \Gamma_2}. \tag{2.38}$$

2.2.1.2 Nakagami Fading

Using (2.34), the closed form Shannon capacity over a correlated Nakagami fading channel is given by substituting (2.27) into (2.32)

$$\bar{C} = \sum_{i=1}^{\mu}\sum_{j=1}^{m\kappa_i} \frac{RD_{ij}\log_2(e)}{\Gamma(j)\left(\frac{\bar{\gamma}_c\lambda_i}{m}\right)^j} f\left(\frac{\bar{\gamma}_c\lambda_i}{m}, j-1\right). \tag{2.39}$$

The special case of constant correlated fading channels can be obtained by substituting (2.28) into (2.32)

$$\begin{aligned}
\bar{C} &= \sum_{j=1}^{m} \frac{(-1)^{m-j}(mMN-j-1)!(1+(MN-1)\rho)^{m(MN-1)-j}(1-\rho)^{m-j}\log_2(e)}{(m-j)!(m(MN-1)-1)!(MN\rho)^{mMN-j}(j-1)!(\frac{\bar{\gamma}_c}{m})^j} \\
&\times f\left(\frac{\bar{\gamma}_c(1+(MN-1)\rho)}{m}, j-1\right) \\
&+ \sum_{j=1}^{m(MN-1)} \frac{(-1)^{m}(mMN-j-1)!(1+(MN-1)\rho)^{m(MN-1)-j}(1-\rho)^{m-j}\log_2(e)}{(m-1)!(m(MN-1)-j)!(MN\rho)^{mMN-j}(j-1)!(\frac{\bar{\gamma}_c}{m})^j} \\
&\times f\left(\frac{\bar{\gamma}_c(1-\rho)}{m}, j-1\right).
\end{aligned} \tag{2.40}$$

By letting $MN = 2$, the corresponding capacity can be obtained for $\mathbf{G}_2$ over Nakagami fading channels with a constant correlation coefficient.

2.2.2 Capacity of q-ary Signal Constellations over Correlated Fading Channels

Both (2.30) and (2.31) were obtained assuming continuous-valued inputs. Here we consider modulation channels with discrete-valued multilevel/phase inputs and continuous-valued outputs. Assuming maximum likelihood (ML) soft decision decoding with perfect channel state information at the receiver, it is known [44][47][48] that the capacity $C^{\star}_{STBC}$ of the STBC channel (2.1) can be obtained by averaging the corresponding conditional capacity $\widetilde{C}^{\star}(\mathbf{H})$ with respect to the joint PDF of the channel matrix $\mathbf{H}$. By doing so, the following expression for the capacity of the fading channel is obtained

$$C^{\star}_{STBC} = \mathrm{E}\left[\widetilde{C}^{\star}(\mathbf{H})\right] = \int \widetilde{C}^{\star}(\mathbf{H}) p(\mathbf{H}) d\mathbf{H} \tag{2.41}$$

with

$$\begin{aligned} \widetilde{C}^{\star}(\mathbf{H}) &= R\log_2 q - \frac{R}{q}\sum_{j=1}^{q} \frac{R}{\pi(\|\mathbf{H}\|_F^2 N_0)} \int_{y\in C} \exp\left(-\frac{\|y - \frac{1}{R}\|\mathbf{H}\|_F^2 \alpha_j\|^2}{\frac{1}{R}\|\mathbf{H}\|_F^2 N_0}\right) \\ &\times \log_2\left[\frac{\sum_{s=1}^{q} \exp\left(\|y - \frac{1}{R}\|\mathbf{H}\|_F^2 \alpha_j\|^2 - \|y - \frac{1}{R}\|\mathbf{H}\|_F^2 \alpha_s\|^2\right)}{\frac{1}{R}\|\mathbf{H}\|_F^2 N_0}\right] dy, \end{aligned} \tag{2.42}$$

where α_j, $j = 1, \ldots, q$ is a real signal in the q-ary PAM constellation or a complex signal in the q-ary PSK/QAM constellation, and $p(\mathbf{H})$ is the joint PDF of the $M \times N$ random elements of the channel matrix $\mathbf{H}$ for the fading channel. Note that (2.41) applies to both real signal constellations such as PAM, and complex signal constellations such as PSK/QAM.

2.2.3 Capacity Comparison

It was shown in [29] that the difference between (2.30) and (2.31) is the capacity loss incurred by using a STBC in a MIMO fading channel with continued-valued inputs. The capacity of a MIMO fading channel with PAM/PSK/QAM modulation is given in [48] as

$$C^{\star}_{M,N} = \int \tilde{C}^{\star}_{M,N}(\mathbf{H}) p(\mathbf{H}) d\mathbf{H} \tag{2.43}$$

where

$$\begin{aligned} \tilde{C}^{\star}_{M,N}(\mathbf{H}) &= N \log_2 q - \left(\frac{1}{q}\right)^N \left(\frac{1}{\pi N_0}\right)^M \sum_{\mathbf{X} \in (A_{\mathbf{X}})^N} \int_{\mathbf{y} \in C} \exp\left(-\frac{\|\mathbf{y} - \mathbf{HX}\|^2}{N_0}\right) \\ &\times \log_2 \left[\sum_{\mathbf{X}' \in (A_{\mathbf{X}})^N} \exp\left(\frac{\|\mathbf{y} - \mathbf{HX}\|^2 - \|\mathbf{y} - \mathbf{HX}'\|^2}{N_0} \right) \right] d\mathbf{y}, \end{aligned} \tag{2.44}$$

and N and M are the number of transmit and receive antenna, respectively, $A_{\mathbf{X}} = \alpha_1, \ldots, \alpha_q$ is the q-ary complex signal constellation, $(A_{\mathbf{X}})^N$ is the N-fold Cartesian product of $A_{\mathbf{X}}$ with itself, the coded vector $\mathbf{X} = [x_1, \ldots, x_N] \in (A_{\mathbf{X}})^N$ is a q^N-variate random variable with outcomes taking values from the expanded signal constellation $(A_{\mathbf{X}})^N$, and $\mathbf{y} = [y_1, \ldots, y_M]^T$ is the M-dimensional output vector of the receive antennas.

It can easily be shown that the second terms in (2.42) and (2.44) vanish as the SNR increases, which implies that the capacity of a MIMO fading channel approaches $N \log_2 q$ bits/channel use while the capacity with STBC approaches only $R \log_2 q$ bits/channel use for large SNR. While the capacity loss of $(N - R) \log_2 q$ bits/channel use incurred by using a STBC is fairly significant, it will be shown that the SNR threshold for reliable data transmission is reduced because of the STBC diversity gain.

2.3 Extension to DS-CDMA Systems with STBC

There is great interest in the application of STBCs to practical wireless systems, such as GSM and CDMA. As part of the 3G UTRA (Universal Terrestrial Radio Access) FDD (Frequency Division Duplex) standard, space-time block codes have been proposed for use in the CDMA downlink to provide transmit diversity. In this section, we extend the results in the previous sections to the analysis of a STBC DS-CDMA downlink system

with correlated fading channels. The capacity is presented in this chapter while the error probability analysis will be derived in the next chapter.

2.3.1 Equivalent Channel Model

The system model is illustrated in Fig. 2.1. To facilitate the analysis, we generalize the CDMA multiple access interference model from [49][50] to accommodate multiple antennas. Without loss of generality, we assume the first user is the desired one. The equivalent channel model for STBC DS-CDMA is then

$$\hat{\mathbf{r}}_{1T} = \frac{1}{R}\sqrt{\frac{P_1}{2}}T_s\|\mathbf{H}\|_F^2\mathbf{b}_{1T} + \eta_T, \tag{2.45}$$

where $\hat{\mathbf{r}}_{1T}$ is the received signal of user 1 over T symbol durations, T_s is the symbol duration, $\mathbf{b}_{1T}$ is the encoded signal of user 1, η has zero mean and its variance is

$$\sigma_{\eta_T}^2 = \frac{1}{R}\|\mathbf{H}\|_F^2\left(N(N-1)\frac{T_s^2}{6G}\sum_{k=1}^{K}P_k + \frac{NN_0T_s}{4}\right), \tag{2.46}$$

G is the processing gain of the CDMA system, P_k is the power of user k, and K is the number of active users. Assuming perfect power control, i.e. $P_k = P$, the effective instantaneous SNR γ_s at the receiver is

$$\gamma_s = \frac{1}{\frac{N(N-1)K}{3G} + \frac{N}{2\frac{E_s}{N_0}}}\frac{1}{R}\|\mathbf{H}\|_F^2. \tag{2.47}$$

2.3.2 Capacity Analysis of DS-CDMA Systems with STBC

To facilitate the capacity analysis, we first normalize the equivalent channel by $\sqrt{\frac{T_s}{2}}$ so that (2.45) can be written in the same form as (2.1)

$$\mathbf{y}_{nT} = \frac{1}{R}\|\mathbf{H}\|_F^2\mathbf{X}_{nT} + \eta_{nT}, \tag{2.48}$$

where $\mathbf{X}_{nT}$ is the $S \times 1$ complex input matrix with each entry having symbol energy E_s, and η_{nT} has zero mean and variance

$$\sigma_{\eta_T}^2 = \frac{1}{R}\|\mathbf{H}\|_F^2 \left[N(N-1)K\frac{E_s}{3G} + \frac{NN_0}{2}\right]. \tag{2.49}$$

The Shannon capacity expressions for STBC CDMA over correlated Rayleigh and Nakagami fading channels can be obtained from (2.35) and (2.39), respectively, by defining

$$\bar{\gamma}_c = \frac{1}{\frac{N(N-1)K}{3G} + \frac{N}{2\frac{E_s}{N_0}}}\frac{1}{R}. \tag{2.50}$$

The capacity of the STBC CDMA system employing a q-ary signal constellation can be obtained directly from (2.41).

2.4 Numerical Results

In this section, some numerical results are presented based on our theoretical results to illustrate the capacity results obtained in this chapter. Simulation results fits well with the theoretical results.

Fig. 2.2 shows the Shannon capacity using STBC $\mathbf{G}_2$ over a correlated Rayleigh fading channel with one receive antenna. As discussed in [51], for the case of an equally spaced linear antenna array, if we assume a Gaussian model for the power correlation among the channels, the correlation coefficient is

$$\rho = \exp\left[-\frac{k}{2}(i-j)^2\left(\frac{d}{\lambda}\right)^2\right] \tag{2.51}$$

where $i, j = 1, \ldots, MN$, d is the physical distance between two adjacent antennas, and λ is the wavelength of the carrier frequency. The coefficient $k = 21.4$ [51]. This correlation model is also used in some of our other simulations to illustrate the relationship between the error probability and the separation distance between adjacent antennas. Results obtained using (2.37) and Monte Carlo simulation were identical, which verifies the analysis.

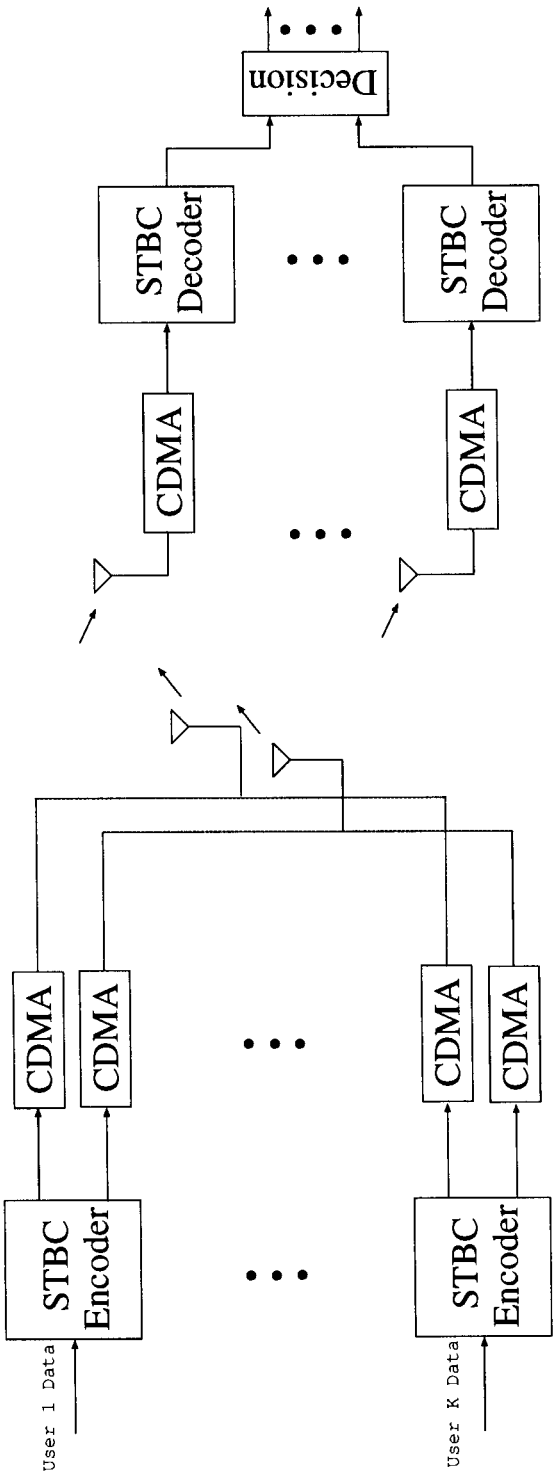

Figure 2.1. *A DS-CDMA System with STBC*

As shown in the figure, the capacity increases as the physical distance between the two adjacent antennas increases when the distance between adjacent antennas is less than half the wavelength. However, as long as the physical distance between two adjacent antennas is larger than half the wavelength, a further increase in the distance has no significant impact on the Shannon capacity. Given this fact, we can conclude that as long as the physical distance between two adjacent antennas is larger than half the wavelength, the fading channels can be considered independent. Fig. 2.3 gives simulation results of the outage capacity using STBC $\mathbf{G}_2$ over a correlated Rayleigh fading channel with one receive antenna.

The capacity of STBC $\mathbf{G}_2$ over a correlated Rician fading channel with one receive antenna and BPSK modulation is given in Fig. 2.4. The Rician parameter in this case is 10 dB. Different correlation coefficients were investigated. This figure shows that for the same capacity, there is approximately a 3-4 dB advantage with independent Rician fading, i.e. $\rho = 0$, over complete correlation, i.e. $\rho = 1$. The capacity of STBC $\mathbf{G}_2$ over a correlated Rician fading channel with one receive antenna and BPSK modulation is given in Fig. 2.5 with the Rician parameter set to 0 dB, i.e. 1. Again, there is approximately a 3-4 dB advantage with independent Rician fading, i.e. $\rho = 0$, over complete correlation, i.e. $\rho = 1$, to achieve same capacity. Comparing Fig. 2.4 and Fig. 2.5, we find that to achieve capacity, an additional 5 dB in SNR is required when the Rician parameter is 10 dB versus the case when the Rician parameter = 0 dB.

The channel capacity of a DS-CDMA system employing STBC $\mathbf{G}_2$ with one receive antenna for BPSK modulation over a correlated Rayleigh fading channel is shown in Fig. 2.6 with the processing gain set to 32. Both single user and multiple user environments are presented with 1 and 30 users, respectively. Again, the capacity increases as the physical distance between two adjacent antennas increases when this distance is less than half the carrier wavelength. When the physical distance between two adjacent antennas is larger than half the carrier wavelength, the fading channels can be considered independent. Note that the capacity is limited by the number of users active in the system. With more than one active user, the system cannot achieve the theoretical channel capacity. As shown in

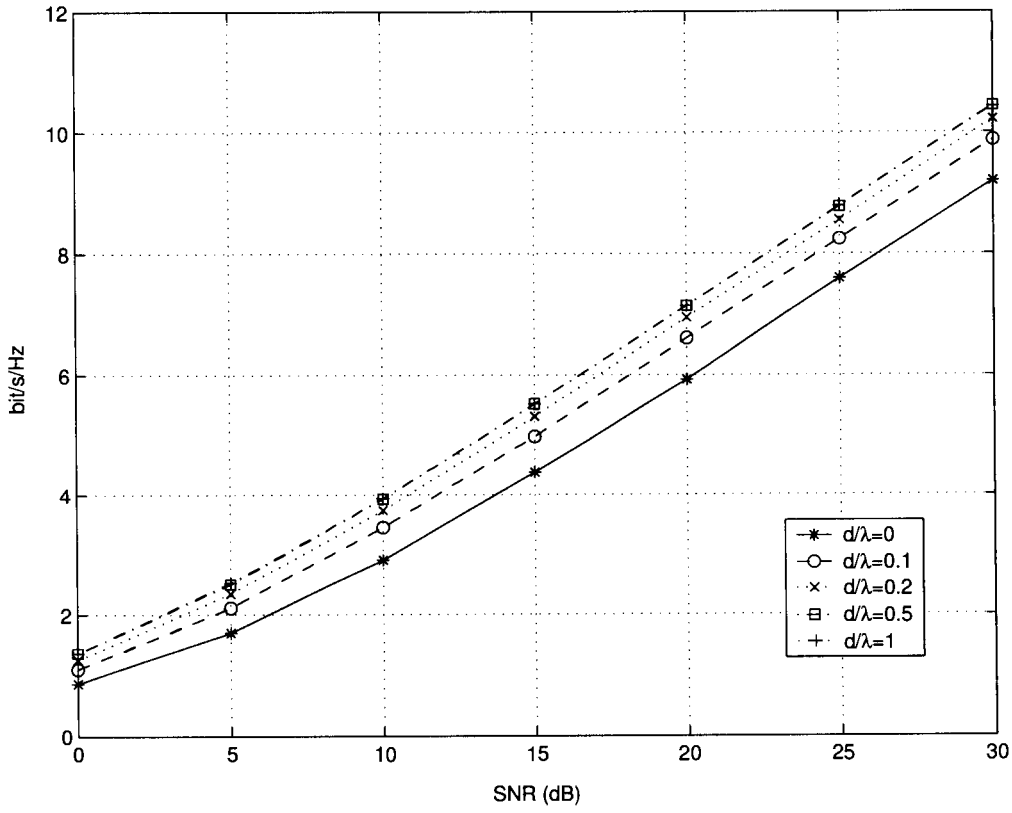

Figure 2.2. *Shannon capacity for STBC* $\mathbf{G}_2$ *with one receive antenna in a correlated Rayleigh fading channel.*

the figure, with 30 synchronous users active in the network, the achievable capacity is 0.75 bits/s/Hz. Thus there is a capacity loss of 25% due to MAI.

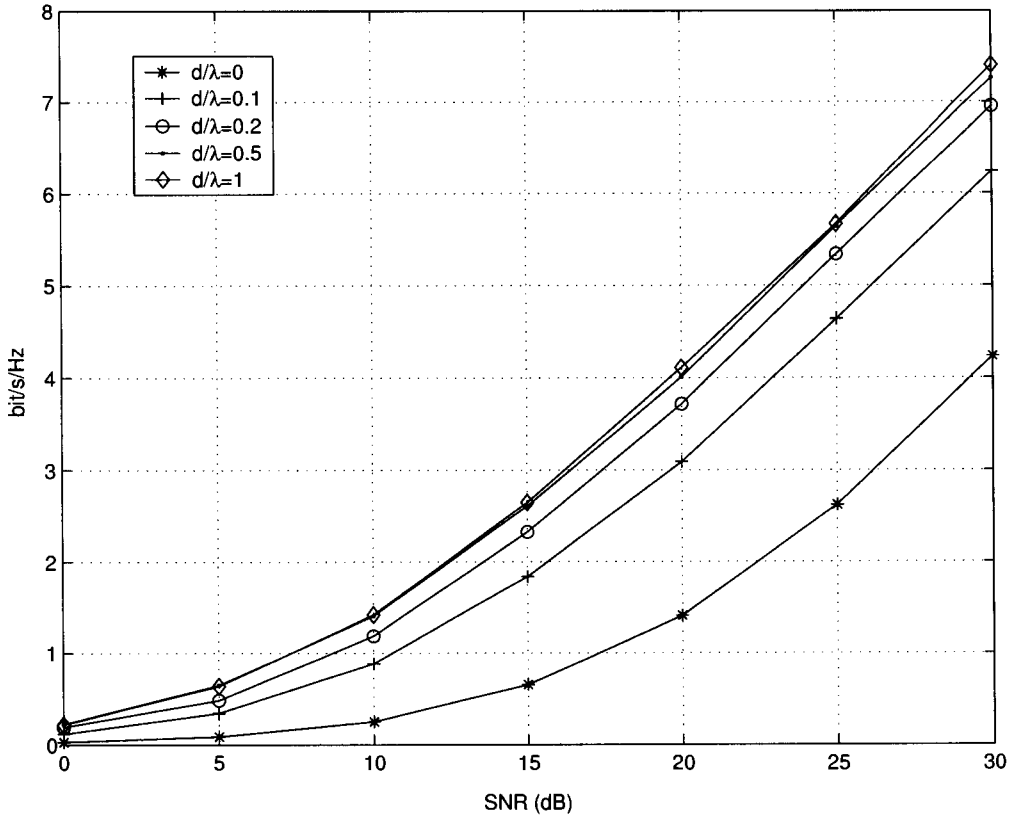

Figure 2.3. *Outage capacity for STBC* $\mathbf{G}_2$ *with one receive antenna in a correlated Rayleigh fading channel.*

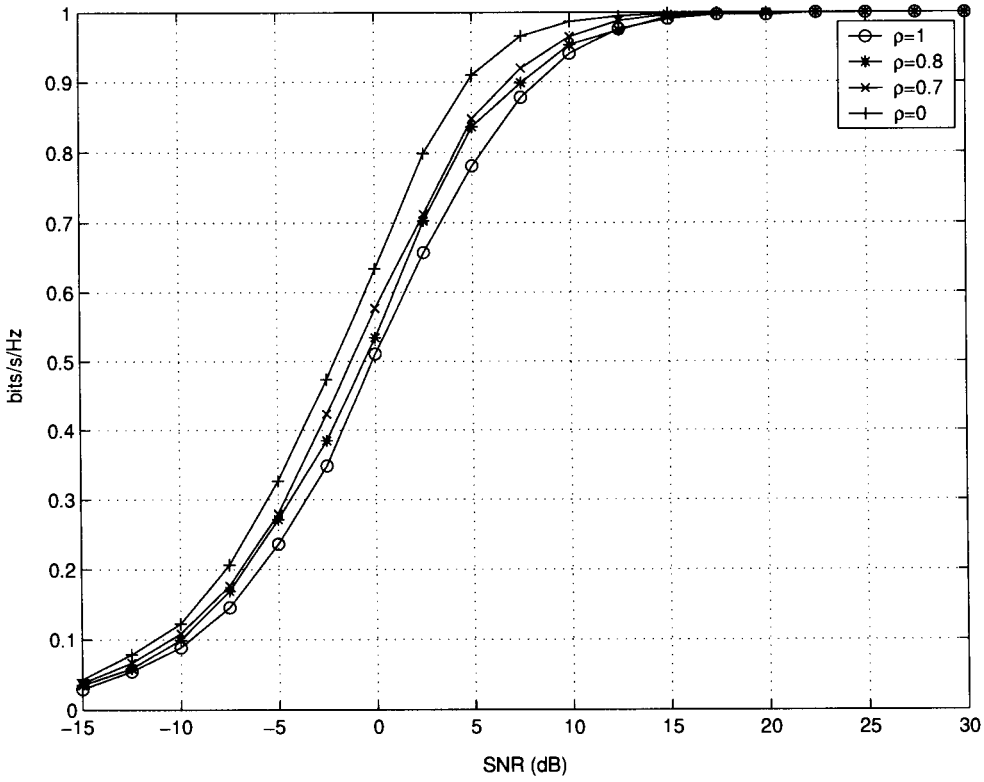

Figure 2.4. *Channel capacity of STBC* $\mathbf{G}_2$ *with BPSK over a correlated Rician fading channel with one receive antenna, Rician parameter=0 dB.*

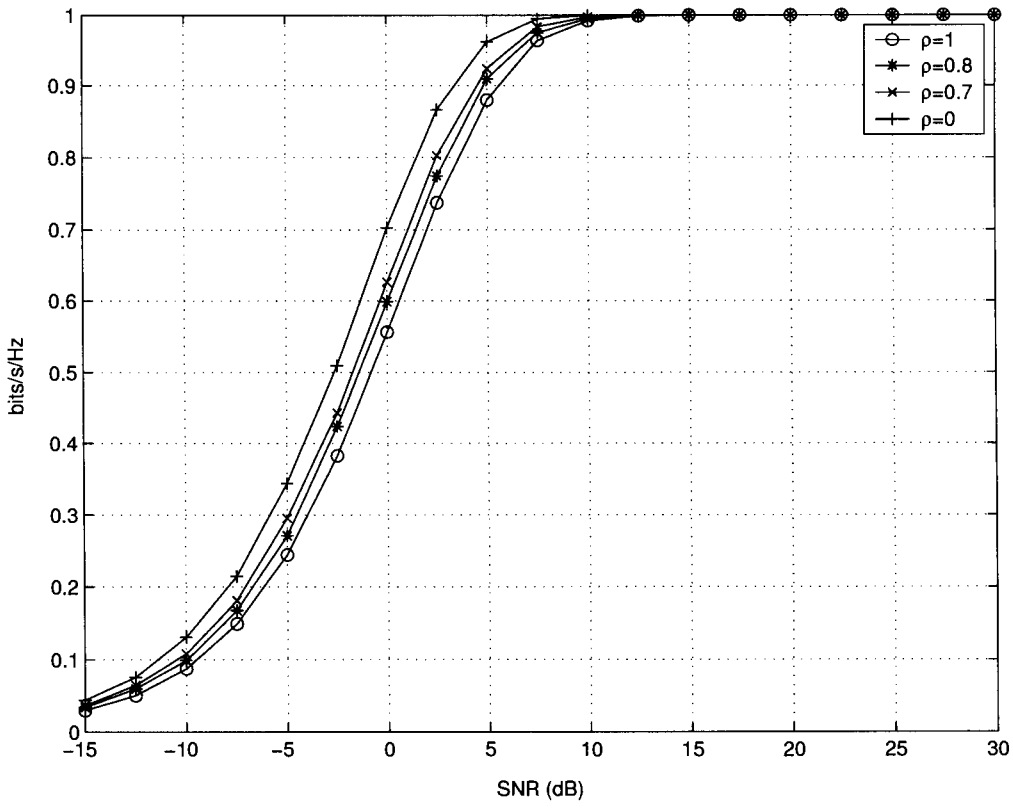

Figure 2.5. *Channel capacity of STBC* $\mathbf{G}_2$ *with BPSK over a correlated Rician fading channel with one receive antenna, Rician parameter=10 dB.*

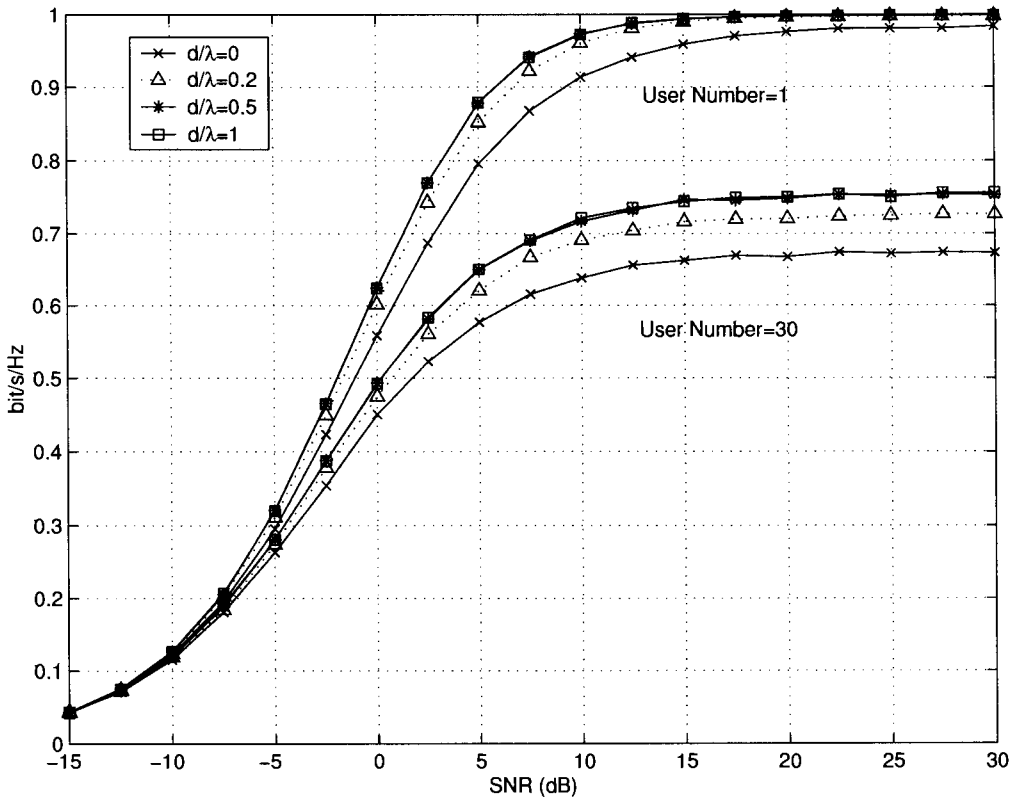

Figure 2.6. *Channel capacity of a DS-CDMA system with STBC* $\mathbf{G}_2$ *and BPSK over a correlated Rayleigh fading channel with one receive antenna, G=32.*

Chapter 3

Error Probability of STBC over Correlated Fading Channels

In this chapter, we analyze the error probability of STBC for PAM/PSK/QAM modulation from an SNR perspective based on the equivalent channel induced by the STBC over correlated fading channels. Using the PDF of the SNR, symbol error probabilities are given for various combinations of modulation and fading channels.

3.1 Error Probability with Correlated Rayleigh Fading

Let $P_q(\gamma_s)$ denote the error probability of a q-ary signal constellation with STBC in an AWGN channel. The error probability of STBC with correlated Rayleigh fading can be obtained by averaging $P_q(\gamma_s)$ over the PDF of γ_s

$$P_{STBC,q} = \int_0^\infty P_q(\gamma_s)p(\gamma_s)d\gamma_s. \tag{3.1}$$

Note that $P_q(\gamma_s)$ can be symbol error probability (SEP) or bit error probability (BEP).

3.1.1 Probability of Error for PAM

Since full rate STBCs exist for any number of transmit antennas using a real PAM constellation [9], we assume $R = 1$ for q-ary PAM. The average SEP for PAM over an AWGN

channel is [1]

$$P_q(\gamma_s) = 2\left(1-\frac{1}{q}\right)\mathrm{Q}\left(\sqrt{\frac{6}{q^2-1}\gamma_s}\right). \tag{3.2}$$

where Q(.) is the Gaussian tail function. Substituting (2.11) and (3.2) into (2.23), the average SEP of PAM with STBC is

$$P_{STBC,PAM,q} = \int_0^\infty 2\left(1-\frac{1}{q}\right)\mathrm{Q}\left(\sqrt{\frac{6}{q^2-1}\gamma_s}\right)\sum_{i=1}^{\mu}\sum_{j=1}^{\kappa_i} D_{ij}\frac{\gamma_s^{j-1}e^{-\frac{\gamma_s}{\bar{\gamma}_c\lambda_i}}}{\Gamma(j)\,(\bar{\gamma}_c\lambda_i)^j}d\gamma_s. \tag{3.3}$$

To evaluate the integral in (3.3), the following integral function was used:

$$f(L) = \int_0^\infty Q(\sqrt{ax})x^{l-1}e^{-\frac{x}{u}}dx = \frac{1}{2}u^L\Gamma(L)\left[1-\sum_{k=0}^{L-1} z\left(\frac{1-z^2}{4}\right)^k\binom{2k}{k}\right] \tag{3.4}$$

where

$$z = \sqrt{\frac{au}{2+au}}. \tag{3.5}$$

Based on (3.4), the closed-form symbol error probability for PAM with STBC is then

$$P_{STBC,PAM,q}(\gamma_s) = \sum_{i=1}^{\mu}\sum_{j=1}^{\kappa_i} D_{ij}(1-\frac{1}{q})\frac{1}{\Gamma(j)(\bar{\gamma}_c\lambda_i)^j}\left[1-\sum_{k=0}^{j-1} u_i\left(\frac{1-u_i^2}{4}\right)^k\binom{2k}{k}\right] \tag{3.6}$$

where

$$u_i = \sqrt{\frac{3\bar{\gamma}_c\lambda_i}{q^2-1+3\bar{\gamma}_c\lambda_i}}. \tag{3.7}$$

3.1.2 Probability of Error for PSK

It is well known [1] that the BEP of BPSK and QPSK over an AWGN channel are

$$P_{BPSK}(\gamma_s) = \mathrm{Q}(\sqrt{2\gamma_s}), \tag{3.8}$$

and

$$P_{QPSK}(\gamma_s) = \mathrm{Q}(\sqrt{\gamma_s}), \tag{3.9}$$

respectively. As shown in [52], the exact symbol error probability of q-ary PSK for an AWGN channel is

$$P_{PSK,AWGN,q}(\gamma_s) = 2\mathrm{Q}\left(\sqrt{2\gamma_s}, \sin\frac{\pi}{q}\right) - \frac{1}{\pi}\int_{\frac{\pi}{2}-\frac{\pi}{q}}^{\frac{\pi}{2}} e^{-\gamma_s \frac{\sin^2\frac{\pi}{q}}{\cos^2\theta}} d\theta. \tag{3.10}$$

For large SNR and large values of q, the SEP of q-ary PSK in an AWGN channel can be approximated as

$$P_q(\gamma_s) \approx 2\mathrm{Q}\left(\sqrt{2\gamma_s}, \sin\frac{\pi}{q}\right). \tag{3.11}$$

and the equivalent BEP is

$$P_{qb} \approx \frac{1}{\log q} P_q. \tag{3.12}$$

where Gray coding is assumed. This approximation is good for large values of q, however for $q = 2$ there is a factor of 2 difference with the exact probability given in (3.8).

By substituting for $P_q(\gamma_s)$ in (3.11) and using (3.4), (3.1) can be written as

$$P_{STBC,PAM,q}(\gamma_s) \approx \sum_{i=1}^{\mu}\sum_{j=1}^{\kappa_i} D_{ij}\left[1 - \sum_{k=0}^{j-1} u_i \left(\frac{1-u_i^2}{4}\right)^k \binom{2k}{k}\right] \tag{3.13}$$

where

$$u_i = \sqrt{\frac{\sin^2\frac{\pi}{q}\bar{\gamma}_c\lambda_i}{1+\sin^2\frac{\pi}{q}\bar{\gamma}_c\lambda_i}} \tag{3.14}$$

Therefore, the BEP can be approximated as

$$P_{STBC,PSK,qb}(\gamma_s) \approx \frac{1}{\log q}\sum_{i=1}^{\mu}\sum_{j=1}^{\kappa_i} D_{ij}\left[1 - \sum_{k=0}^{j-1} u_i \left(\frac{1-u_i^2}{4}\right)^k \binom{2k}{k}\right] \tag{3.15}$$

By substituting for $P_q(\gamma_s)$ in (3.8) and (3.9), and using (2.26), the exact bit error probability for BPSK and QPSK can be derived from (3.1) as

$$P_{STBC,PSK,q}(\gamma_s) = \frac{1}{2}\sum_{i=1}^{\mu}\sum_{j=1}^{\kappa_i} D_{ij}\left[1 - \sum_{k=0}^{j-1} u_i \left(\frac{1-u_i^2}{4}\right)^k \binom{2k}{k}\right] \tag{3.16}$$

where

$$u_i = \sqrt{\frac{\bar{\gamma}_c\lambda_i}{1+\bar{\gamma}_c\lambda_i}} \tag{3.17}$$

for BPSK and

$$u_i = \sqrt{\frac{\bar{\gamma}_c\lambda_i}{2+\bar{\gamma}_c\lambda_i}} \tag{3.18}$$

for QPSK. Note that

$$\bar{\gamma}_c = \frac{E_s}{2NRN_0} \tag{3.19}$$

for QPSK.

3.1.3 Probability of Error for QAM

Rectangular QAM signal constellations are frequently employed because they can be considered as two PAM signals on quadrature carriers. For q-ary, $q = 2^k$ (k even), rectangular QAM, the symbol error probability is given in [1] as

$$P_q = 1 - \left(1 - P_{\sqrt{q}}\right)^2, \tag{3.20}$$

where

$$P_{\sqrt{q}} = 2\left(1 - \frac{1}{\sqrt{q}}\right) \mathrm{Q}\left(\sqrt{\frac{1}{q-1}\gamma_s}\right). \tag{3.21}$$

By substituting for $P_q(\gamma_s)$ in (3.21), (3.1) can be written as

$$P_{STBC,PAM,\sqrt{q}} = \int_0^\infty 2\left(1-\frac{1}{\sqrt{q}}\right) \mathrm{Q}\left(\sqrt{\frac{1}{q-1}\gamma_s}\right) \sum_{i=1}^{\mu}\sum_{j=1}^{\kappa_i} D_{ij} \frac{\gamma_s^{j-1} e^{-\frac{\gamma_s}{\bar{\gamma}_c\lambda_i}}}{\Gamma(j)\,(\bar{\gamma}_c\lambda_i)^j} d\gamma_s. \quad (3.22)$$

Using (3.4), the closed-form symbol error probability for rectangular q-ary QAM with STBC is then

$$P_{STBC,QAM,q} = (1 - P_{STBC,PAM,\sqrt{q}})^2, \quad (3.23)$$

where

$$P_{STBC,PSK,qb}(\gamma_s) = \sum_{i=1}^{\mu}\sum_{j=1}^{\kappa_i} D_{ij}(1-\frac{1}{\sqrt{q}}) \left[1 - \sum_{k=0}^{j-1} u_i \left(\frac{1-u_i^2}{4}\right)^k \binom{2k}{k}\right] \quad (3.24)$$

and for $\sqrt{q}$-ary PAM in q-ary rectangular QAM

$$u_i = \sqrt{\frac{3\bar{\gamma}_c\lambda_i}{2\mathbf{q} - 2 + 3\bar{\gamma}_c\lambda_i}}. \quad (3.25)$$

Derivation of the closed form SEP for special cases like constant correlation, and STBC $\mathbf{G}_2$ with one receive antenna over balanced or unbalanced fading channels, is straightforward.

3.2 Error Probability with Nakagami Fading

Following the same procedure as in the previous sections, the error probability over Nakagami fading can be obtained from the results for Rayleigh fading by increasing the diversity order. The SEP for STBC over a correlated Nakagami fading channel is then

$$P_{STBC,PSK,q}(\gamma_s) = \xi \sum_{i=1}^{q}\sum_{j=1}^{m\kappa_i} D_{ij} \left[1 - \sum_{k=0}^{j-1} u_i \left(\frac{1-u_i^2}{4}\right)^k \binom{2k}{k}\right] \quad (3.26)$$

where, for q-ary PAM

$$u_i = \sqrt{\frac{3\bar{\gamma}_c\lambda_i}{m(q^2-1)+3\bar{\gamma}_c\lambda_i}}, \tag{3.27}$$

and $\xi = 1 - \frac{1}{q}$, for q-ary PSK

$$u_i = \sqrt{\frac{\sin^2\frac{\pi}{q}\bar{\gamma}_c\lambda_i}{m+\sin^2\frac{\pi}{q}\bar{\gamma}_c\lambda_i}} \tag{3.28}$$

and with $\xi = \frac{1}{2}$ for $q = 2$ and $\xi = 1$ for $q > 2$, and for $\sqrt{q}$-ary PAM in q-ary rectangular QAM

$$u_i = \sqrt{\frac{3\bar{\gamma}_c\lambda_i}{2m(\mathbf{q}-1)+3\bar{\gamma}_c\lambda_i}} \tag{3.29}$$

and $\xi = 1 - \frac{1}{\sqrt{q}}$. The SEP of q-ary rectangular QAM can then be calculated from (3.23). Again, the derivation of the closed form error probabilities expressions for the special cases is straightforward.

3.3 A Unified Approach to the Error Probability on Correlated Fading Channels

In the previous sections, the error probabilities of PAM/PSK/QAM modulation with correlated Rayleigh and Nakagami fading channels were obtained. Closed form expressions were derived based on the integral function (3.4). However, as stated above, applying the same approach to correlated Rician fading channels involves significant difficulty due to the exponential component of the characteristic function. Though one can perform a Laguerre-series expansion to transform the PDF into the desired form, the coefficients of the expanded terms are very complex as they involve the Laguerre polynomial. In this section, we introduce a unified approach to the error probability analysis [4] over correlated Rician fading channels based on the characteristic function of the instantaneous SNR γ_s. A simple error probability expression is obtained utilizing an integral transformation of the

Gaussian tail function. Though numerical integration is required for the error probability evaluation, this approach is more tractable than using Laguerre-series. Furthermore, the approach can easily be extended to correlated Nakagami fading channels. The error probability for correlated Rayleigh fading channels can also be obtained from both the Rician and Nakagami fading channel expressions as a special case.

To facilitate the error probability analysis, we first write the Gaussian tail function in the following form [4]

$$\mathrm{Q}(\sqrt{ax}) = \frac{1}{\pi}\int_0^{\frac{\pi}{2}} \exp\left(-\frac{ax}{2\sin^2\phi}\right) d\phi \tag{3.30}$$

Then we have

$$\begin{aligned} P &= \int_0^{\infty} \mathrm{Q}(\sqrt{a\gamma_s})p(\gamma_s)d\gamma_s \\ &= \frac{1}{\pi}\int_0^{\infty}\int_0^{\frac{\pi}{2}} \exp\left(-\frac{a\gamma_s}{2\sin^2\phi}\right) p(\gamma_s)d\phi d\gamma_s \\ &= \frac{1}{\pi}\int_0^{\frac{\pi}{2}} G_{\gamma_s}\left(\frac{ax}{2\sin^2\phi}\right) d\phi \end{aligned} \tag{3.31}$$

and the STBC SEP over a correlated Rician fading channel is

$$P_{STBC,Rician,q} = \frac{\xi}{\pi}\int_0^{\frac{\pi}{2}} \frac{\exp\left[-\frac{a\gamma_s}{2\sin^2\phi}(\mathrm{E}[\mathbf{z}])^{\dagger}\left(\frac{1}{\bar{\gamma}_c}\mathbf{I} + \frac{a\gamma_s}{2\sin^2\phi}\mathbf{R}^*\right)^{-1}\mathrm{E}[\mathbf{z}]\right]}{|\mathbf{I} + \frac{a\gamma_s}{2\sin^2\phi}\bar{\gamma}_c\mathbf{R}^*|} d\phi \tag{3.32}$$

where, for q-ary PAM $a = \sqrt{\frac{6}{q^2-1}}$ and $\xi = 2(1-\frac{1}{q})$; for q-ary PSK $a = 2\sin^2\frac{\pi}{q}$ and $\xi = 1$ for $q = 2$ and $\xi = 2$ for $q > 2$; and for $\sqrt{q}$-ary PAM in q-ary rectangular QAM $a = \frac{2}{q-1}$ and $\xi = 2(1-\frac{1}{\sqrt{q}})$; The SEP of q-ary rectangular QAM can then be calculated from (3.23).

Similarly, the STBC SEP over a correlated Nakagami fading channel is

$$P_{STBC,Nakagami,q} = \frac{\xi}{\pi}\int_0^{\frac{\pi}{2}} \frac{1}{|\mathbf{I} + \frac{a\gamma_s}{2\sin^2\phi}\bar{\gamma}_c\mathbf{R}^*|^m} d\phi \tag{3.33}$$

where, for q-ary PAM $a = \sqrt{\frac{6}{q^2-1}}$ and $\xi = 2(1-\frac{1}{q})$; for q-ary PSK $a = 2\sin^2\frac{\pi}{q}$ and $xi = 1$ for $q = 2$ and $\xi = 2$ for $q > 2$; and for $\sqrt{q}$-ary PAM in q-ary rectangular QAM $a = \frac{2}{q-1}$ and $\xi = 2(1-\frac{1}{\sqrt{q}})$;

The SEP of q-ary rectangular QAM can then be calculated from (3.24). Note that (3.32) and (3.33) coincide in the Rayleigh fading case, i.e. $\mathrm{E}[\mathbf{z}] = 0$ and $m = 1$, respectively. For noncoherent detection of binary signals in an AWGN channel, the error probability with an optimum matched filter receiver is given by

$$P(\gamma_s) = \frac{1}{2}\exp(-\gamma_s), \tag{3.34}$$

for DPSK. In this case, the error probability of STBC with binary DPSK over correlated fading channels can be obtained from (3.1) as

$$\begin{aligned} P_{STBC} &= \int_0^\infty \frac{1}{2}\exp(-a\gamma_s)p(\gamma_s)d\gamma_s \\ &= \frac{1}{2}G_{\gamma_s}(a). \end{aligned} \tag{3.35}$$

3.4 Extension to DS-CDMA System with STBC

Based on the results in Chapter 2, the error probability results in the previous sections for correlated fading channels can be directly applied to the STBC DS-CDMA case. In particular, the exact BEP of BPSK is given by

$$P_{STBC,PSK,q}(\gamma_s) = \frac{1}{2}\sum_{i=1}^{\mu}\sum_{j=1}^{\kappa_i} D_{ij}\left[1 - \sum_{k=0}^{j-1} u_i\left(\frac{1-u_i^2}{4}\right)^k \binom{2k}{k}\right] \tag{3.36}$$

where $u_i = \sqrt{\frac{\bar{\gamma}_c\lambda_i}{1+\bar{\gamma}_c\lambda_i}}$ for Rayleigh fading;

$$P_{STBC,Rician,q} = \frac{1}{\pi}\int_0^{\frac{\pi}{2}} \frac{\exp\left[-\frac{a}{2\sin^2\phi}(E[\mathbf{z}])^\dagger\left(\frac{1}{\bar{\gamma}_c}\mathbf{I} + \frac{a}{2\sin^2\phi}\mathbf{R}^*\right)^{-1}E[\mathbf{z}]\right]}{|\mathbf{I} + \frac{a}{2\sin^2\phi}\bar{\gamma}_c\mathbf{R}^*|}d\phi \tag{3.37}$$

for Rician fading where $a = 2$; and

$$P_{STBC,PSK,q}(\gamma_s) = \frac{1}{2}\sum_{i=1}^{q}\sum_{j=1}^{m\kappa_i} D_{ij}\left[1 - \sum_{k=0}^{j-1} u_i \left(\frac{1-u_i^2}{4}\right)^k \binom{2k}{k}\right] \tag{3.38}$$

for Nakagami fading, where

$$u_i = \sqrt{\frac{\bar{\gamma}_c \lambda_i}{m + \bar{\gamma}_c \lambda_i}}, \tag{3.39}$$

and $\bar{\gamma}_c$ is given in (2.50). Note that there are two factors in $\bar{\gamma}_c$ which determine the BEP of the system, $\frac{N(N-1)K}{3G}$ and $\frac{N}{2E_s/N_0}$. The first term corresponds to the MAI from other users and the self-interference from different transmit antennas. The second term corresponds to the system noise (AWGN). For large SNR, $\bar{\gamma}_c$ will be dominated by the MAI, i.e., the number of users limits the performance, as expected.

3.5 Numerical Results

In this part of the thesis, we give the theoretical results obtained in this chapter. Simulation was performed and verified the exact closed form error probability expressions.

In Fig. 3.1, the bit error probability of BPSK with STBC $\mathbf{G}_2$ and one receive antenna is presented for correlated Nakagami fading with $m = 1$, i.e. Rayleigh fading. This shows that the simulation results are identical to those obtained using (3.16). There is approximately a 12dB gain in SNR with independent fading channels over the fully correlated case at a BER of 10^{-3}.

In Fig. 3.2, the bit error probability of BPSK with STBC $\mathbf{G}_2$ and one receive antennas is presented for correlated Nakagami fading with $m = 2$. Again, the simulation results match perfectly with those obtained using (3.26). There is approximately an 8 dB gain in SNR with independent fading channels over the fully correlated case at a BER of 10^{-5}. Comparing Fig. 3.1 and Fig. 3.2, it is interesting to note that the fully correlated Nakagami-2 fading channel has the same performance as the independent Rayleigh fading channel, i.e. a Nakagami-1 fading channel.

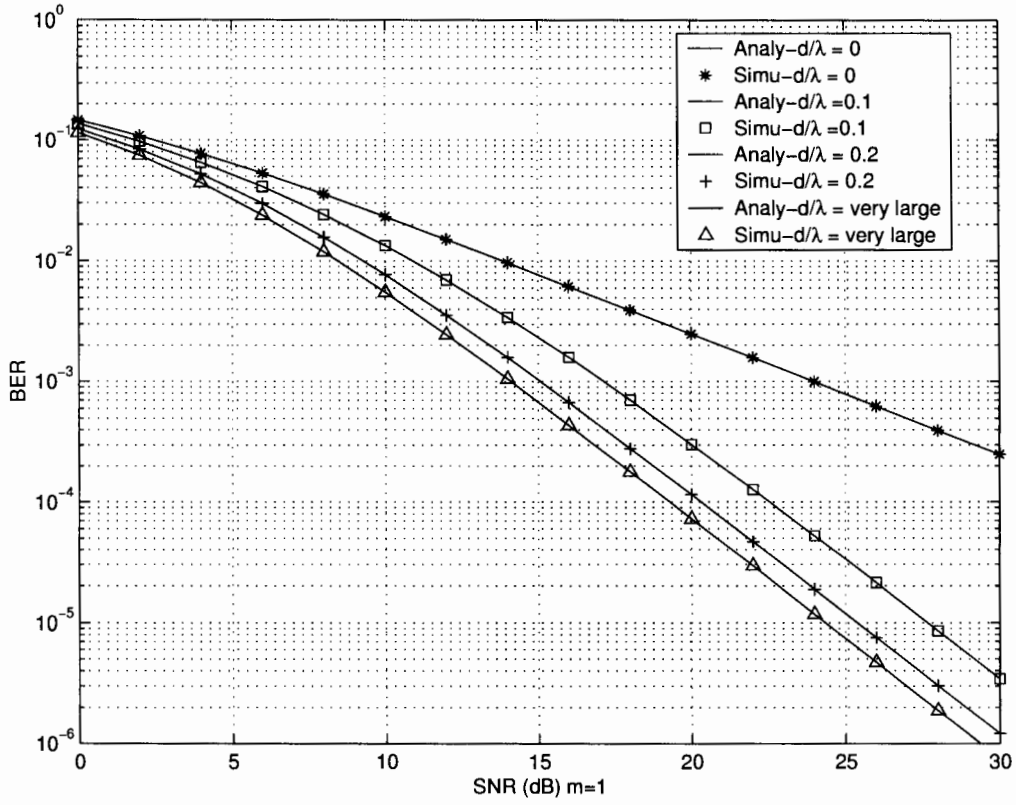

Figure 3.1. *Bit error probability of* $\mathbf{G}_2$ *code with BPSK for STBC with one receive antenna over correlated Nakagami (m=1, i.e. Rayleigh) fading channels.*

Fig. 3.3 presents the BER of STBC $\mathbf{G}_2$ with BPSK and one receive antenna over correlated Rician fading channels. This shows that as the Rician parameter increases, the channel approaches AWGN, which explains why the correlation has almost no impact on the performance when the Rician parameter is set to 100 dB, i.e. the channel is almost Gaussian. In Fig. 3.4, the bit error probability of QPSK with STBC $\mathbf{G}_2$ and one receive antennas is presented for correlated Rician channel.

Fig. 3.5 shows the SER of STBCs $\mathbf{G}_3$, $\mathbf{G}_4$, $\mathbf{H}_3$ and $\mathbf{H}_4$ with QPSK and two receive antennas over correlated Nakagami fading channels, with $m = 2$.

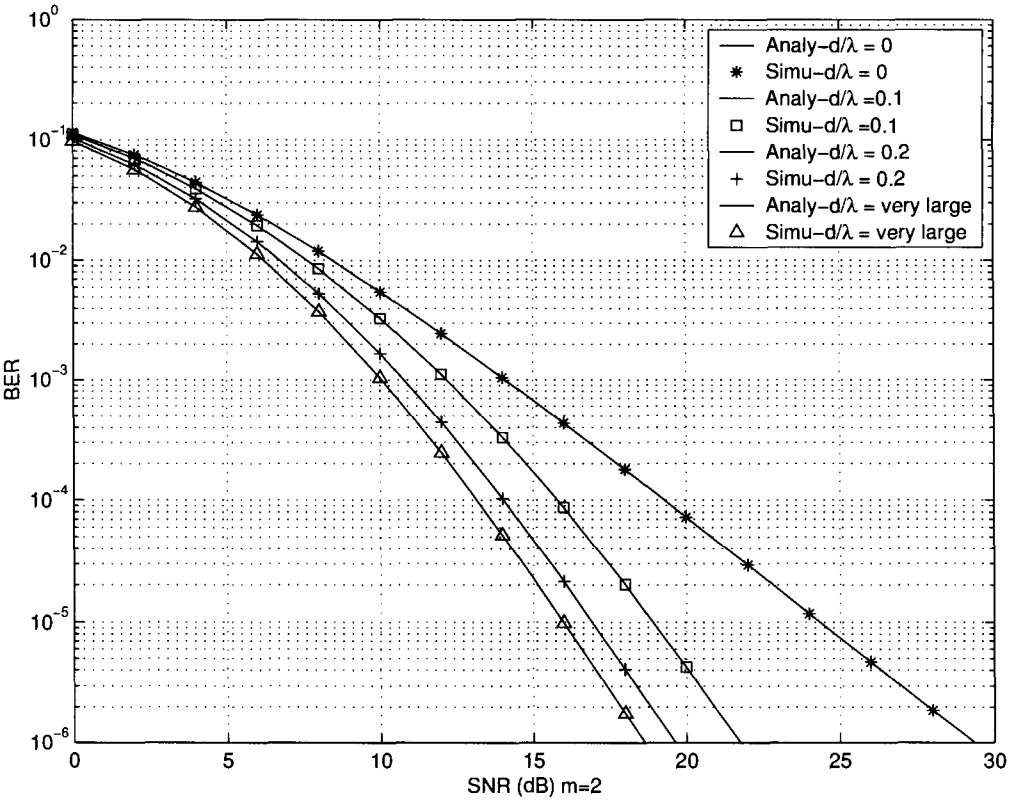

Figure 3.2. *Bit error probability of* $\mathbf{G}_2$ *code with BPSK for STBC with one receive antenna over correlated Nakagami (m=2) fading channels.*

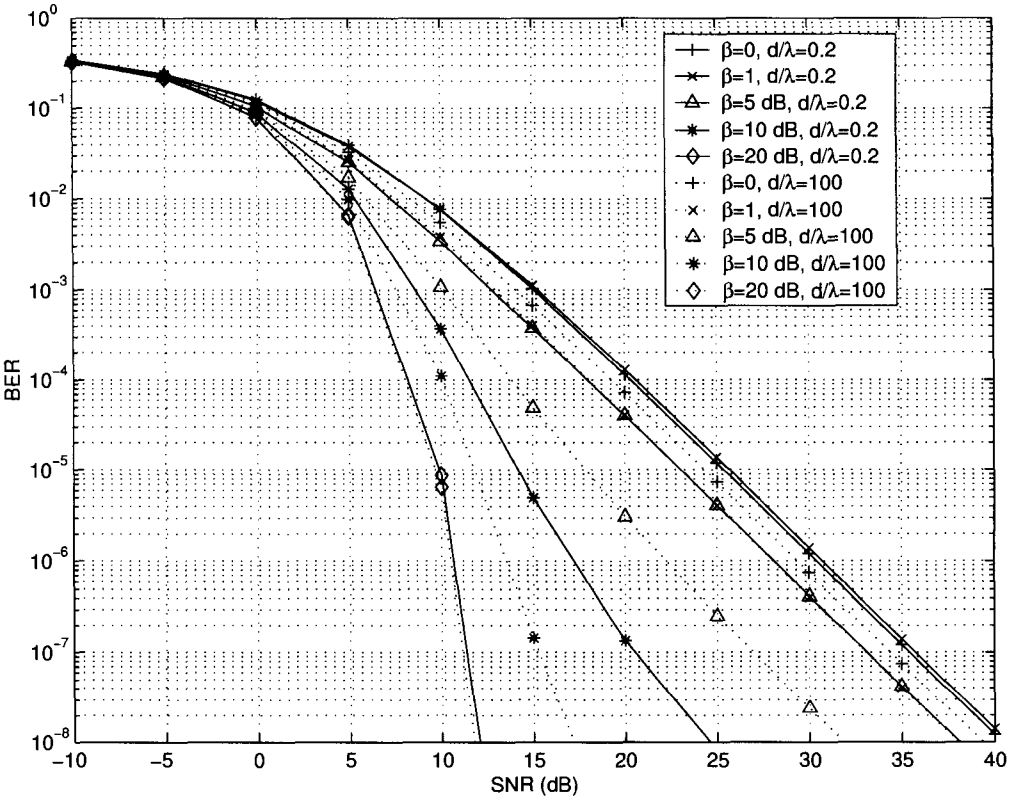

Figure 3.3. *Symbol error probability of STBC* $\mathbf{G}_2$ *BPSK and one receive antenna over a correlated Rician fading channel.*

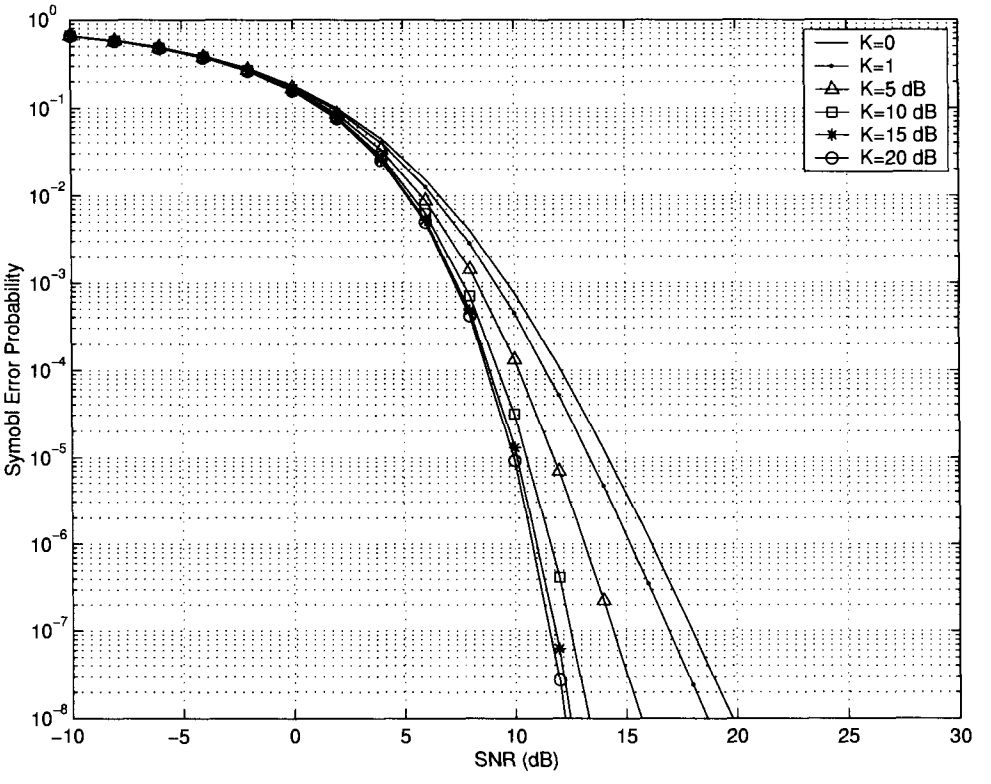

Figure 3.4. *Symbol error probability of STBC* $\mathbf{G}_2$ *QPSK over a correlated Rician fading channel.*

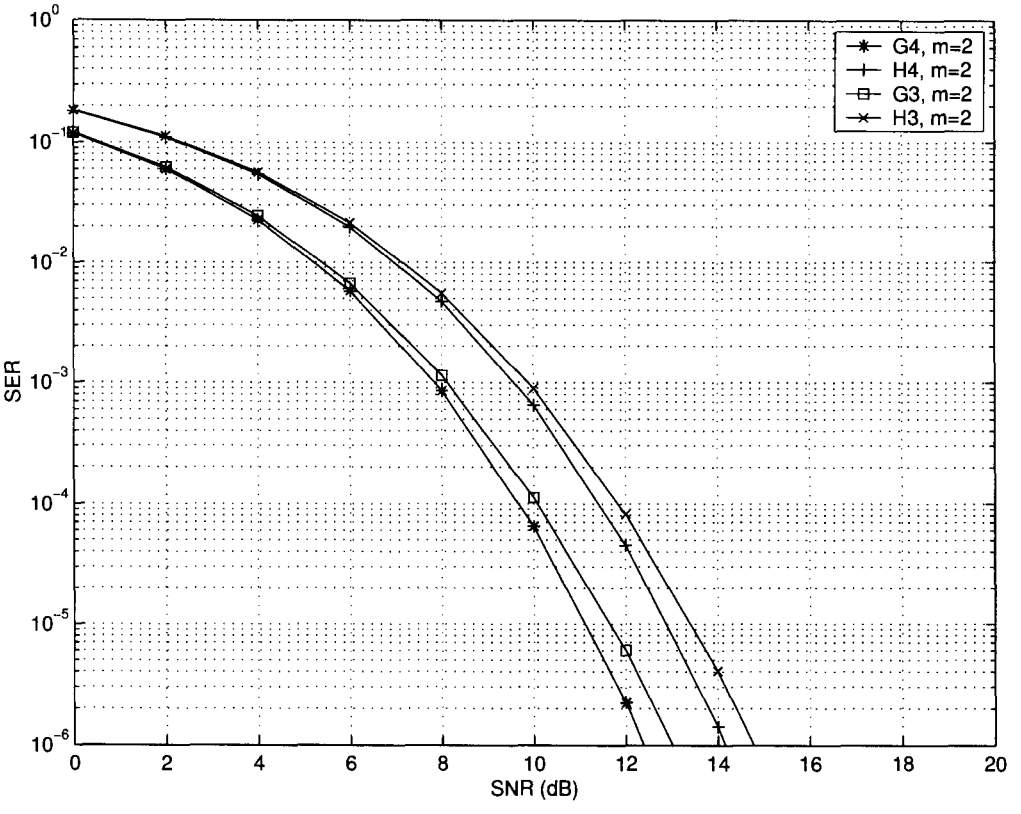

Figure 3.5. *Symbol error probability of STBC* $\mathbf{G}_2$ *with QPSK and two receive antennas over correlated Nakagami fading channels, m=2.*

Chapter 4

Capacity and Error Probability of MRC over Correlated Nakagami Fading Channels

In this chapter, employing the same approach as in Chapters 2 and 3, we extend the error probability and capacity analysis to MRC on correlated Nakagami fading channels. We present simple error probability expressions for MRC multichannel reception of q-ary coherent systems over flat Nakagami fading channels. Closed-form symbol error probabilities for q-ary PAM, PSK and rectangular QAM systems are given in a very simple form. Closed form Shannon capacity expressions are also derived for correlated Nakagami fading channels.

4.1 CF and PDF of the Output SNR for MRC on Nakagami Fading Channels

4.1.1 The Effective Scaled AWGN Channel

We consider a wireless system employing an M-branch MRC receiver. The channel is assumed to be frequency-non-selective slow fading. Let T represent the number of times slots used to transmit S symbols, the equivalent AWGN scaled channel for an MRC receiver

is

$$\mathbf{y}_T = \|\mathbf{H}\|_F^2 \mathbf{X}_T + \mathbf{w}_T, \tag{4.1}$$

where $\mathbf{y}_T$ is the $S \times 1$ complex matrix after MRC combining from the received matrix $\mathbf{Y}_T$, $\mathbf{H}$ is an $M \times 1$ fading channel coefficient matrix with correlated entries modeled as complex random variables, $\mathbf{X}_T$ is the $S \times 1$ complex input matrix with each entry having energy E_s, E_s is the maximum total energy transmitted per symbol time, $\mathbf{w}_T$ is complex Gaussian noise with zero mean and variance $\|\mathbf{H}\|_F^2 \frac{N_0}{2}$ in each real dimension, $\|H\|_F^2 = \sum_{j=1}^{M} \|h_j\|^2$ is the squared Frobenius norm of $\mathbf{H}$, and h_j is the channel gain for the jth diversity path. Therefore, the effective instantaneous combined SNR, denoted as γ_s, at the MRC receiver is

$$\gamma_s = \frac{E_s}{N_0}\|\mathbf{H}\|_F^2 = \bar{\gamma}_c \|\mathbf{H}\|_F^2 = \sum_{j=1}^{M} \bar{\gamma}_c \|h_j\|^2 = \sum_{j=1}^{M} \gamma_j, \tag{4.2}$$

where $\bar{\gamma}_c = \frac{E_s}{N_0}$ is the average SNR of each fading path per symbol, and γ_j is the instantaneous SNR of the jth fading path. It can easily be shown that the instantaneous SNR per bit γ_b has the same PDF as γ_j except that

$$\bar{\gamma}_c = \frac{E_s}{N_0 \log_2 q}, \tag{4.3}$$

for a q-ary signal constellation.

4.1.2 CF and PDF of SNR on Correlated Nakagami Fading Channel

To facilitate our analysis, we first define an $M \times 1$ column complex matrix $\mathbf{z} = [h_1, h_2, \ldots, h_M]$. Then (4.2) can be written as

$$\gamma_s = \mathbf{z}^\dagger \bar{\gamma}_c \mathbf{z}, \tag{4.4}$$

where the superscript † denotes matrix transpose and conjugate. The complex covariance among the h_j are given by the elements R_{kl} of the $M \times M$ covariance matrix $\mathbf{R}$

$$\mathbf{R} = \mathrm{E}\left[[\mathbf{z} - \mathrm{E}[\mathbf{z}]]^* [\mathbf{z} - \mathrm{E}[\mathbf{z}]]' \right], \tag{4.5}$$

where E[.] is the expected value operator, $*$ is the conjugate operator, and $'$ is the transpose operator.

For Nakagami fading, the amplitude of the channel coefficient $\|h_j\|$ for the jth diversity path has a Nakagami distribution with variance σ_j^2 in each dimension. The random variable $y = \|h_j\|^2$ then has PDF

$$p(y) = \frac{m^m}{(2\sigma_j^2)^m \Gamma(m)} y^{m-1} e^{-\frac{y}{2\sigma_j^2}}, \tag{4.6}$$

which follows a chi-square distribution. Based on the results in Chapters 2 and 3, the instantaneous SNR γ_s can then be written as

$$\gamma_s = \bar{\gamma}_c \sum_{j=1}^{M} \|h_j\|^2 = \bar{\gamma}_c \sum_{j=1}^{M} \sum_{k=1}^{2m} a_{jk}^2, \tag{4.7}$$

where a_{jk}^2 is a Gaussian variable with zero mean and unit variance. Again, we transform the distribution of γ_s to a Hermitian quadratic form distribution in complex Gaussian variates. The joint PDF of the instantaneous SNR of each multipath γ_j is then

$$p(\gamma_1, \ldots, \gamma_M) = \frac{\exp\left(-\frac{1}{2}\sum_{i=1}^{2m} \mathbf{a}_i^T \mathbf{R}^{-1} \mathbf{a}_i\right)}{(2\pi)^{mM} |\mathbf{R}|^m}, \tag{4.8}$$

where $\mathbf{a_i}$ is an independent random Gaussian vector with dimension M. The characteristic function (CF) of γ_s is then

$$\begin{aligned} G_{\gamma_s}(s) &= \int_0^\infty p(\gamma_s) \exp(-s\gamma_s) d\gamma_s \\ &= \frac{1}{|\mathbf{I} + s\frac{\bar{\gamma}_c}{m}\mathbf{R}|^m} \end{aligned} \tag{4.9}$$

Assume the convariance matrix $\mathbf{R}$ has μ distinct nonzero eigenvalues, with the ith nonzero distinct eigenvalue denoted as λ_i, and repeated κ_i times. Then (4.9) can be written as

$$G_{\gamma_s}(s) = \frac{1}{\prod_{i=1}^{\mu} |1 + s\frac{\bar{\gamma}_c}{m}\lambda_i|^{m\kappa_i}}. \tag{4.10}$$

Using a partial fractions expansion, (4.10) becomes

$$G_{\gamma_s}(s) = \sum_{i=1}^{\mu}\sum_{j=1}^{m\kappa_i} \frac{D_{ij}}{\left(1 + s\frac{\bar{\gamma}_c}{m}\lambda_i\right)^j}. \tag{4.11}$$

where the coefficient D_{ij} is given as

$$D_{ij} = \frac{1}{(m\kappa_i - j)!\left(\frac{\bar{\gamma}_c}{m}\lambda_i\right)^{m\kappa_i - j}} \frac{\partial^{m\kappa_i - j}}{\partial s^{m\kappa_i - j}} \left[\left(1 + s\frac{\bar{\gamma}_c}{m}\lambda_i\right)^{m\kappa_i} G_{\gamma_s}(s)\right] |_{s=\frac{m}{\bar{\gamma}_c\lambda_i}} \tag{4.12}$$

An inverse Laplace transform will provide the PDF of γ_s. Utilizing the linearity of the Laplace transform, the PDF of γ_s is

$$p(\gamma_s) = \sum_{i=1}^{\mu}\sum_{j=1}^{m\kappa_i} D_{ij} \frac{\gamma_s^{j-1} e^{-\frac{m\gamma_s}{\bar{\gamma}_c\lambda_i}}}{\Gamma(j)\left(\frac{\bar{\gamma}_c}{m}\lambda_i\right)^j}. \tag{4.13}$$

As a special case, for constant correlation with correlation coefficient ρ, i.e. $R_{kl} = \rho$ for $k \neq l$, and balanced fading channels, i.e. $\sigma_j^2 = \sigma^2$, the covariance matrix will have two distinct eigenvalues $\lambda_1 = 2\sigma^2(1 + (M-1)\rho)$ and $\lambda_k = 2\sigma^2(1-\rho)$ for $k = 2, 3, \ldots, M$. The PDF of the instantaneous SNR γ_s from (4.13) is therefore

$$\begin{aligned} p(\gamma_s) &= \sum_{j=1}^{m} \frac{(-1)^{m-j}(mM - j - 1)!(1 + (M-1)\rho)^{m(M-1)-j}(1-\rho)^{m-j}\gamma_s^{j-1}}{(m-j)!(m(M-1)-1)!(M\rho)^{mM-j}(j-1)!(\frac{\bar{\gamma}_c}{m})^j} \\ &\times \exp\left(-\frac{m\gamma_s}{\bar{\gamma}_c(1 + (M-1)\rho)}\right) \\ &+ \sum_{j=1}^{m(M-1)} \frac{(-1)^{m}(mM - j - 1)!(1 + (M-1)\rho)^{m(M-1)-j}(1-\rho)^{m-j}\gamma_s^{j-1}}{(m-1)!(m(M-1)-j)!(M\rho)^{mM-j}(j-1)!(\frac{\bar{\gamma}_c}{m})^j} \\ &\times \exp\left(-\frac{m\gamma_s}{\bar{\gamma}_c(1-\rho)}\right). \end{aligned} \tag{4.14}$$

4.2 Capacity of MRC on Nakagami Fading Channels

4.2.1 Shannon Capacity over Nakagami Fading Channels

The Shannon capacity $C = W\log_2(1 + SNR)$, where SNR is the signal-to-noise ratio and W is channel bandwidth, predicts the channel capacity C for an AWGN channel with continuous-valued inputs and outputs. However, a channel employing MRC with PAM/PSK/QAM modulation has discrete-valued inputs and continuous-valued outputs, which imposes an additional constraint on the capacity calculation.

The capacity of a multiple antenna wireless system over a fading channel with continuous-valued inputs and continuous-valued outputs is given as

$$C = \mathrm{E}\left[\log_2 \det\left(\mathbf{I} + \frac{E_s}{N_0}\mathbf{H}\mathbf{H}^{\dagger}\right)\right], \tag{4.15}$$

where E[.] is the expected value operator, $\mathbf{I}$ is an identity matrix with dimension M, $\det(x)$ denotes the determinant of matrix $\mathbf{X}$, and the superscript † denotes matrix transpose and conjugate. The capacity of the equivalent MRC channel in (4.1) with continuous-valued inputs and continuous-valued outputs for complex signals is given as

$$\bar{C} = \mathrm{E}\left[\log_2\left(1 + \frac{E_s}{N_0}\|\mathbf{H}\|_F^2\right) = \mathrm{E}[\log_2(1+\gamma_s)]\right], \tag{4.16}$$

Given the PDF of γ_s, the capacity of the equivalent MRC channel can be obtained from

$$\bar{C} = \int_0^{\infty} \log_2(1+\gamma_s)p(\gamma_s)d\gamma_s, \tag{4.17}$$

Monte Carlo simulation can be employed to evaluate (4.17). However, in the rest of this section, closed form Shannon capacity expressions are derived for Nakagami fading channels. To evaluate (4.17), we introduce the following integral function

$$f(\bar{\gamma}_c, n) = \int_0^{\infty} \ln(1+\gamma_s)\gamma_s^n e^{-\frac{\gamma_s}{\bar{\gamma}_c}} d\bar{\gamma}_c$$

$$
\begin{aligned}
&= (-1)^{n-1}\bar{\gamma}_c e^{\frac{1}{\bar{\gamma}_c}} Ei\left(-\frac{1}{\bar{\gamma}_c}\right) \\
&+ \sum_{k=1}^{n} \frac{n!}{(n-k)!}\left[\sum_{j=0}^{k}\sum_{i=0}^{j-k-1} \frac{(-1)^{n-k}}{(k-j)(k-j-i-1)!}\bar{\gamma}_c^{\,i+j+2}\right] \\
&+ \sum_{k=1}^{n} \frac{n!}{(n-k)!}\left[(-1)^{n-k-1}\bar{\gamma}_c^{\,k+1} e^{\frac{1}{\bar{\gamma}_c}} \mathrm{Ei}\left(-\frac{1}{\bar{\gamma}_c}\right)\right]. \qquad (4.18)
\end{aligned}
$$

The proof of (4.18) is given in Appendix A. Ei(.) denotes the exponential integral function. Based on (4.18), the closed form Shannon capacity over correlated Nakagami fading channels is given by substituting (4.13) into (4.17)

$$
\bar{C} = \sum_{i=1}^{\mu}\sum_{j=1}^{m\kappa_i} \frac{D_{ij}\log_2(e)}{\Gamma(j)\left(\frac{\bar{\gamma}_c\lambda_i}{m}\right)^j} f\left(\frac{\bar{\gamma}_c\lambda_i}{m}, j-1\right). \qquad (4.19)
$$

The capacity for constant correlated fading channels can also be obtained by substituting (13) into (16)

$$
\begin{aligned}
\bar{C} &= \sum_{j=1}^{m} \frac{(-1)^{m-j}(mM-j-1)!(1+(M-1)\rho)^{m(M-1)-j}(1-\rho)^{m-j}\log_2(e)}{(m-j)!(m(M-1)-1)!(M\rho)^{mM-j}(j-1)!(\frac{\bar{\gamma}_c}{m})^j} \\
&\times f\left(\frac{\bar{\gamma}_c(1+(M-1)\rho)}{m}, j-1\right) \\
&+ \sum_{j=1}^{m(M-1)} \frac{(-1)^{m}(mM-j-1)!(1+(M-1)\rho)^{m(M-1)-j}(1-\rho)^{m-j}\log_2(e)}{(m-1)!(m(M-1)-j)!(M\rho)^{mM-j}(j-1)!(\frac{\bar{\gamma}_c}{m})^j} \\
&\times f\left(\frac{\bar{\gamma}_c(1-\rho)}{m}, j-1\right). \qquad (4.20)
\end{aligned}
$$

4.2.2 Capacity of q-ary Signals on Correlated Nakagami Fading Channels

Both (4.15) and (4.16) were obtained assuming continuous-valued inputs. Here we consider modulation channels with discrete-valued multilevel/phase inputs and continuous-valued outputs. Assuming maximum likelihood (ML) soft decoding with perfect channel state information at the receiver, following the same approach as in Chapter 2, the capacity

of the MRC channel (4.1) can be obtained by averaging the corresponding conditional capacity with respect to the joint PDF of the channel matrix $\mathbf{H}$. By doing so, the following expression for the capacity of the fading channel is obtained

$$C^{\star}_{MRC} = \mathrm{E}\left[\tilde{C}^{\star}(\mathbf{H})\right] = \int \tilde{C}^{\star}(\mathbf{H}) p(\mathbf{H}) d\mathbf{H} \tag{4.21}$$

with

$$\begin{aligned} \tilde{C}^{\star}(\mathbf{H}) &= \log_2 q - \frac{1}{q}\sum_{j=1}^{q} \frac{1}{\pi(\|\mathbf{H}\|_F^2 N_0)} \int_{y\in C} \exp\left(-\frac{\|y - \|\mathbf{H}\|_F^2 \alpha_j\|^2}{\|\mathbf{H}\|_F^2 N_0}\right) \\ &\times \log_2 \left[\frac{\sum_{s=1}^{q} \exp\left(\|y - \|\mathbf{H}\|_F^2 \alpha_j\|^2 - \|y - \|\mathbf{H}\|_F^2 \alpha_s\|^2\right)}{\|\mathbf{H}\|_F^2 N_0}\right] dy, \end{aligned} \tag{4.22}$$

where α_j, $j = 1, \ldots, q$ is a real signal in the q-ary PAM constellation or a complex signal in the q-ary PSK/QAM constellation, and $p(\mathbf{H})$ is the joint PDF of the M random elements of the channel matrix $\mathbf{H}$ for the fading channel. Note that (4.21) applies to both real signal constellations such as PAM, and complex signal constellations such as PSK/QAM.

4.3 Error Probability over Nakagami Fading Channels

Let $P_q(\gamma_s)$ denote the error probability of a q-ary signal constellation with MRC in an AWGN channel. The error probability of MRC with correlated Nakagami fading can be obtained by averaging $P_q(\gamma_s)$ over the PDF of γ_s

$$P_{MRC,q} = \int_0^{\infty} P_q(\gamma_s) p(\gamma_s) d\gamma_s. \tag{4.23}$$

Note that $P_q(\gamma_s)$ can be symbol error probability (SEP) or bit error probability (BEP).

4.3.1 Probability of Error for PAM

The average SEP for PAM over an AWGN channel is (4.24)

$$P_q(\gamma_s) = 2\left(1 - \frac{1}{q}\right) \mathrm{Q}\left(\sqrt{\frac{6}{q^2-1}\gamma_s}\right), \tag{4.24}$$

where Q(.) is the Gaussian tail function. Substituting (4.13) and (4.24) into (4.23), the average SEP of PAM for Nakagami fading with MRC is

$$P_{MRC,PAM,q} = \int_0^\infty 2\left(1 - \frac{1}{q}\right) \mathrm{Q}\left(\sqrt{\frac{6}{q^2-1}\gamma_s}\right) \sum_{i=1}^{\mu} \sum_{j=1}^{m\kappa_i} D_{ij} \frac{\gamma_s^{j-1} e^{-\frac{m\gamma_s}{\bar{\gamma}_c \lambda_i}}}{\Gamma(j)\left(\frac{\bar{\gamma}_c}{m}\lambda_i\right)^j} d\gamma_s. \tag{4.25}$$

To evaluate the integral in (4.25), we use the following integral function

$$f(L) = \int_0^\infty \mathrm{Q}(\sqrt{ax}) x^{l-1} e^{-\frac{x}{u}} dx = \frac{1}{2} u^L \Gamma(L) \left[1 - \sum_{k=0}^{L-1} z \left(\frac{1-z^2}{4}\right)^k \binom{2k}{k}\right] \tag{4.26}$$

where

$$z = \sqrt{\frac{au}{2+au}}. \tag{4.27}$$

Based on (4.26), the closed-form symbol error probability for PAM with MRC is then

$$P_{MRC,PAM,q}(\gamma_s) = \xi \sum_{i=1}^{q} \sum_{j=1}^{m\kappa_i} D_{ij} \left[1 - \sum_{k=0}^{j-1} \mu_i \left(\frac{1-\mu_i^2}{4}\right)^k \binom{2k}{k}\right] \tag{4.28}$$

where

$$\mu_i = \sqrt{\frac{3\bar{\gamma}_c \lambda_i}{m(q^2-1) + 3\bar{\gamma}_c \lambda_i}} \tag{4.29}$$

and

$$\xi = 1 - \frac{1}{q}. \tag{4.30}$$

4.3.2 Probability of Error for PSK

We rewrite the BEP of BPSK and QPSK over an AWGN channel here as

$$P_{BPSK}(\gamma_s) = Q(\sqrt{2\gamma_s}), \tag{4.31}$$

and

$$P_{QPSK}(\gamma_s) = Q(\sqrt{\gamma_s}), \tag{4.32}$$

respectively. The exact symbol error probability of q-ary PSK for an AWGN channel is

$$P_{PSK,AWGN,q}(\gamma_s) = 2Q\left(\sqrt{2\gamma_s}, \sin\frac{\pi}{q}\right) - \frac{1}{\pi}\int_{\frac{\pi}{2}-\frac{\pi}{q}}^{\frac{\pi}{2}} e^{-\gamma_s \frac{\sin^2\frac{\pi}{q}}{\cos^2\theta}} d\theta. \tag{4.33}$$

For large SNR and large values of q, the SEP of q-ary PSK in an AWGN channel can be approximated as

$$P_q(\gamma_s) \approx 2Q\left(\sqrt{2\gamma_s}, \sin\frac{\pi}{q}\right). \tag{4.34}$$

and the equivalent BEP is

$$P_{qb} \approx \frac{1}{\log q} P_q. \tag{4.35}$$

where Gray coding is assumed. This approximation is good for large values of q, however for $q = 2$ there is a factor of 2 difference with the exact probability given in (4.31). By substituting for $P_q(\gamma_s)$ in (4.34) and using (4.26), (4.23) can be written as

$$P_{MRC,PAM,q}(\gamma_s) \approx \xi \sum_{i=1}^{q} \sum_{j=1}^{m\kappa_i} D_{ij} \left[1 - \sum_{k=0}^{j-1} u_i \left(\frac{1-u_i^2}{4}\right)^k \binom{2k}{k}\right], \tag{4.36}$$

where

$$u_i = \sqrt{\frac{\sin^2\frac{\pi}{q}\bar{\gamma}_c\lambda_i}{m + \sin^2\frac{\pi}{q}\bar{\gamma}_c\lambda_i}}, \tag{4.37}$$

and $\xi = \frac{1}{2}$ for $q = 2$ and $\xi = 1$ for $q > 2$. Therefore, the BEP can be approximated as

$$P_{MRC,PSK}(\gamma_s) \approx \frac{1}{\log q}\xi \sum_{i=1}^{q}\sum_{j=1}^{m\kappa_i} D_{ij}\left[1 - \sum_{k=0}^{j-1} u_i \left(\frac{1-u_i^2}{4}\right)^k \binom{2k}{k}\right] \tag{4.38}$$

By substituting for $P_q(\gamma_s)$ in (4.31) and (4.32), and using (4.26), the exact bit error probability for BPSK and QPSK can be derived from (4.23) as

$$P_{MRC,PSK,qb}(\gamma_s) = \frac{1}{2}\xi \sum_{i=1}^{q}\sum_{j=1}^{m\kappa_i} D_{ij}\left[1 - \sum_{k=0}^{j-1} u_i \left(\frac{1-u_i^2}{4}\right)^k \binom{2k}{k}\right] \tag{4.39}$$

where

$$u_i = \sqrt{\frac{\frac{\bar{\gamma}_c}{m}\lambda_i}{1+\frac{\bar{\gamma}_c}{m}\lambda_i}} \tag{4.40}$$

and

$$u_i = \sqrt{\frac{\frac{\bar{\gamma}_c}{m}\lambda_i}{2+\frac{\bar{\gamma}_c}{m}\lambda_i}} \tag{4.41}$$

for BPSK and QPSK, respectively. Note that

$$\bar{\gamma}_c = \frac{E_s}{2N_0} \tag{4.42}$$

for QPSK.

4.3.3 Probability of Error for QAM

Rectangular QAM signal constellations can be considered as equivalent to two PAM signals on quadrature carriers. For q-ary, $q = 2^k$ (k even), rectangular QAM, the symbol error probability is given as

$$P_q = 1 - \left(1 - P_{\sqrt{q}}\right)^2, \tag{4.43}$$

where

$$P_{\sqrt{q}} = 2\left(1 - \frac{1}{\sqrt{q}}\right) Q\left(\sqrt{\frac{1}{q-1}\gamma_s}\right). \tag{4.44}$$

By substituting in (4.44), (4.23) can be written as

$$P_{MRC,PAM,\sqrt{q}} = \int_0^\infty 2\left(1 - \frac{1}{\sqrt{q}}\right) Q\left(\sqrt{\frac{1}{q-1}\gamma_s}\right) \sum_{i=1}^{\mu} \sum_{j=1}^{m\kappa_i} D_{ij} \frac{\gamma_s^{j-1} e^{-\frac{m\gamma_s}{\bar{\gamma}_c \lambda_i}}}{\Gamma(j)\left(\frac{\bar{\gamma}_c}{m}\lambda_i\right)^j} d\gamma_s. \tag{4.45}$$

Using (4.26), the closed-form symbol error probability for rectangular q-ary QAM with MRC is then

$$P_{MRC,QAM,q} = (1 - P_{MRC,PAM,\sqrt{q}})^2, \tag{4.46}$$

where

$$P_{MRC,PSK,qb}(\gamma_s) = \xi \sum_{i=1}^{q} \sum_{j=1}^{m\kappa_i} D_{ij} \left[1 - \sum_{k=0}^{j-1} u_i \left(\frac{1-u_i^2}{4}\right)^k \binom{2k}{k}\right] \tag{4.47}$$

and for $\sqrt{q}$-ary PAM in q-ary rectangular QAM

$$u_i = \sqrt{\frac{3\bar{\gamma}_c \lambda_i}{2m(q-1) + 3\bar{\gamma}_c \lambda_i}} \tag{4.48}$$

and $\xi = 1 - \frac{1}{\sqrt{q}}$. The SEP of q-ary rectangular QAM can then be calculated from (4.46). Again, the derivation of the closed form error probabilities expressions for the special cases is straightforward.

4.4 Numerical Results

In this section, some numerical results are presented to illustrate the capacity and error probability results obtained in the previous sections. Simulation is performed and confirmed the theoretical results.

Fig. 4.1 shows the Shannon capacity for MRC in a correlated Nakagami fading channel with different correlation parameters. In Fig. 4.1 we have 4 diversity paths, i.e. $M = 4$, and

the Nakagami parameter is $m = 2$. The figure shows results using both (4.20) and Monte Carlo simulation, and illustrates that the results using the two methods are identical. Fig. 4.1 also shows that the capacity increases as the channel correlation decreases, however, the capacity increase is not apparent when the channel correlation parameter ρ is greater than 0.5.

The Shannon capacity of MRC over a correlated Nakagami fading channel with different numbers of multipath signals is given in Fig. 4.2. Here $\rho = 0.5$ and the Nakagami parameter is again $m = 2$. In this figure, we can see that the capacity is greatly increased by combining more diversity paths. For example, when SNR=5dB, the system capacity increases from about 2.6 bit/s/Hz to 4.7 bit/s/Hz when the number of multipath signals combined increases from 2 to 8.

Fig. 4.3 presents the channel capacity of MRC over a correlated Nakagami fading channel with BPSK modulation, $M = 4$, Nakagami parameter $m = 2$, and different correlation parameters. This shows that to obtain the same capacity, the fully correlated channel ($\rho = 1$) needs about 2-5 dB more SNR than the non-correlated channel ($\rho = 0$).

Simulation was used to verify the exact closed form error probability expressions obtained in this chapter. In Fig. 4.4, the bit error rate of MRC over a correlated Nakagami fading channel with BPSK modulation is given for different correlation parameters. There is approximately an 8 dB gain with independent fading over the fully correlated case at a BER of 10^{-3}.

In Fig. 4.5, the bit error probability of MRC with BPSK and different Nakagami parameters m is presented for $M = 2$ and $\rho = 0.8$. As m increases, fluctuations in the signal strength diminish compared to Rayleigh fading, so the system performance will improve. This is shown clearly in Fig. 4.5 where results are given for $m = 1, 3, 5, 7$.

In Fig. 4.6, the bit error probability of MRC with BPSK and different numbers of combined multipath signals is presented for a correlated Nakagami fading channel with $m = 2$ and $\rho = 0.8$. Again, the simulation results match perfectly with those obtained from the analysis. Note that the BER improves as the number of combined paths increases.

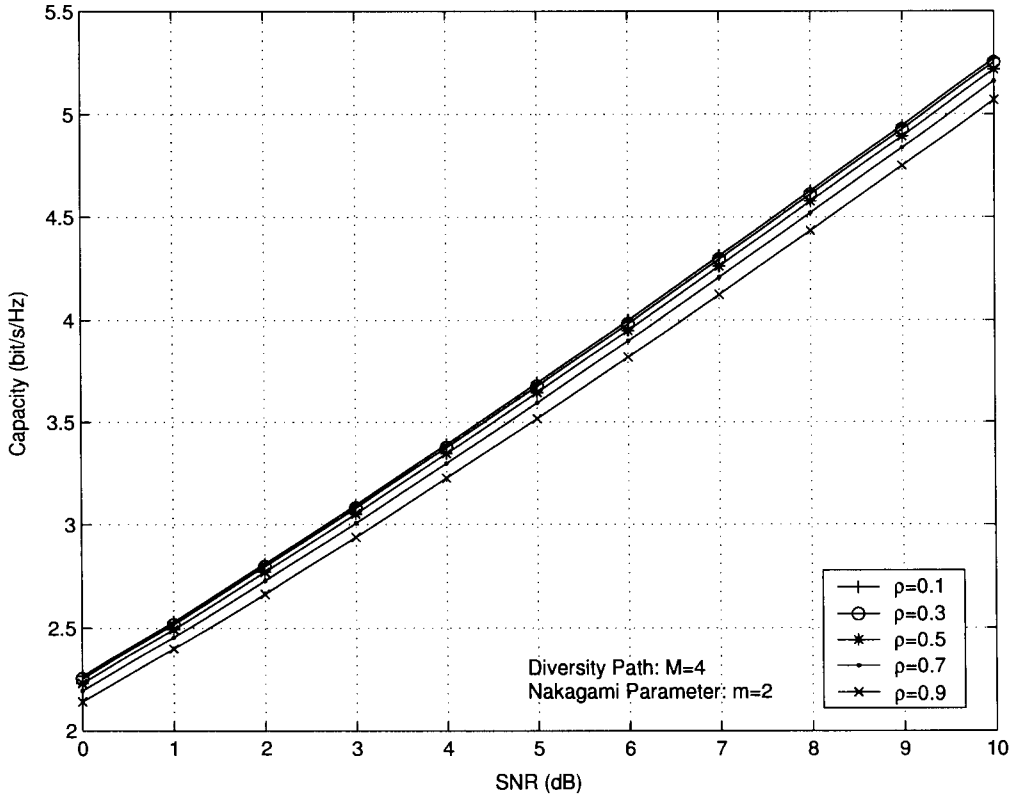

Figure 4.1. *Shannon capacity for MRC in a correlated Nakagami fading channel with different correlation parameters.*

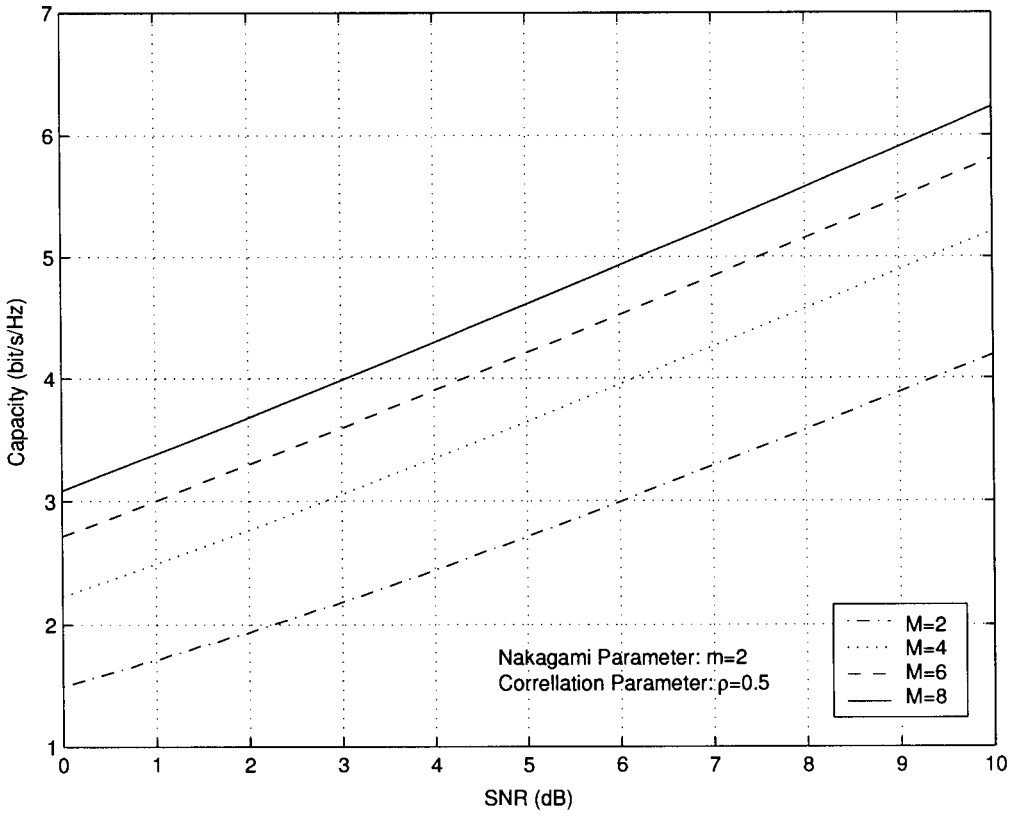

Figure 4.2. *Shannon capacity of MRC over correlated Nakagami fading channel with different number of multipath signals.*

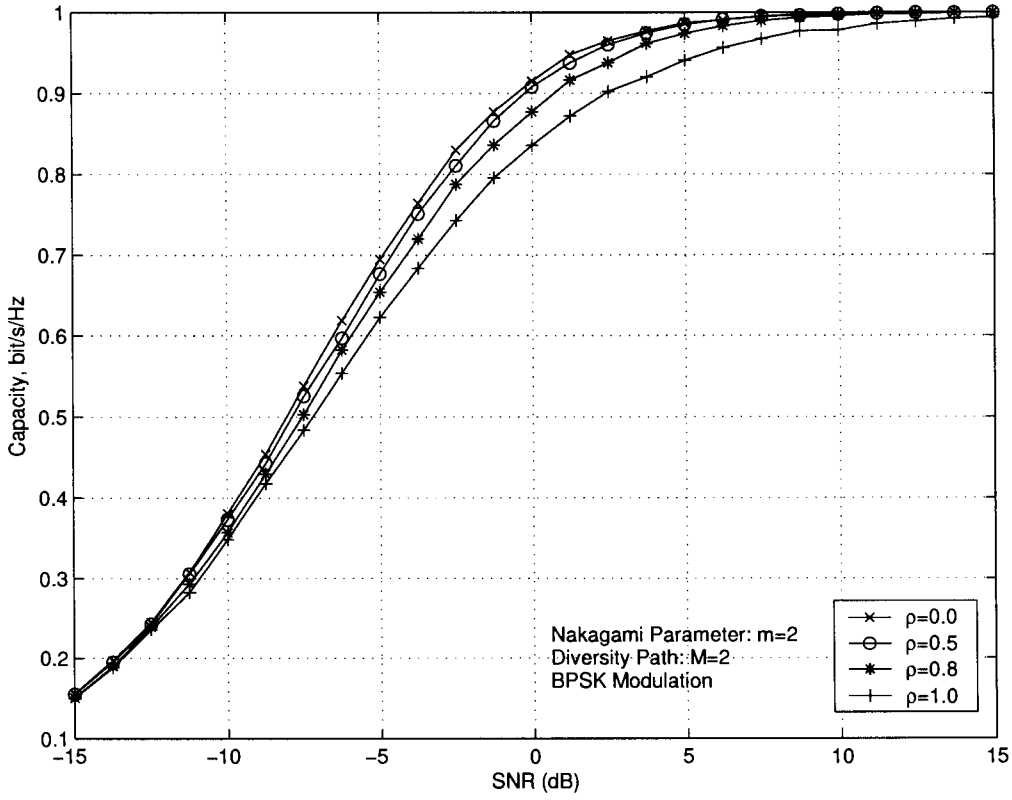

Figure 4.3. *Channel capacity of MRC over correlated Nakagami fading with different correlation parameters.*

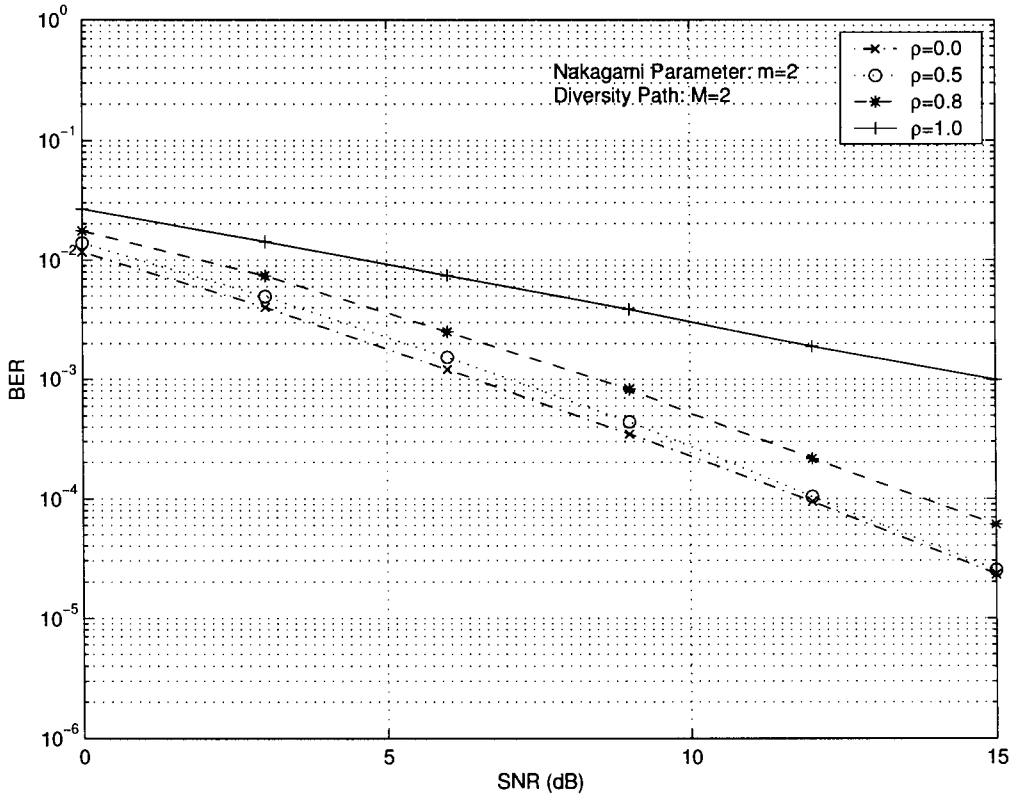

Figure 4.4. *BER of MRC over correlated Nakagami fading channels with BPSK and different correlation parameters.*

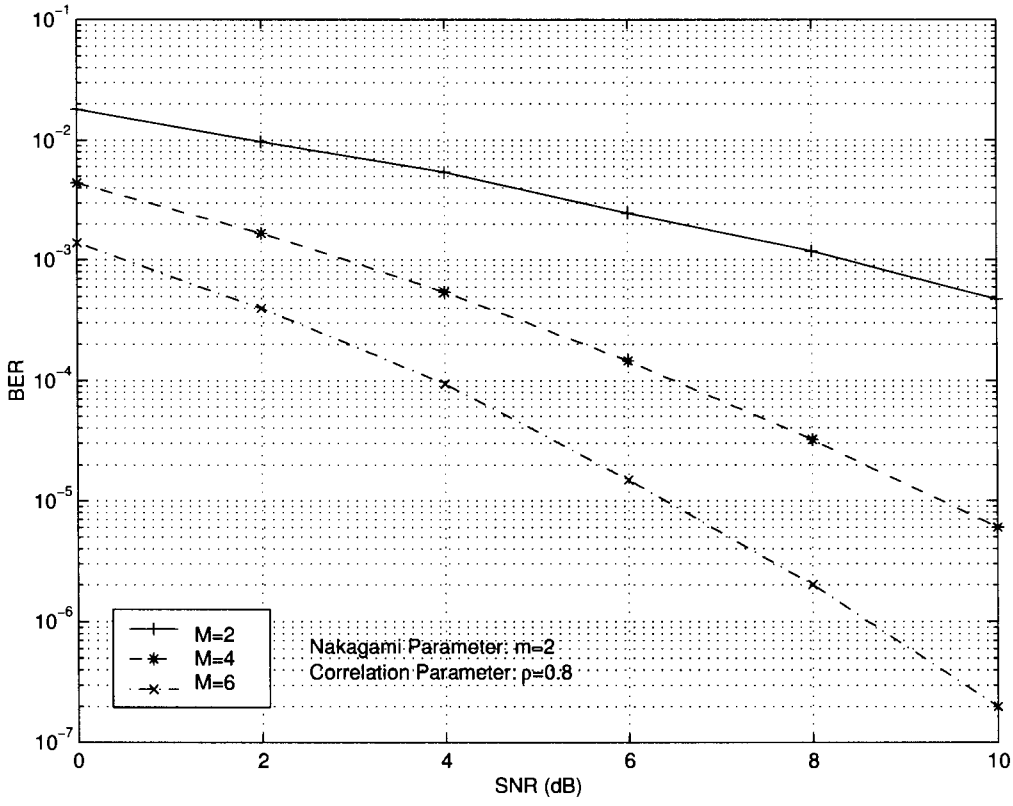

Figure 4.5. *BER of MRC over correlated Nakagami fading channels with BPSK and different Nakagami parameters.*

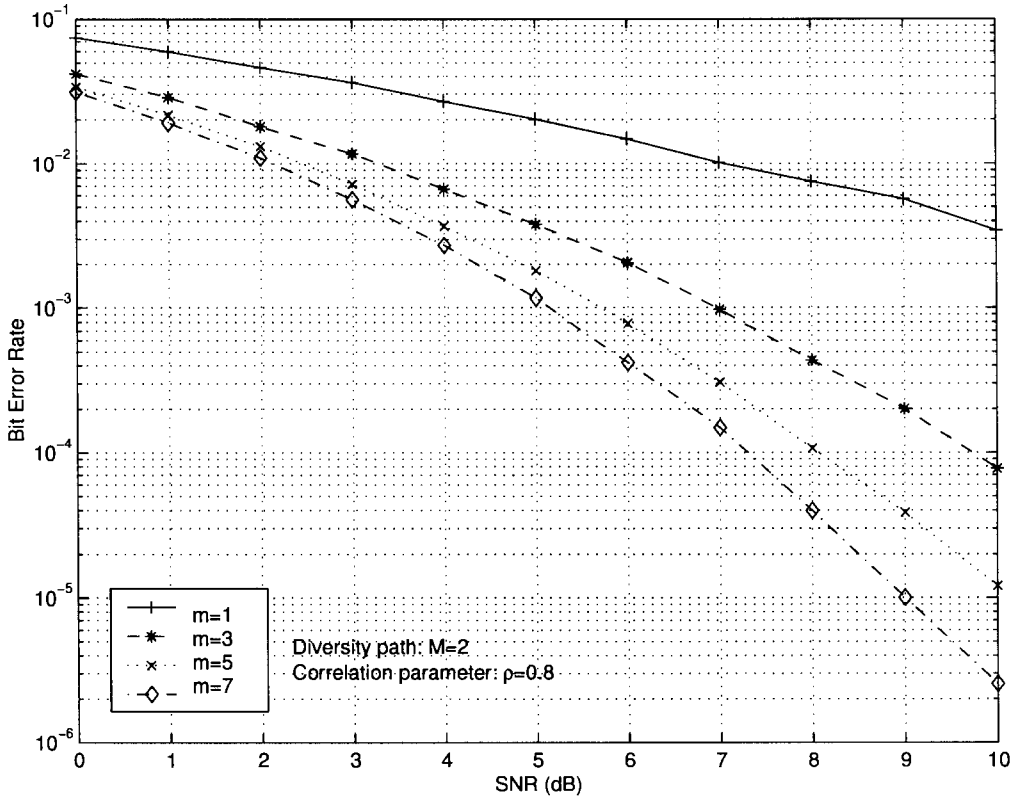

Figure 4.6. *MRC over correlated Nakagami fading channels with BPSK and different number of multipath signals.*

Chapter 5

Rake Receiver Performance Analysis

In this chapter, we analyze the performance of a practical RAKE receiver with MRC combining over fading channels.

5.1 System Model and Operation

5.1.1 System Model

We assume a block fading channel. Specifically, fading is assumed to be constant during each channel coherence time, but becomes independent after one coherence time. We also assume that there are L resolvable diversity paths, all of which are i.i.d. with the same average SNR $\bar{\gamma}$. We will discuss the unequal average SNR case at the end of this chapter.

A RAKE receiver essentially consists of a set of individual correlators (fingers). Because of the hardware complexity constraint, it is usually not practical to implement the same number of fingers as the number of resolvable paths. We assume that there are L_c fingers. Fig. 5.1 shows the structure of a RAKE receiver with four fingers, i.e. $L_c = 4$. The signals on each finger is correlated with the spreading sequence and integrated over the symbol interval. After that, the output from the fingers are weighted according to the MRC algorithm and combined to form the receiver output.

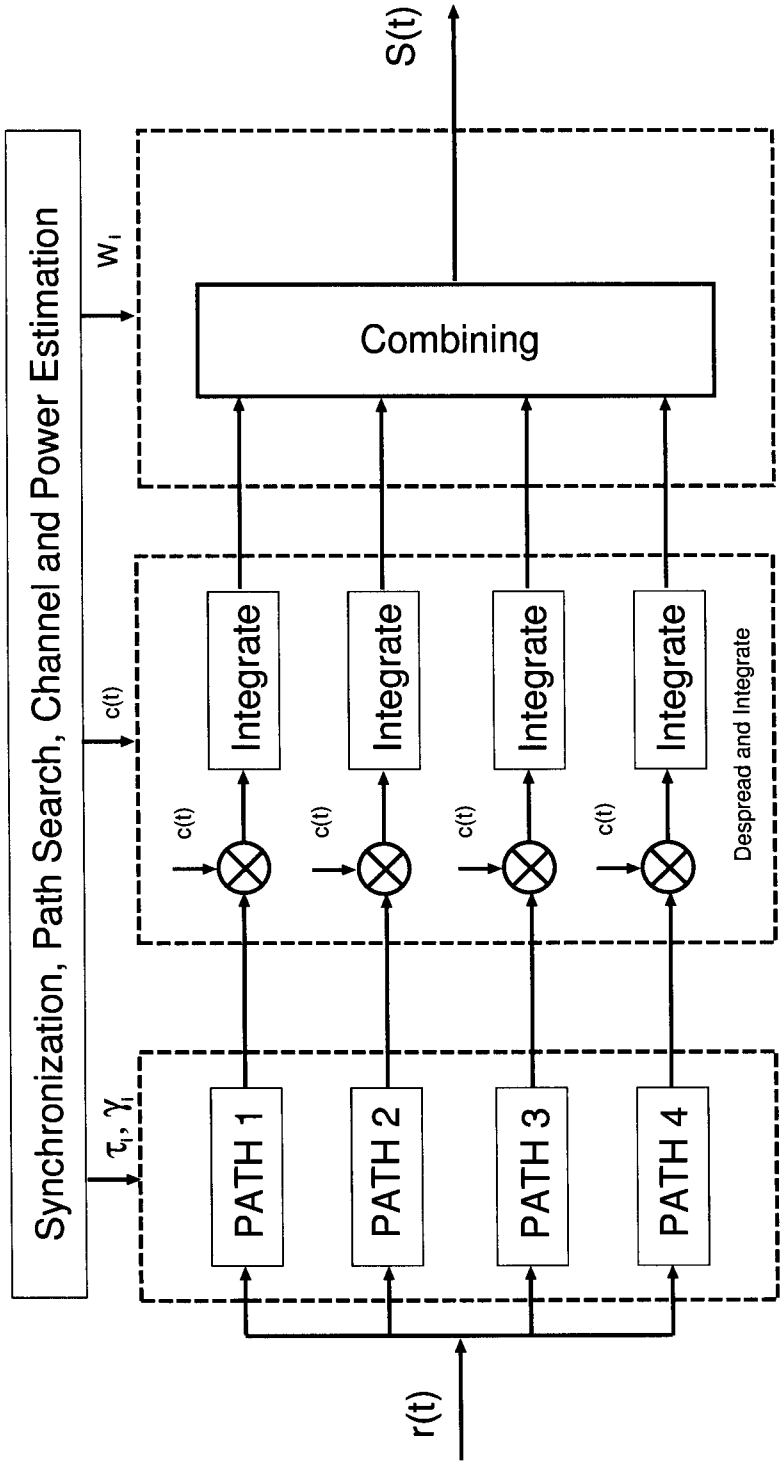

Figure 5.1. *The structure of a RAKE receiver.*

5.1.2 Mode of Operation

In practical CDMA systems, the RAKE receiver finds the first multipath, i.e. the path with the smallest system delay, through the synchronization process. The remaining paths are located by determining their excess delays with respect to the first path.

In this paper, we assume that the first finger always follows the path found through synchronization. Only when the system loses synchronization and/or the performance becomes unacceptable will the receiver update this path through a new synchronization process. The receiver attempts to choose acceptable paths from the remaining $L-1$ available multipaths for the other L_c-1 fingers. This is achieved by sequentially comparing the instantaneous SNR of each path with a fixed threshold, denoted by γ_T. When the receiver finds the (L_c-1)th acceptable path, the search process is terminated and the path parameters are fed into the MRC combiner. Note that the receiver may not find L_c-1 acceptable paths after examining all resolvable paths. In this case, the receiver uses only the acceptable paths it finds in addition to the first path. Therefore the number of paths used in the RAKE receiver, or active fingers, ranges from 1 to L_c. We assume that the path selection for the L_c-1 fingers is updated periodically, usually at the rate of the channel coherence time.

By combining only those paths with sufficient SNR, energy usage is reduced and the mobile terminal battery life is increased. Also we can avoid the noise increase caused by combining paths with poor SNR.

5.2 MGF of the Combined SNR

5.2.1 General Case

To analyze the performance of the RAKE receiver in fading channels, we require the statistical characterization of the combined output SNR. In this section of the thesis, we derive the MGF of the output SNR.

Based on the mode of operation, the combined output SNR, S, after MRC combining is

$$S = \gamma_0 + \sum_{k=1}^{i} \gamma_k, \tag{5.1}$$

where γ_0 is the instantaneous SNR of the first path, i, $0 \leq i \leq L_c - 1$, is the number of acceptable diversity paths combined by the RAKE receiver except for the first path, and γ_k is the instantaneous SNR of the kth acceptable path. Note that the SNR of the first path follows a standard fading distribution since we do not apply any threshold to it. For the the remaining i paths, however, the SNR follow a truncated distribution according to the SNR threshold γ_T.

Notice that the RAKE receiver using different number of paths, i.e. $i = 0, 1, \cdots, L_c - 1$ are mutually exclusive events. Based on the total probability theorem, the MGF of the combined output signal $M_S(t)$ is

$$M_S(t) = M_{\gamma_0}(t) \times \sum_{i=0}^{L_c-1} w_i M_S^i(t), \tag{5.2}$$

where $M_{\gamma_0}(t)$ is the MGF of the SNR for the first path, w_i is the probability that i paths out of a maximum of $L - 1$ paths have an SNR greater than γ_T, and $M_S^i(t)$ is the MGF of S corresponding to the event that there i paths out of a maximum of $L - 1$ paths with an SNR greater than γ_T, and

$$M_S^i(t) = \prod_{k=1}^{i} M_{\gamma_k}(t), \tag{5.3}$$

where $M_{\gamma_k}(t)$ is the MGF of the SNR of the kth acceptable path. Since all the diversity

paths are i.i.d. faded with average SNR $\bar{\gamma}$, w_i is given by

$$w_i = \begin{cases} \binom{L-1}{i}[P_\gamma(\gamma_T)]^{L-1-i}[1-P_\gamma(\gamma_T)]^i, \\ \qquad\qquad i = 0, ..., L_c - 2 \\ \sum_{j=L_c-1}^{L-1} \binom{L-1}{j}[P_\gamma(\gamma_T)]^{L-1-j}[1-P_\gamma(\gamma_T)]^j, \\ \qquad\qquad i = L_c - 1, \end{cases} \tag{5.4}$$

where $P_\gamma(\gamma_T)$ is the Cumulative Distribution Function (CDF) of the received SNR for a path.

Since all the selected paths have the same truncated distribution, it can be shown that $M_S^i(t)$ is given by

$$M_S^i(t) = [M_s^+(t)]^i, \tag{5.5}$$

where

$$M_s^+(t) = \frac{1}{1-P_\gamma(\gamma_T)} \int_{\gamma_T}^{+\infty} p_\gamma(x) e^{tx} dx. \tag{5.6}$$

In the equation above, $p_\gamma(\gamma_T)$ is the Probability Density Function (PDF) of the SNR of the received signals.

Substituting (5.4), (5.5) and (5.6) into (5.2) we have

$$\begin{aligned} M_S(t) &= M_{\gamma_0}(t) \sum_{i=0}^{L_c-2} \binom{L-1}{i} [P_\gamma(\gamma_T)]^{L-1-i}[1-P_\gamma(\gamma_T)]^i [M_s^+(t)]^i \\ &+ M_{\gamma_0}(t) \sum_{j=L_c-1}^{L-1} \binom{L-1}{j} [P_\gamma(\gamma_T)]^{L-1-j}[1-P_\gamma(\gamma_T)]^j [M_s^+(t)]^{L_c}. \end{aligned} \tag{5.7}$$

5.2.2 Rayleigh Fading Channel

For a Rayleigh fading channel, the PDF, CDF and MGF of the SNR of a single path are given by

$$p_\gamma(x) = \frac{1}{\bar{\gamma}} e^{-\frac{x}{\bar{\gamma}}}, \tag{5.8}$$

$$P_\gamma(x) = 1 - e^{-\frac{x}{\bar{\gamma}}}, \tag{5.9}$$

and

$$M_{\gamma_0} = \frac{1}{1 - t\bar{\gamma}}, \tag{5.10}$$

respectively. Substituting (5.8) and (5.9) into (5.6), we have

$$M_s^+ = \frac{1}{1 - t\bar{\gamma}} e^{t\gamma_T}. \tag{5.11}$$

Then substituting (5.9), (5.10) and (5.11) into (5.7), the MGF for the combined output SNR of a RAKE receiver over Rayleigh fading channels is

$$\begin{aligned} M_S(t) &= \sum_{i=0}^{L_c-2} \binom{L-1}{i} \left(1 - e^{-\frac{\gamma_T}{\bar{\gamma}}}\right)^{L-1-i} e^{-\frac{i\gamma_T}{\bar{\gamma}}} e^{i\gamma_T t} \left(\frac{1}{1 - t\bar{\gamma}}\right)^{i+1} \\ &+ \sum_{j=L_c-1}^{L-1} \binom{L-1}{j} \left(1 - e^{-\frac{\gamma_T}{\bar{\gamma}}}\right)^{L-1-j} e^{-\frac{j\gamma_T}{\bar{\gamma}}} e^{(L_c-1)\gamma_T t} \left(\frac{1}{1 - t\bar{\gamma}}\right)^{L_c}. \end{aligned} \tag{5.12}$$

5.2.3 Rician Fading Channel

For Rician fading, the PDF, CDF and MGF of the SNR of a single path are

$$p_\gamma(x) = \frac{1+K}{\bar{\gamma}} e^{-K - \frac{1+K}{\bar{\gamma}}x} I_0\left(2\sqrt{\left(\frac{1+K}{\bar{\gamma}}Kx\right)}\right), \tag{5.13}$$

$$P_\gamma(x) = 1 - Q_1\left(\sqrt{2K}, \sqrt{\frac{2(1+K)}{\bar{\gamma}}x}\right), \tag{5.14}$$

and

$$M_{\gamma_0} = \frac{1+K}{1+K-t\bar{\gamma}} e^{\frac{t\bar{\gamma}K}{1+K-t\bar{\gamma}}}, \tag{5.15}$$

respectively, where K is the Rician fading parameter. Following the same procedure as in section 2.2, for Rician fading channels we have

$$M_s^+ = \frac{1+K}{1+K-t\bar{\gamma}} e^{\frac{t\bar{\gamma}K}{1+K-t\bar{\gamma}}} \frac{Q_1\left(\sqrt{\frac{2K(1+K)}{1+K-t\bar{\gamma}}}, \sqrt{2(1+K-t\bar{\gamma})\frac{\gamma_T}{\bar{\gamma}}}\right)}{Q_1\left(\sqrt{2K}, \sqrt{2(1+K)\frac{\gamma_T}{\bar{\gamma}}}\right)}. \tag{5.16}$$

Then the MGF for the SNR of the combined output signal of a RAKE receiver over Rician fading channels is

$$\begin{aligned} M_S(t) &= \sum_{i=0}^{L_c-2} \binom{L-1}{i} \left(\frac{1+K}{1+K-t\bar{\gamma}} e^{\frac{t\bar{\gamma}K}{1+K-t\bar{\gamma}}}\right)^{i+1} \\ &\times \left[1-Q_1(\sqrt{2K}, \sqrt{2(1+K)\frac{\gamma_T}{\bar{\gamma}}})\right]^{L-i-1} \left[Q_1(\sqrt{\frac{2K(1+K)}{1+K-t\bar{\gamma}}}, \sqrt{2(1+K-t\bar{\gamma})\frac{\gamma_T}{\bar{\gamma}}})\right]^{i} \\ &+ \sum_{j=L_c-1}^{L-1} \binom{L-1}{j} \left(\frac{1+K}{1+K-t\bar{\gamma}} e^{\frac{t\bar{\gamma}K}{1+K-t\bar{\gamma}}}\right)^{L_c} \left[1-Q_1(\sqrt{2K}, \sqrt{2(1+K)\frac{\gamma_T}{\bar{\gamma}}})\right]^{L-j-1} \\ &\times \left[Q_1(\sqrt{2K}, \sqrt{2(1+K)\frac{\gamma_T}{\bar{\gamma}}})\right]^{i+1-L_c} \left[Q_1(\sqrt{\frac{2K(1+K)}{1+K-t\bar{\gamma}}}, \sqrt{2(1+K-t\bar{\gamma})\frac{\gamma_T}{\bar{\gamma}}})\right]^{L_c-1} \end{aligned} \quad (5.17)$$

5.2.4 Nakagami Fading Channel

For Nakagami-m fading, the PDF, CDF and MGF of the SNR of a single path are

$$p_\gamma(x) = \left(\frac{m}{\bar{\gamma}}\right)^m \frac{x^{m-1}}{\Gamma(m)} e^{-\frac{mx}{\bar{\gamma}}}, \quad (5.18)$$

$$P_\gamma(x) = 1 - \frac{\Gamma(m, \frac{m}{\bar{\gamma}}x)}{\Gamma(m)}, \quad (5.19)$$

and

$$M_{\gamma_0} = \left(1 - \frac{t\bar{\gamma}}{m}\right)^{-m}, \quad (5.20)$$

respectively, where m is the Nakagami fading parameter. Following the same procedure as in the previous section, for Nakagami-m fading we have

$$M_s^+ = \left(1 - \frac{t\bar{\gamma}}{m}\right)^{-m} \frac{\Gamma(m, \frac{m\gamma_T}{\bar{\gamma}} - t\gamma_T)}{\Gamma(m, \frac{m\gamma_T}{\bar{\gamma}})} \quad (5.21)$$

The MFG for the combined output SNR of a RAKE receiver for Nakagami fading is

$$\begin{aligned} M_S(t) &= \left(1 - \frac{t\bar{\gamma}}{m}\right)^{-(i+1)m} \sum_{i=0}^{L_c-2} \binom{L-1}{i} \left[1 - \frac{\Gamma(m, \frac{m\gamma_T}{\bar{\gamma}})}{\Gamma(m)}\right]^{L-1-i} \left[\frac{\Gamma(m, \frac{m\gamma_T}{\bar{\gamma}} - t\gamma_T)}{\Gamma(m)}\right]^{i} \\ &+ \left(1 - \frac{t\bar{\gamma}}{m}\right)^{-(L_c+1)m} \sum_{i=L_c-1}^{L-1} \binom{L-1}{j} \left[1 - \frac{\Gamma(m, \frac{m\gamma_T}{\bar{\gamma}})}{\Gamma(m)}\right]^{L-j} \frac{\Gamma(m, \frac{m\gamma_T}{\bar{\gamma}} - t\gamma_T)^{L_c-1}}{\Gamma(m)^j \Gamma(m, \frac{m\gamma_T}{\bar{\gamma}})^{L_c-1-j}}. \end{aligned} \quad (5.22)$$

5.3 Performance Analysis

In this part of the thesis, we evaluate the RAKE receiver performance based on the MGF results in section 5.2. The average combined SNR and SEP are investigated. Results for system outage probability and number of channels estimated are also given.

5.3.1 Average Combined SNR

The average combined SNR of a RAKE receiver can be calculated as the first moment of the MGF

$$\bar{\gamma}_c = \frac{dM_S(t)}{dt}|_{t=0}. \tag{5.23}$$

For example, the average combined SNR for a RAKE receiver over Rayleigh fading channels is

$$\begin{aligned}\bar{\gamma}_{Rayleigh} &= \sum_{i=0}^{L_c-2} \binom{L-1}{i} \left(1-e^{-\frac{\gamma_T}{\bar{\gamma}}}\right)^{L-1-i} e^{-\frac{i\gamma_T}{\bar{\gamma}}} [i\gamma_t + (i+1)\bar{\gamma}] \\ &+ [L_c\bar{\gamma} + (L_c-1)\gamma_T] \sum_{j=L_c-1}^{L-1} \binom{L-1}{j} \left(1-e^{-\frac{\gamma_T}{\bar{\gamma}}}\right)^{L-1-j} e^{-\frac{j\gamma_T}{\bar{\gamma}}}. \end{aligned} \tag{5.24}$$

5.3.2 Symbol Error Probability

With the closed-form expression for the MGF obtained in section 5.2, we can evaluate the RAKE receiver SEP performance for different modulation schemes [53]. For example, the average symbol error probability with M-ary PSK modulation is

$$P_{MPSK} = \frac{1}{\pi}\int_0^{\frac{(M-1)\pi}{M}} M_S(f(\phi))d\phi, \tag{5.25}$$

where $f(\phi)$ is given by

$$f(\phi) = -\frac{\sin^2\left(\frac{\pi}{M}\right)}{\sin^2(\phi)}. \tag{5.26}$$

The average symbol error probability for a RAKE receiver over Rayleigh fading channels with M-ary PSK modulation is

$$P_S = \sum_{i=0}^{L_c-2} \binom{L-1}{i} \left(1-e^{-\frac{\gamma_T}{\bar{\gamma}}}\right)^{L-1-i} e^{-\frac{i\gamma_T}{\bar{\gamma}}} \frac{1}{\pi}\int_0^{\frac{(M-1)\pi}{M}} e^{\frac{-i\gamma_T \sin^2(\frac{\pi}{M})}{\sin^2\phi}}$$

$$\times \left(\frac{\sin^2\phi}{\sin^2\phi + \bar{\gamma}\sin^2(\frac{\pi}{M})}\right)^{i+1} d\phi$$
$$+ \sum_{j=L_c-1}^{L-1} \binom{L-1}{j} (1-e^{-\frac{\gamma_T}{\bar{\gamma}}})^{L-1-j} e^{-\frac{j\gamma_T}{\bar{\gamma}}} \frac{1}{\pi} \int_0^{\frac{(M-1)\pi}{M}} e^{-\frac{(L_c-1)\gamma_T \sin^2(\frac{\pi}{M})}{\sin^2(\phi)}}$$
$$\times \left(\frac{\sin^2\phi}{\sin^2\phi + \bar{\gamma}\sin^2(\frac{\pi}{M})}\right)^{L_c} d\phi. \tag{5.27}$$

5.3.3 Outage Probability

Outage probability P_{out} is a very important performance measure for wireless communication systems. For RAKE receiver, it is defined as the probability that the signal-to-noise ratio of the combined signal is below a threshold γ_{out}. To investiage the outage probability of RAKE receiver, we first derive the PDF $p_S(x)$ for the SNR of the combined signal S by applying an inverse Laplace transform to its MGF $M_S(t)$

$$p_S(x) = L^{-1}\left[M_S(t)\right]. \tag{5.28}$$

The CDF of the SNR of the combined signal is obtained by integrating to $p_S(x)$

$$P_S(x) = Pr[S \le x] = \int_0^x p_S(u)du. \tag{5.29}$$

Similar results for Rician and Nakagami fading are very hard to get. Here we give the results for a Rayleigh fading channel as an example. Following the procedure given above, with the result in (5.7), we can get the PDF for the SNR of the combined signal S

$$\begin{aligned} p_S(t) &= \sum_{i=0}^{L_c-2} \binom{L-1}{i} \left(1-e^{-\frac{\gamma_T}{\bar{\gamma}}}\right)^{L-1-i} e^{-\frac{i\gamma_T}{\bar{\gamma}}} (-\frac{1}{\bar{\gamma}})^{i+1} \frac{1}{i!} e^{-\frac{x-i\gamma_T}{\bar{\gamma}}} u[x-i\gamma T] \\ &+ \sum_{j=L_c-1}^{L-1} \binom{L-1}{j} \left(1-e^{-\frac{\gamma_T}{\bar{\gamma}}}\right)^{L-1-j} e^{-\frac{j\gamma_T}{\bar{\gamma}}} \\ &\times (-\frac{1}{\bar{\gamma}})^{L_c} \frac{1}{(L_c-1)!} [x-(L_c-1)\gamma_T]^{L_c-1} e^{-\frac{x-(L_c-1)\gamma_T}{\bar{\gamma}}} u[x-(Lc-1)\gamma_T] \end{aligned} \tag{5.30}$$

Substituting (5.30) into (5.29), the CDF for the SNR of the combined signal S is

$$
\begin{aligned}
P_S(x) &= \sum_{i=0}^{L_c-2} \binom{L-1}{i} \left(1-e^{-\frac{\gamma_T}{\bar{\gamma}}}\right)^{L-1-i} e^{-\frac{i\gamma_T}{\bar{\gamma}}} \\
&\times \left[1-e^{-\frac{x-i\gamma T}{\bar{\gamma}}} \sum_{k=0}^{i,i\leq\frac{x}{\gamma T}} \frac{1}{k!}\left(\frac{x-i\gamma T}{\bar{\gamma}}\right)^k\right] \\
&+ \sum_{j=L_c-1}^{L-1} \binom{L-1}{j} \left(1-e^{-\frac{\gamma_T}{\bar{\gamma}}}\right)^{L-1-j} e^{-\frac{j\gamma_T}{\bar{\gamma}}} \\
&\times I_{(L_c-1)\gamma T}(x)\left[1-e^{-\frac{x-(L_c-1)\gamma T}{\bar{\gamma}}} \sum_{k=0}^{L_c-1} \frac{1}{k!}\left(\frac{x-(L_c-1)\gamma T}{\bar{\gamma}}\right)^k\right]. \qquad (5.31)
\end{aligned}
$$

where $I_{(L_c-1)\gamma_T}(x)$ is an indicator function, which is equal to 1 if $x \geq (L_c-1)\gamma_T$ and zero otherwise. Let $x = \gamma_{out}$ in (5.31), then we have the outage probability for a threshold γ_{out}.

5.3.4 Number of Channels Estimated

It is interesting to study the algorithm complexity when the RAKE receiver updates its diversity paths. We denote the number of channels estimated as N, with $0 \leq N \leq L$. When $L_c = 1$, since we assume there will always be one path from synchronization, we do not need to estimate any channel, so we have $N = 0$. When $2 \leq L_c \leq L$, we have two cases: when there are less than $L_c - 1$ acceptable paths, and when there are at least $L_c - 1$ acceptable paths. For the first case, the receiver must have tested all L paths before it stops searching. The probability that there are less than $L_c - 1$ acceptable paths is

$$
P_B = \sum_{k=L-L_c+1}^{L-1} \binom{L-1}{k} [1-P_\gamma(\gamma_T)]^{L-k-1}[P_\gamma(\gamma_T)]^k \qquad (5.32)
$$

For the second case, with k paths tested, we have the probability $P_A^{(k)}$

$$
P_A^{(k)} = \sum_{k=L_c-1}^{L-1} \binom{k-1}{k-L_c+1} [1-P_\gamma(\gamma_T)]^{Lc}[P_\gamma(\gamma_T)]^{k-L_c}. \qquad (5.33)
$$

Combining these two cases we have

$$
\begin{aligned}
N &= \sum_{k=L_c-1}^{L-1} kP_A^{(k)} + (L-1)P_B \\
&= \sum_{k=L_c-1}^{L-1} k\binom{k-1}{k-L_c+1}[1-P_\gamma(\gamma_T)]^{Lc-1}[P_\gamma(\gamma_T)]^{k-L_c+1} \\
&+ (L-1)\sum_{k=L-L_c+1}^{L-1}\binom{L-1}{k}[1-P_\gamma(\gamma_T)]^{L-k-1}[P_\gamma(\gamma_T)]^k
\end{aligned} \tag{5.34}
$$

As expected, when $\gamma_T = 0$, we have $P_\gamma(\gamma_T) = 0$, so that $N = L_c - 1$. When $\gamma_T \to +\infty$, we have $P_\gamma(\gamma_T) = 1$, so that $N = L - 1$.

5.4 Performance Analysis over Fading Paths with Unequal Average SNR

5.4.1 Channel Model and MGF of the Combined Output SNR

In the previous section we assume the synchronized channel follows standard fading, and all the diversity paths are i.i.d. and have the same average SNR. In this section of the paper, we employ a more practical channel model. For the synchronized path, since synchronization requires a certain SNR threshold, which we denote as γ_{syn}, we assume it also follows the truncated fading with threshold γ_{syn}. Also, it is not practical to assume that all the paths are i.i.d. distributed. Actually, for a RAKE receiver, the average SNR decreases when the path delay increases. Between different paths, we assume

$$\gamma_k = \gamma_0 e^{-\delta k}, \tag{5.35}$$

where γ_i is the average SNR of the ith diversity path, and δ is a constant between 0 and 1. Now we derive the MGF of the combined signal over fading paths with unequal average SNR using the approach in section 5.2. Based on (5.35), we have $\gamma_0 > \gamma_1 > ... > \gamma_{L-1}$, and assuming exactly $i+1$ out of L paths are combined, the combined SNR S is

$$S = \gamma_0 + \sum_{k=1}^{i} \gamma_k, \tag{5.36}$$

where i is the number of combined paths except the synchronized one. The MGF of S is

$$M_S(t) = M^*_{\gamma_0}(t) \times \sum_{l=0}^{L_c-1} w_l M^l_S(t), \tag{5.37}$$

where $M^*_{\gamma_0}(t)$ is the MGF of the synchronized path with SNR threshold γ_{syn}, $M^l_S(t)$ is the MGF of S corresponding to the event that l out of $L_c - 1$ paths have an SNR greater than γ_T. We derive the MGF of S.

When $l = L_c - 1$

$$\begin{aligned} M^{L_c}_S(t) &= M^*_{\gamma_0}(t) Pr[\{n_i\}_{i=1}^{L_c-1}] M_S^{\{n_i\}_{i=1}^{L_c-1}}(t) \\ &= M^*_{\gamma_0}(t) \sum_{\{n_i\}_{i=1}^{L_c-1}} \left\{ \prod_{j=1}^{L_c-1} \left[\prod_{k=n_{j-1}+1}^{n_j-1} P_{\gamma_j}(\gamma_T) \right] [1 - P_{\gamma_j}(\gamma_T)] \right\} \\ &\times \prod_{i=1}^{L_c-1} M^+_{\gamma_{n_i}}(t), \end{aligned} \tag{5.38}$$

where $\{n_i\}_{i=1}^{l}$ denotes a path selection set which has l diversity paths.

When $1 \le l \le L_c - 2$

$$\begin{aligned} M^l_S(t) &= M^*_{\gamma_0}(t) \sum_{n_i{}_{i=1}^{l}} Pr[\{n_i\}_{i=1}^{l}] M_S^{\{n_i\}_{i=1}^{l}}(t) \\ &= M^*_{\gamma_0}(t) \sum_{\{n_i\}_{i=1}^{l}} \left\{ \prod_{j=1}^{L_c-1} \left[\prod_{k=n_{j-1}+1}^{n_j-1} P_{\gamma_j}(\gamma_T) \right] [1 - P_{\gamma_j}(\gamma_T)] \right\} \\ &\times \prod_{j=n_l+1}^{L-1} P_{\gamma_j}(\gamma_T) \prod_{i=1}^{L-1} M^+_{\gamma_{n_i}}(t). \end{aligned} \tag{5.39}$$

When $l = 0$, we only have one path, the synchronized path, so that

$$M^0_S(t) = Pr[l = 0] M_S^{l=0}(t)$$

$$= M^*_{\gamma_0}(t) \prod_{j=1}^{L-1} P_{\gamma_j}(\gamma_T). \tag{5.40}$$

Combining (5.38) (5.39) and (5.40), we have

$$\begin{aligned} M_S(t) &= M^*_{\gamma_0}(t) \prod_{j=1}^{L-1} P_{\gamma_j}(\gamma_T) \\ &+ M^*_{\gamma_0}(t) \sum_{n_i{}_{i=1}^{L_c-1}} \left\{ \prod_{j=1}^{L_c-1} \left[\prod_{k=n_{j-1}+1}^{n_j-1} P_{\gamma_j}(\gamma_T) \right] [1 - P_{\gamma_j}(\gamma_T)] \right\} \prod_{i=1}^{L_c-1} M^+_{\gamma_{n_i}}(t) \\ &+ M^*_{\gamma_0}(t) \sum_{n_i{}_{i=1}^{l}} \left\{ \prod_{j=1}^{L_c-1} \left[\prod_{k=n_{j-1}+1}^{n_j-1} P_{\gamma_j}(\gamma_T) \right] [1 - P_{\gamma_j}(\gamma_T)] \right\} \\ &\times \prod_{j=n_l+1}^{L-1} P_{\gamma_j}(\gamma_T) \prod_{i=1}^{L-1} M^+_{\gamma_{n_i}}(t). \end{aligned} \tag{5.41}$$

With the closed-form MGF $M_S(t)$ for the SNR of the combined signal S in (5.41) we can get the error probability.

5.4.2 Average Number of Diversity Path Estimates

The number of channels estimated is N, with $0 \leq N \leq L$. When $L_c = 1$, we do not need to estimate any paths, so we have $N = 0$. When $2 \leq L_c \leq L$ we have

$$\begin{aligned} N &= N^{l=L_c-1} + (L-1)Pr[0 \leq l \leq L_c - 2] \\ &= \sum_{\{n_i\}_{i=1}^{L_c-1}} n(L_c - 1) \prod_{j=1}^{L_c-1} \left[\prod_{k=n_{j-1}+1}^{n_j-1} P_{\gamma_j}(\gamma_T) \right] [1 - P_{\gamma_j}(\gamma_T)] \\ &+ (L-1) \left\{ 1 - \sum_{\{n_i\}_{i=1}^{L_c-1}} n(L_c - 1) \prod_{j=1}^{L_c-1} \left[\prod_{k=n_{j-1}+1}^{n_j-1} P_{\gamma_j}(\gamma_T) \right] [1 - P_{\gamma_j}(\gamma_T)] \right\} \end{aligned} \tag{5.42}$$

5.5 Numerical Results

In this section, we study the average SNR, error performance, outage probability and average number of channels estimated by a RAKE receiver. Results are given for both i.i.d.

and non-i.i.d cases. Theoretical results given in this part of the thesis are confirmed by computer simulation.

Fig. 5.2 shows the average combined SNR of a RAKE receiver over a Rayleigh fading channel with $L = 6$. We examine the situations when different numbers of fingers are used in the RAKE receiver. From Fig. 5.2, we clearly see that the combined output SNR increases with each additional finger employed in the receiver. However, it is not necessary to use the same number of fingers as the number of resolvable multipath signals to obtain near-optimal performance. For example, in Fig. 5.1 with $L = 6$, performance is very near to optimal when $L_c = 5$. Fig. 5.3 shows the SEP in Rayleigh fading with different numbers of RAKE fingers. This figure shows that the system performance is greatly improved with an increased number of fingers. Note that for typical SNR values, the curves for $L_c = 5$ and $L_c = 6$ are identical, which supports the conclusion based on Fig. 5.2.

Figs. 5.4 and 5.5 show the effects of different selection thresholds γ_T on the SEP performance and average output SNR with $L = 4$. Notice that the optimal threshold changes according to the number of fingers used in the receiver. These fingers also show that when the threshold is large compared to the average SNR (larger than 20dB in the figure), all the paths will be discarded except the first one, so the output SNR is simply the SNR of the first path. The results in Figs. 5.4 and 5.5 are also useful to determine the optimal threshold for a RAKE receiver with a given L_c.

Fig. 5.6 shows the outage probability of a RAKE receiver with different normalized outage threshold γ_{out}, which is defined as the ratio between the outage threshold and the average SNR per path. In Fig. 5.6 we have $\bar{\gamma} = 10dB$ and $\gamma_T = 7dB$. As we can see, the outage probability decreases as L_c increases, and when the normalized outage threshold is high, the outage probability equal to one. Fig. 5.7 shows the number of channels estimated. As expected, $N = L_c - 1$ when γ_T is very small, and $N = L - 1$ when γ_T is large. In Fig. 5.7 we have $\bar{\gamma} = 10dB$.

Figs. 5.8, 5.9 and 5.10 shows results for the case with unequal SNR for each diversity path and the synchronized path follows truncated Rayleigh distribution with the synchro-

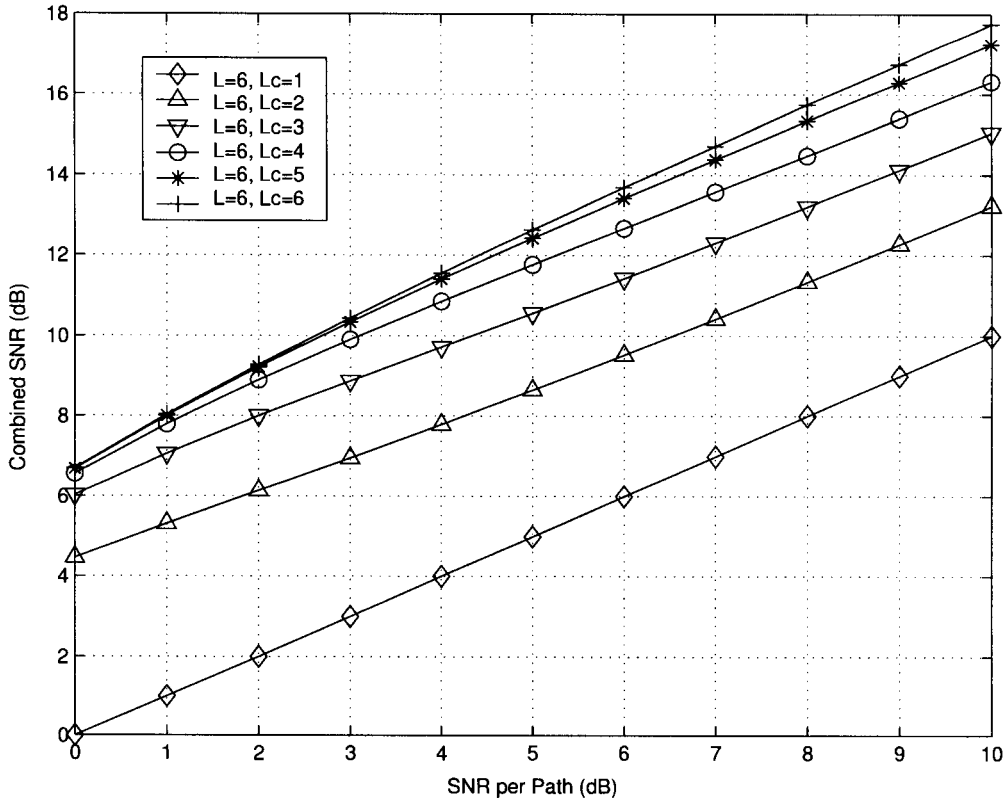

Figure 5.2. *Combined SNR of a RAKE receiver over a Rayleigh fading channel,* $\gamma_T = 10dB$.

nize threshold $\gamma_{syn} = 10dB$. Fig. 5.8 shows the BER performance with differnt average SNRs for the first (synchronized) diversity path. From this figure we can see that the contribution of each diversity path decreases as the average SNR decreases. Fig. 5.9 shows the BER performance with different choosing threshold. The results show that for different δ we have different optimum threshold for best BER performance, and when the choosing threshold is too high we have only the first path used in the RAKE receiver. Fig. 5.10 shows the number of channels estimated when we have different γ_T, with $L = 4$ and $L_c = 2$.

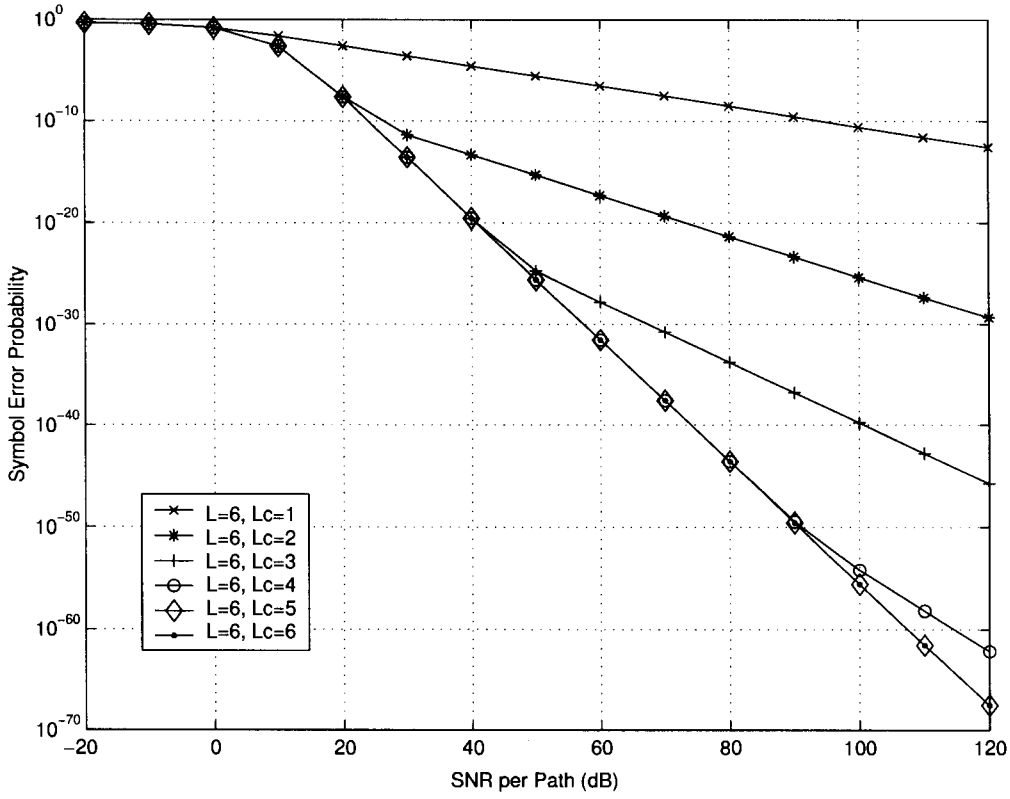

Figure 5.3. *Symbol error probability of a RAKE receiver over a Rayleigh fading channel,* $\gamma_T = 10dB$.

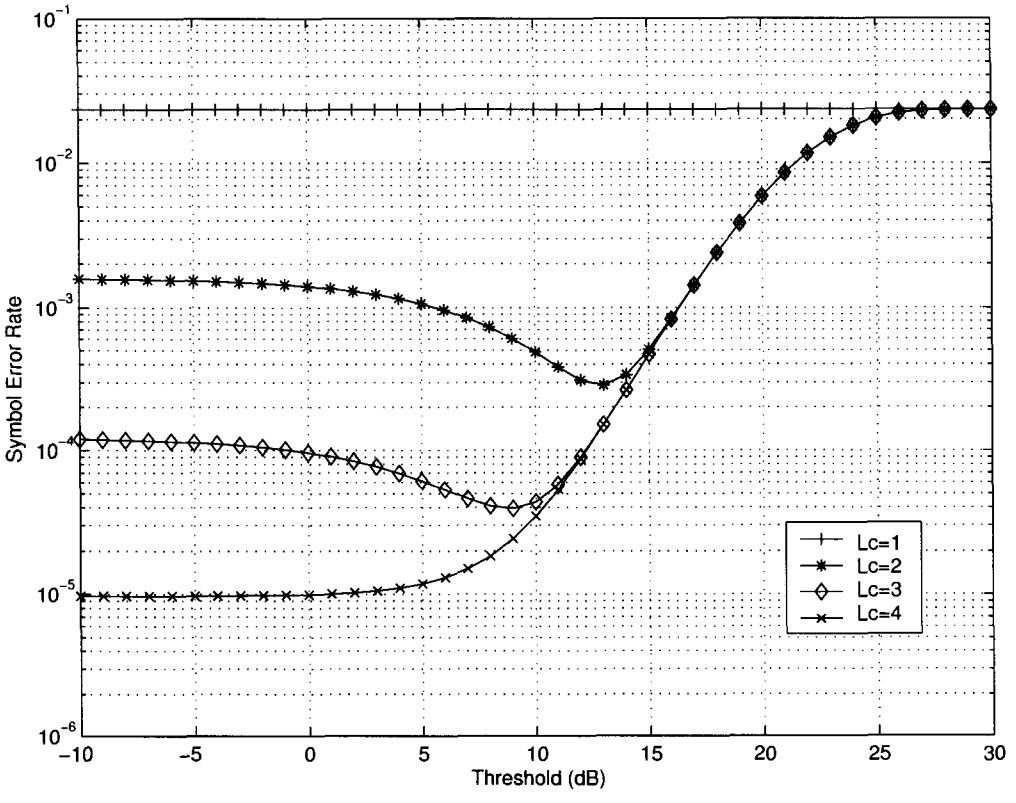

Figure 5.4. *Symbol error probability of a RAKE receiver over a Rayleigh fading channel with different selection thresholds,* $L = 4$, $\bar{\gamma} = 10dB$.

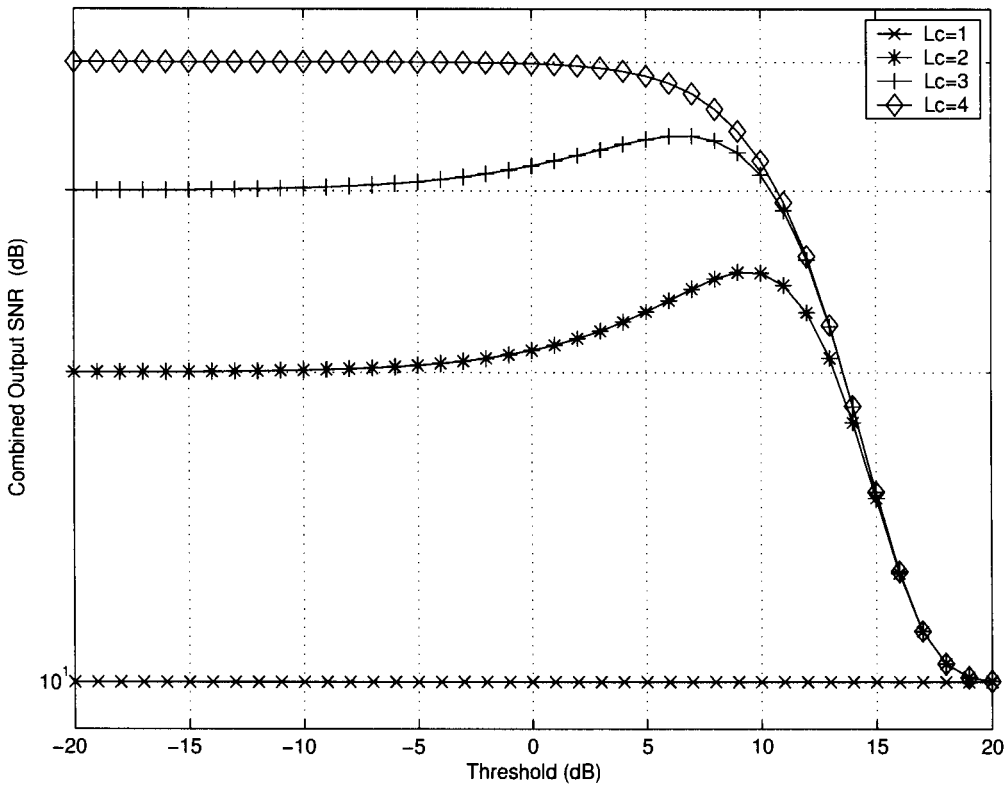

Figure 5.5. *Combined SNR of a RAKE receiver over a Rayleigh fading channel with different selection thresholds,* $L = 4$, $\bar{\gamma} = 10dB$.

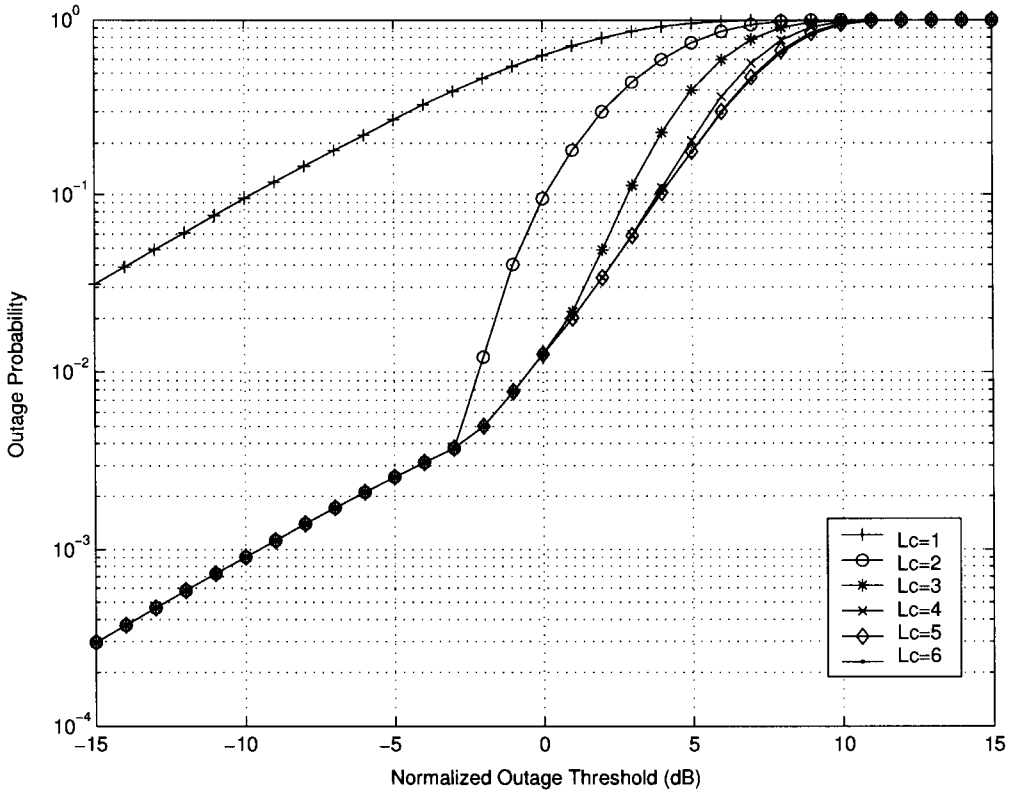

Figure 5.6. *Outage Probability of a RAKE receiver over a Rayleigh fading channel* $L = 6$, $\bar{\gamma} = 10dB$, *and* $\gamma_T = 7dB$.

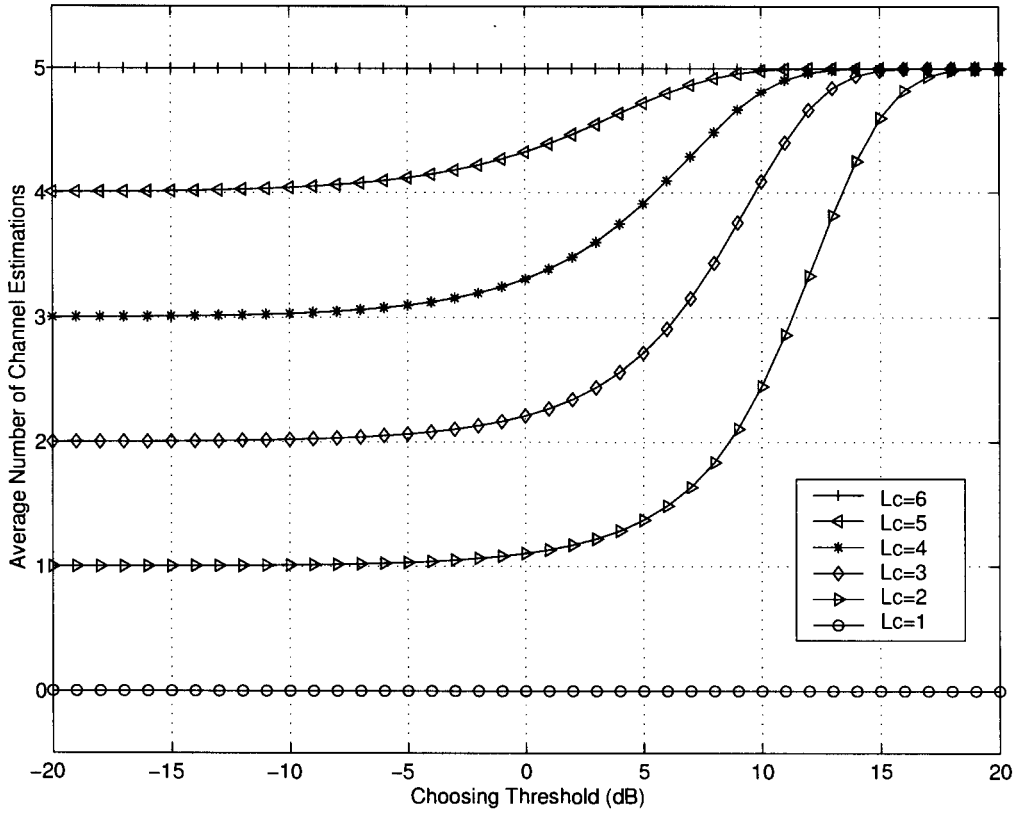

Figure 5.7. *Number of Channels Estimated of a RAKE receiver over a Rayleigh fading channel* $L = 6$, $\bar{\gamma} = 10dB$.

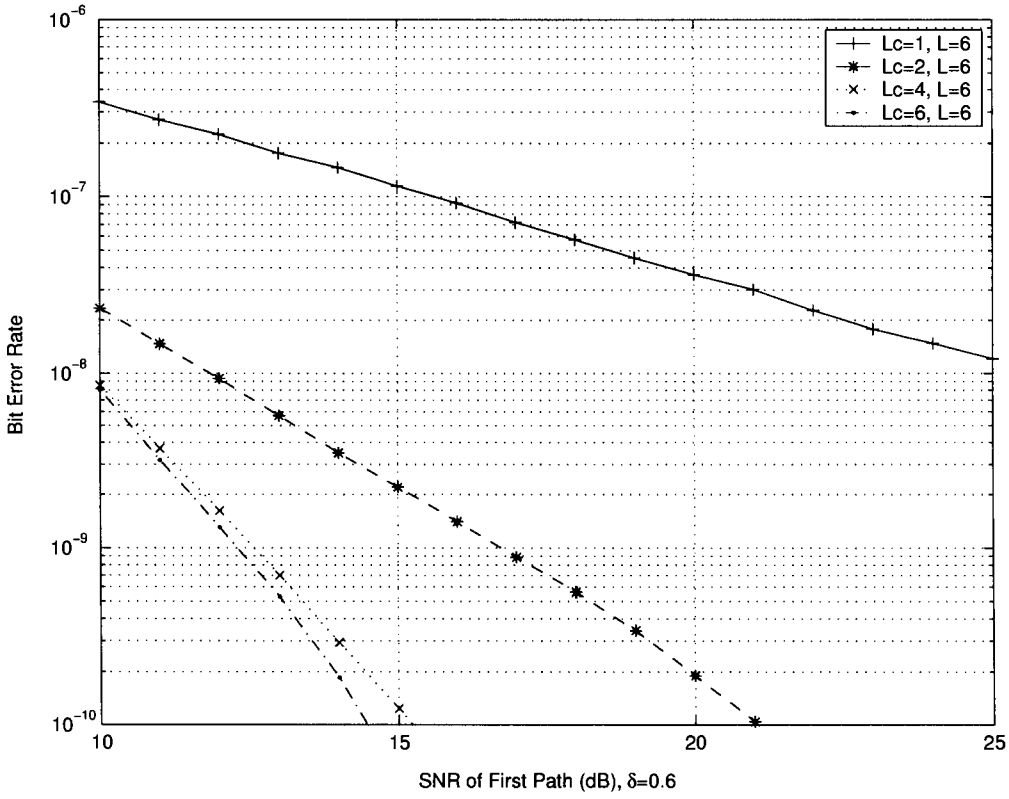

Figure 5.8. *BER of a RAKE receiver over a Rayleigh fading channel with different average SNR for the first diversity path,* $\gamma_T = 10dB$, $\gamma_{syn} = 10dB$ *and* $\delta = 0.6$.

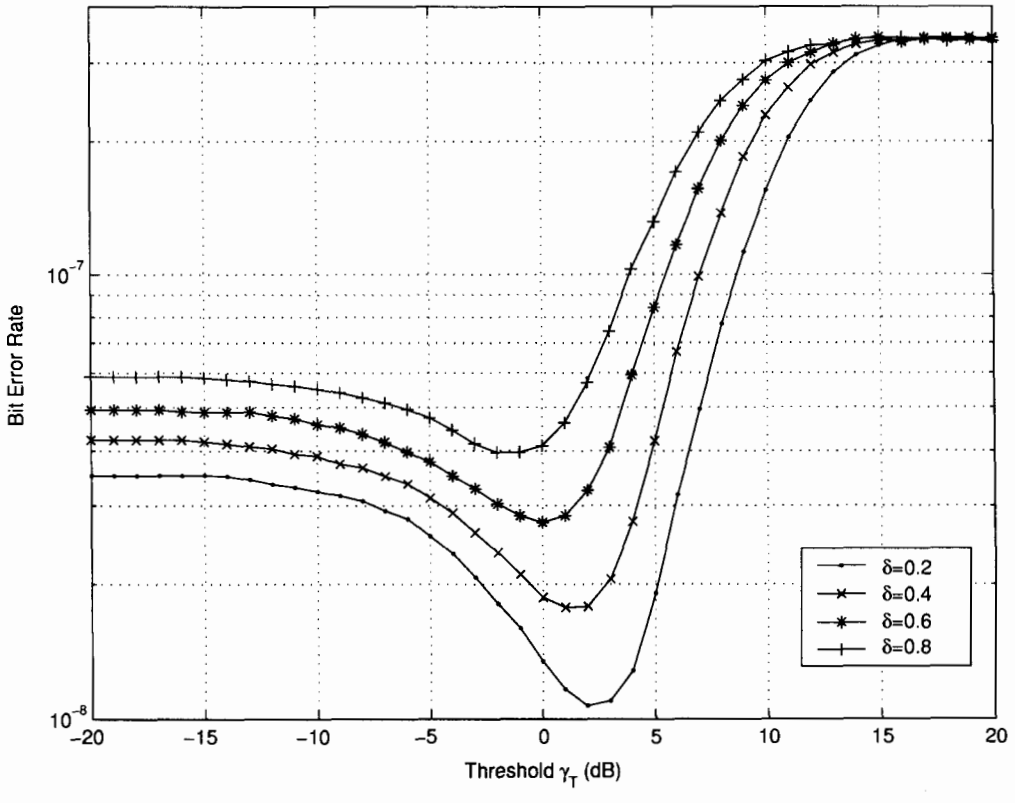

Figure 5.9. *BER of a RAKE receiver over a Rayleigh fading channel with different choosing threshold* γ_T, $\gamma_{syn} = 10dB$, $\gamma_T = 10dB$, $L = 4$ *and* $L_c = 2$.

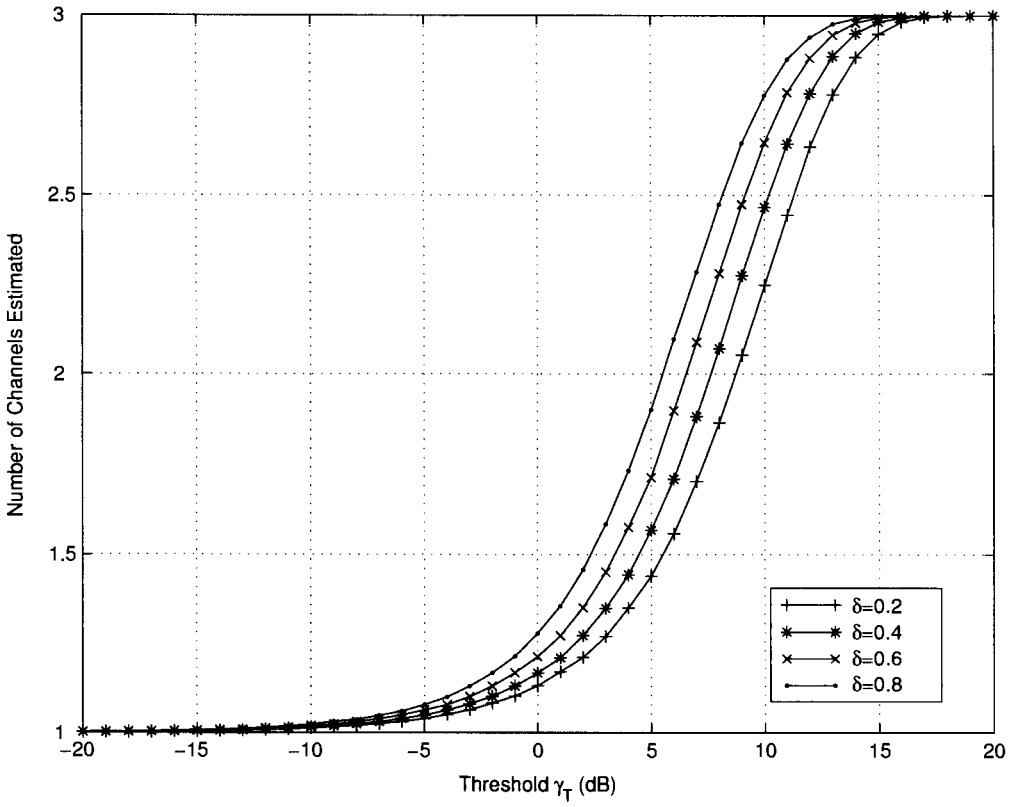

Figure 5.10. *Number of channels estimated of a RAKE receiver over a Rayleigh fading channel with different choosing threshold* γ_T, $\gamma_{syn} = 10dB$, $\gamma_T = 10dB$, $L = 4$ *and* $L_c = 2$.

Chapter 6

Summary

In this thesis, a comprehensive analysis for the capacity and error probability of orthogonal space-time block codes has been presented in correlated fading channels. Correlated Rayleigh, Rician and Nakagami fading are considered for PAM, PSK and QAM modulations. Closed form Shannon capacity expressions of STBC are derived for the correlated Rayleigh and Nakagami fading channels. Channel capacities for STBC employing PAM/PSK/QAM over correlated fading channels are also investigated. Closed-form error probabilities are derived for correlated Rayleigh and Nakagami fading channels and various modulation schemes. A unified approach is also introduced for the error probability analysis with correlated Rayleigh, Rician, and Nakagami fading channels. A simple expression based on the characteristics function of the instantaneous SNR is presented for different fading channels and modulation schemes. This analysis is also employed to determine the performance of a STBC multiuser DS-CDMA system.

As a further step of our research, we apply the same approach used to get the performance of STBC to MRC system. We investigated the error probability and system capacity for q-ary linearly modulated systems with MRC multichannel reception over correlated Nakagami fading channels. Closed-form expressions were derived for the error probability of q-ary PAM, PSK and QAM when perfect channel state information is available at the receiver. Error probabilities over Rayleigh fading channels were also presented as a special case.

In this thesis, we considered the performance of a practical RAKE receiver in a CDMA

system employing maximal-ratio combining (MRC). We derived closed-form expression of average combined SNR and SEP over i.i.d. fading channels based on the Moment Generating Functions (MGF) of the combined output signal. Outage probability and the number of channels estimated are also given. Performance of RAKE receiver in a more general non-identically fading channel scenario is also studied. Selected numerical results were given to support the analysis.

Our future research work will still focus on diversity. We will study Transmit/Receive Diversity for Wireless Communication Systems, which combine the benefit of both transmit and receive diversity. Multi-User Detection (MUD) schemes for systems with transmit and/or receive diversity are also a possible direction for our future research. As part of our ongoing effort, we would like to investigate the performance of RAKE receivers for UWB Transmission. Performance of the systems mentioned above over different channel models is also a good topic to work on.

Bibliography

[1] J. Proakis, *Digital Communications*, 4th ed. McGraw-Hill, 2001.

[2] W. C. Jakes, *Microwave Mobile Communications*. IEEE Press, New Jersey, 1974.

[3] M. Schwatz, W. R. Bennett, and S. Stein, *Communication Systems and Techniques*. McGraw-Hill, 1966.

[4] A. Paulraj, *Diversity Techniques in Mobile Communications*. CRC Press, 1996.

[5] V. Tarokh, N. Seshadri, and A. Calderbank, "Space-time codes for high data rate wireless communication: Performance criterion and code construction," *IEEE Trans. Inform. Theory*, vol. 44, no. 2, pp. 744–765, 1998.

[6] A. Wittneben, "A new bandwidth efficient transmit antenna modulation diversity scheme for linear digital modulation," *Proceedings of ICC*, pp. 1630–1634, May 1993.

[7] N. Seshadri and J. H. Winters, "Two signalling schemes for improving the error performance of frequency-division-duplex (FDD) transmission systems using transmitter antenna diversity," *Int. J. Wireless Inform.*, vol. 1, no. 1, pp. 49–60, 1994.

[8] S. Alamouti, "A simple transmit diversity technique for wireless communications," *IEEE J. Select. Areas Commun.*, vol. 16, no. 8, pp. 1452–1458, 1988.

[9] V. Tarokh, H. Jafarkhani, and A. Calderbank, "Space-time block codes from orthogonal designs," *IEEE Trans. Inform. Theory*, vol. 45, pp. 1456–1467, 1999.

[10] ——, "Space-time block coding for wireless communications: Performance results," *IEEE J. Select. Areas Commun.*, vol. 17, no. 3, pp. 451–460, 1999.

[11] B. M. Hochwald, T. L. Marzetta, and C. B. Papadias, "A transmitter diversity scheme for wideband CDMA systems based on space time spreading," *IEEE J. Select. Areas Commun.*, vol. 19, pp. 48–60, 2001.

[12] G. Ganesan and P. Stoica, "Space time block codes: A maximum SNR approach," *IEEE Trans. Inform. Theory*, vol. 47, pp. 1650–1656, 2001.

[13] O. Tirkkonen and A. Hottinen, "Square-matrix embeddable space time block codes for complex signal constellations," *IEEE Trans. Inform. Theory*, vol. 48, pp. 1122–1126, 2002.

[14] G. B. S. Baro and A. Hansmann, "Improved codes for space-time trellis-coded modulation," *IEEE Comm. Lett.*, vol. 4, pp. 20–22, 2000.

[15] J. Yuan, Z. Chen, B. Vucetic, and W. Firmanto, "Performance analysis and design of space-time coding on fading channels," *Proc. 2001 IEEE International Symposium on Information Theory*, p. 153, 2001.

[16] H. Boleskei and A. J. Paulraj, "Performance of space-time codes in the presence of spatial fading correlation," *Proc. of Asilomar Conf. on Signals, Systems, and Computeres*, pp. 235–238, 2000.

[17] S. Siwamogsatham and M. O. Fitz, "Robust space-time coding for correlated rayleigh fading channels," *Proc. 38th Annual Allerton Conf. on Communication, Control, and Computing*, pp. 115–118, 2000.

[18] B. Hochwald, W. S. T. Marzetta, and R. Urbanke, "Systematic design of unitary space-time constellations," *IEEE Trans. Inform. Theory*, vol. 46, no. 6, pp. 1962–1973, 2000.

[19] S. Sandhu and A. J. Paulraj, "Unified design of linear space-time block codes," pp. 1073–1077, 2001.

[20] X. Lin and R. S. Blum, "Systematic design of space-time codes employing multiple trellis coded modulation," *IEEE Trans. on Commun.*, vol. 50, no. 4, pp. 608–615, 2002.

[21] R.A.Stirling-Gallacher and Z. Wang, "Improving performance of coherent coded ofdm systems using space-time transmit diveresity," *Electronic Lett.*, vol. 7, pp. 302–307, 2001.

[22] W. Lindsey, "Error probability for rician fading multichannel reception of binary and N-ary signals," *IEEE Trans. Inform. Theory*, vol. 10, pp. 339–350, 1964.

[23] T. Staley, R. North, J. L. W. Ku, and J. Zeidler, "Performance evaluation for multichannel reception of coherent mpsk over slowly fading frequency selective fading channels," *IEEE Trans. Vehic. Technol.*, vol. 50, pp. 877–894, 2001.

[24] ——, "Error probability performance prediction for multichannel reception of linearly modulated coherent systems on fading channels," *IEEE Trans. Commun.*, vol. 50, pp. 1423–1428, 2002.

[25] M.-S. Alouini and A. Goldsmith, "A unified approach for calculating error rates of linearlymodulated signals over generalized fading channels," *IEEE Trans. Commun.*, vol. 47, no. 9, pp. 1324–1334, 1999.

[26] P. Lombardo, G. Fedele, and M. Rao, "MRC performance for binary signals in nak-

agami fading with general branch correlation," *IEEE. Trans. Commun.*, vol. 47, no. 1, pp. 44–52, 1999.

[27] M. Kang and M.-S. Alouini, "Performance analysis of MIMO MRC systems over rician fading channels," *Proc. IEEE Vehic. Tech. Conf.*, pp. 869–873, Sept. 2002.

[28] M. Win and J. Winters, "Virtual branch analysis of symbol error probability for hybrid selection/maximal-ratio combining in rayleigh fading," *IEEE Trans. Commun.*, vol. 49, no. 11, pp. 1926–1934, 2001.

[29] S. Sandhu and A. Paulraj, "Space-time block codes: A capacity perspective," *IEEE Commun. Letters*, vol. 4, no. 12, pp. 384–386, 2000.

[30] H. Espinosa, J. Fonollosa, and J. D. Penin, "Channel capacity of space-time block coding," *Proc. IST Mobile Communications*, pp. 507–511, Sept. 2001.

[31] R. Price and J. P. Green, "A communication technique for multipath channels," *Proc. IRE*, pp. 46:555–570, March 1958.

[32] S. Tantikovit, A. Sheikh, and M. Wang, "Combining schemes in rake receiver for low spreading factor long-code-CDMA systems," *IEE Elect. Letts*, vol. 36, pp. 1872–1874, 2000.

[33] N. Kong and L. B. Milstein, "Average SNR of a generalized diversity selection combiniing scheme," *IEEE Commun. Letters*, vol. 3, no. 3, pp. 57–59, 1999.

[34] M. Z. Win and J. H. Winters, "Analysis of hybrid selection/maximal-ratio combining for Rayleigh fading," *IEEE Trans. Commun.*, vol. 47, no. 12, pp. 1773–1776, 1999.

[35] M. S. Alouini and M. K. Simon, "An MGF-based performance analysis of generalized selective combining over Rayleigh fading channels," *IEEE Trans. Commun.*, vol. 48, no. 3, pp. 401–415, 2000.

[36] Y. Ma and C. Chai, "Unified error probability analysis for generalized selection combining in Nakagami fading channels," *IEEE J. Select. Areas Commun.*, vol. 18, no. 11, pp. 2198–2210, 2000.

[37] A. Annamalai and C. Tellambura, "Analysis of hybrid selection/maximal-ratio diversity combiner with Gaussian errors," *IEEE Trans. Wireless Commun.*, vol. 1, no. 3, pp. 498–512, 2002.

[38] S. Kim, D. Ha, and J. Reed., "Minimum selection GSC and adaptive low-power RAKE combining scheme," *IEEE Int. Symp. Circuits and Systems*, pp. IV–357–IV–360, May 2003.

[39] M. Simon and M.-S. Alouini, "Performance analysis of generalized selection combining with threshold test per branch (T-GSC)," *IEEE Trans. Vehic. Technol.*, vol. 51, pp. 1018–1029, 2002.

[40] A. Oppenheim, A. Willsky, and S. Nawab, *Signals and Systems*. Prentice-Hall, 1998.

[41] W. Yee, *Mobile Communications Engineering*. McGraw-Hill, 1982.

[42] R. Nabar, H. Bolcskei, and A. Paulraj, "Outage properties of space-time block codes in correlated rayleigh or ricean fading environments," pp. 2381–2384, May 2002.

[43] H. Zhang and T. A. Gulliver, "Capacity and error probability analysis for space-time block codes over fading channels," *accepted for publication by IEEE Trans. Wireless Comm.*, 2004.

[44] E. Baccarelli, "Evaluation of the reliable data rates supported by multiple-antenna coded wireless links for QAM transmissions," *IEEE J. Select. Areas Commun.*, vol. 19, no. 2, pp. 295–304, 2001.

[45] N. Johnson and S. Kotz, *Distribution in Statistics: Continuous Multivariate Distributions*. New York: Wiley, 1972.

[46] G. Foschini and M. Gans, "On limits of wireless communications in a fading environment when using multiple antennas," *Wireless Personal Commun.*, vol. 6, pp. 311–335, 1998.

[47] G. Ungerboeck, "Channel coding with multilevel/phase signals," *IEEE Trans. Inform. Theory*, vol. 28, no. 1, pp. 55–67, 1982.

[48] E. Baccarelli and A. Fasano, "Some simple bounds on the symmetric capacity and outage probability for QAM wireless channels with Rice and Nakagami fadings," *IEEE J. Select. Areas Commun.*, vol. 18, no. 3, pp. 361–368, 2000.

[49] S. Wei, "An alternative derivation for the signal-to-noise ratio of a SSMA system," *IEEE Trans. Commun.*, vol. 42, pp. 2224–2226, 1994.

[50] T. Rappaport, *Wireless Communications:Principles and Practice*, 1st ed. Prentice-Hall, 1996.

[51] J. Salz and J. H. Winters, "Effect of fading correlation on adaptive arrays in digital mobile radio," *IEEE Trans. Vehic. Technol.*, vol. 43, pp. 1049–1057, 1994.

[52] M. Shayesteh and A. Aghamohammadi, "On the error probability of linearly modulated signals on frequency-flat Ricean, Rayleigh, and AWGN channels," *IEEE Trans. Commun.*, vol. 43, pp. 1454–1466, 1995.

[53] M. K. Simon and M. S. Alouini, *Digital Communications over Generalized Fading Channels: A Unified Approach to Performance Analysis*. John Wiley&Sons, 2000.

Appendix A

Derivation of (2.34) and (4.18)

Consider the following integral

$$\begin{aligned} p(n) &= \int_0^\infty \ln(1+\gamma x) x^n e^{-x} dx \\ &= \frac{e^{\frac{1}{\gamma}}}{\gamma^{n+1}} \sum_{k=0}^{n} \binom{n}{k} (-1)^{n-k} \int_1^\infty \ln(t) t^k e^{\frac{1}{\gamma}} dt. \end{aligned} \tag{A.1}$$

It is known that

$$\begin{aligned} g(k) &= \int_1^\infty \ln(t) t^k e^{-\frac{t}{\gamma}} dt \\ &= \gamma \int_1^\infty t^{k-1} e^{-\frac{t}{\gamma}} dt + \gamma \int_1^\infty k t^{k-1} \ln(t) e^{-\frac{t}{\gamma}} dt \\ &= \gamma \int_1^\infty t^{k-1} e^{-\frac{t}{\gamma}} dt + \gamma k g(k-1) \\ &= \gamma e^{-\frac{1}{\gamma}} \sum_{j=0}^{k} \sum_{i=0}^{k-j-1} \frac{k!}{(k-j)(k-j-i-1)!} \gamma^{i+j+1} - \gamma^{k+1} k! \mathrm{Ei}\left(-\frac{1}{\gamma}\right), \end{aligned} \tag{A.2}$$

so substituting (A.2) into (A.1) gives

$$\begin{aligned} p(n) &= \sum_{k=1}^{n} \frac{n!}{(n-k)!} \left[\sum_{j=0}^{k} \sum_{i=0}^{j-k-1} \frac{(-1)^{n-k}}{(k-j)(k-j-i-1)!} \bar{\gamma_c}^{i+j+2} \right] \\ &+ \sum_{k=1}^{n} \frac{n!}{(n-k)!} \left[(-1)^{n-k-1} \bar{\gamma_c}^{k+1} e^{\frac{1}{\bar{\gamma_c}}} \mathrm{Ei}\left(-\frac{1}{\bar{\gamma_c}}\right) \right]. \end{aligned} \tag{A.3}$$

Then (2.34) is obtained as required

$$
\begin{aligned}
f(n) &= \int_0^{\infty} \ln(1+\gamma_s)\gamma_s^n e^{-\frac{\gamma_s}{\bar{\gamma}_c}} d\bar{\gamma}_c \\
&= \bar{\gamma}_c{}^{n+1} \times p(n) \\
&= (-1)^{n-1}\bar{\gamma}_c e^{\frac{1}{\bar{\gamma}_c}} Ei\left(-\frac{1}{\bar{\gamma}_c}\right) \\
&+ \sum_{k=1}^{n} \frac{n!}{(n-k)!}\left[\sum_{j=0}^{k}\sum_{i=0}^{j-k-1} \frac{(-1)^{n-k}}{(k-j)(k-j-i-1)!}\bar{\gamma}_c{}^{i+j+2}\right] \\
&+ \sum_{k=1}^{n} \frac{n!}{(n-k)!}\left[(-1)^{n-k-1}\bar{\gamma}_c{}^{k+1} e^{\frac{1}{\bar{\gamma}_c}} \mathrm{Ei}\left(-\frac{1}{\bar{\gamma}_c}\right)\right]. \qquad \text{(A.4)}
\end{aligned}
$$